Field Guide to
Infrared Optics, Materials, and Radiometry

Arnold Daniels

SPIE Terms of Use: This SPIE eBook is DRM-free for your convenience. You may install this eBook on any device you own, but not post it publicly or transmit it to others. SPIE eBooks are for personal use only. For details, see the SPIE Terms of Use. To order a print version, visit SPIE.

SPIE.

Field Guide to

Infrared Optics, Materials, and Radiometry

Arnold Daniels

SPIE Field Guides
Volume FG39

John E. Greivenkamp, Series Editor

SPIE PRESS
Bellingham, Washington USA

The content of this book reflects the thought of the author. Every effort has
been made to publish reliable and accurate information herein, but the
publisher is not responsible for the validity of the information or for any
outcomes resulting from reliance thereon.

Printed in the United States of America.
First printing.
For updates to this book, visit http://spie.org and type "FG39" in the search
field.

SPIE.

Introduction to the Series

Welcome to the *SPIE Field Guides*—a series of publications written directly for the practicing engineer or scientist. Many textbooks and professional reference books cover optical principles and techniques in depth. The aim of the *SPIE Field Guides* is to distill this information, providing readers with a handy desk or briefcase reference that provides basic, essential information about optical principles, techniques, or phenomena, including definitions and descriptions, key equations, illustrations, application examples, design considerations, and additional resources. A significant effort will be made to provide a consistent notation and style between volumes in the series.

Each *SPIE Field Guide* addresses a major field of optical science and technology. The concept of these *Field Guides* is a format-intensive presentation based on figures and equations supplemented by concise explanations. In most cases, this modular approach places a single topic on a page, and provides full coverage of that topic on that page. Highlights, insights, and rules of thumb are displayed in sidebars to the main text. The appendices at the end of each *Field Guide* provide additional information such as related material outside the main scope of the volume, key mathematical relationships, and alternative methods. While complete in their coverage, the concise presentation may not be appropriate for those new to the field.

The *SPIE Field Guides* are intended to be living documents. The modular page-based presentation format allows them to be updated and expanded. We are interested in your suggestions for new *Field Guide* topics as well as what material should be added to an individual volume to make these *Field Guides* more useful to you. Please contact us at **fieldguides@SPIE.org**.

<div align="right">

John E. Greivenkamp, *Series Editor*
College of Optical Sciences
The University of Arizona

</div>

The Field Guide Series

Keep information at your fingertips with the *SPIE Field Guides*:

Field Guide to Infrared Optics, Materials, and Radiometry

The amount of new material added to the second edition of the *Field Guide to Infrared Systems, Detectors, and FPAs* (2010) was quite extensive. As a result, the third edition (2018) of that Field Guide is accompanied by this "companion" publication, *Field Guide to Infrared Optics, Materials, and Radiometry*.

These Field Guides cover a broad range of technical topics necessary to understand the principles of modern infrared technology. They combine numerous engineering disciplines essential for the development of infrared systems. The mathematical equations and physical concepts in these Field Guides are in sequence. Therefore, although the two publications are available separately, it is highly recommended that readers acquire the two books as a set.

The *Field Guide to Infrared Optics, Materials, and Radiometry* includes a detailed explanation of monochromatic and chromatic optical aberrations as well as a comprehensive introduction to the optical, mechanical, and thermal properties of infrared materials. It provides important concepts such as depth of focus, depth of field, hyperfocal distance, warm shields, aspheric surfaces, kinoforms, optical scatter, etc. It also includes an overview of the best and most common infrared glasses and mirror substrates. This Field Guide also covers the essentials of radiometry necessary for the quantitative understanding of infrared signatures and flux transfer, spectral atmospheric transmittance, and path radiance.

Field Guide to Infrared Optics, Materials, and Radiometry

Above all, I voice a special note of gratitude to my kids Becky and Alex, and my wife Rosa for their love and support.

Lastly, I would particularly like to thank you, the reader, for selecting these books and taking the time to explore the topics related to this motivating and exciting field. I trust that the contents of these Field Guides will prove interesting and useful to engineers and scientists working in one of the various infrared fields.

These Field Guides are dedicated to the memory of my father and brothers.

Arnold Daniels
September 2018

Table of Contents

Table of Contents

Table of Contents

Glossary of Symbols

a_{lattice}	Lattice constant
A	Area
A_{d}	Detector area
A_{enp}	Area of an entrance pupil
A_{exp}	Area of an exit pupil
$A_{\text{footprint}}$	Footprint area
A_{img}	Area of an image
A_{lens}	Lens area
A_{obj}	Area of an object
A_{opt}	Area of an optical component
A_{s}	Source area
AMTIR	Amorphous materials transmitting infrared radiation
b.f.l.	Back focal length
Bi	Biot number
BSDF	Bidirectional scatter distribution function
c	Speed of light in vacuum
C_{p}	Heat capacitance at constant pressure
CoC	Circle of confusion
CVD	Chemical vapor deposition
d_{diff}	Diameter of a diffraction-limited spot
D_{enp}	Diameter of an entrance-pupil
D_{exp}	Diameter of an exit-pupil
D_{img}	Image diameter
D_{in}	Input diameter
D_{lens}	Lens diameter
D_{obj}	Object diameter
D_{opt}	Optics diameter
D_{out}	Output diameter
e	Energy-based unit subscript
E'	Young's modulus
$E_{\text{e,bkg}}$	Background irradiance–energy units
$E_{\text{e,img}}$	Image irradiance–energy units
$E_{\text{p,bkg}}$	Background irradiance–photon units
$E_{\text{p,img}}$	Image irradiance–photon units
E_{source}	Source irradiance
$\mathcal{E}$	Energy of a photon
f	Focal length
f_{eff}	Effective focal length

Glossary of Symbols

f.f.l.	Front focal length
F_B	Back focal point
F_F	Front focal point
F_s	Force
FOR	Field of regard
FOV	Full-angle field of view
$FOV_{half\text{-}angle}$	Half-angle field of view
F/#	F-number
GASIR	Germanium arsenic selenium infrared
h	Planck's constant
$\bar{h}$	Mean coefficient of heat transfer
h_{img}	Image height
h_{obj}	Object height
H	Hardness
HFD	Hyperfocal distance
IDCA	Integrated dewar/detector cooler assembly
k	Conic constant
k	Boltzmann's constant
k'	Thermal conductivity
K_{Ic}	Fracture toughness
k_s	Spring stiffness
L	Radiance
L_{bkg}	Background radiance
L_λ	Spectral radiance
LWIR	Longwave infrared
m_e^*	Effective mass of an electron
M	Exitance
M_{meas}	Measured exitance
M_{obj}	Exitance of an object
M_λ	Spectral exitance
MTF	Modulation transfer function
MWIR	Midwave infrared
$\mathcal{M}$	Magnification
$\mathcal{M}_{ang}$	Angular magnification
n	Refractive index
n_e	Extraordinary refractive index
n_o	Ordinary refractive index
NSA	Nanostructure array
p	Object distance

Glossary of Symbols

p	Photon-based unit subscript
p_m	Momentum of a photon
P_f	Load at fracture
PSD	Power spectral density
PSF	Point spread function
q	Image distance
r	Pupil radius
R	Exit-pupil-to-image distance
R	Resistance
SF	Safety factor
SNR	Signal-to-noise ratio
SR	Strehl-intensity ratio
T	Temperature
T_b	Brightness temperature
T_{bkg}	Background temperature
T_c	Color temperature
T_{curie}	Curie temperature
T_d	Detector temperature
T_{load}	Load temperature
T_{rad}	Radiation temperature
T_{source}	Source temperature
T_{target}	Target temperature
TIS	Total integrated scatter
v	Speed of light in a medium
V	Abbe number
W_{abr}	Aberrated wavefront
W_{PV}	Peak-to-valley wavefront error
W_{ref}	Reference wavefront
WFE	Wavefront error
x_i, y_i	Image coordinates
x_o, y_o	Object coordinates
x_p, y_p	Pupil coordinates
α	Coefficient of absorption
α'	Coefficient of thermal expansion (CTE)
β	Blur angle caused by diffraction
γ	Surface energy density
δ	Depth of field
δ'	Depth of focus
δ_f	Shift in focus

Glossary of Symbols

δ_y	Transverse aberration
δ_z	Longitudinal aberration
ΔT	Temperature difference
ΔW	Optical path difference (OPD)
$\Delta\lambda$	Wavelength interval
ε	Emissivity
ε'	Strain
η	Spatial frequency in the vertical direction
η_{kino}	Diffraction efficiency of kinoforms
θ	Angle variable
θ_{max}	Maximum angle subtense
λ	Subscript indicating a spectral radiometric quantity
λ	Wavelength
λ_{cutoff}	Cutoff wavelength
λ_{cuton}	Cuton wavelength
λ_{max}	Maximum wavelength
$\lambda_{\text{max-cont}}$	Maximum contrast wavelength
λ_o	Fixed wavelength
λ_{peak}	Peak wavelength
ν	Optical frequency
ν'	Poisson ratio
ξ	Spatial frequency in the horizontal direction
ρ	Normalized pupil radius
ρ	Reflectance
ρ'	Material density
ρ_p	Reflectance: p-polarization
ρ_s	Reflectance: s-polarization
σ'	Stress
σ_e	Stefan–Boltzmann constant in energy units
σ_f	Ultimate tensile stress
σ_{max}	Maximum stress
σ_p	Stefan–Boltzmann constant in photon units
σ_{rms}	Surface roughness
τ	Transmittance
τ_{atm}	Atmospheric transmittance
τ_{external}	External transmittance
τ_{int}	Integration time
τ_{internal}	Internal transmittance

Glossary of Symbols

τ_{opt}	Optical transmittance
τ_p	Transmittance: p-polarization
τ_s	Transmittance: s-polarization
φ	Angular aberration
ϕ	Flux
ϕ_{abs}	Absorbed flux
ϕ_{bkg}	Background flux
ϕ_d	Detector flux
ϕ_{img}	Flux incident on an image
ϕ_{inc}	Incident flux
ϕ_{obj}	Flux radiated by an object
ϕ_{sig}	Signal flux
ϕ_{trans}	Transmitted flux
ϕ_λ	Spectral flux
χ	Empirical constant
ω	RMS wavefront error
Ω	Solid angle
Ω_d	Detector solid angle
Ω_{bkg}	Background solid angle
Ω_{enp}	Entrance pupil solid angle
Ω_{exp}	Exit pupil solid angle
Ω_{img}	Image solid angle
Ω_{lens}	Lens solid angle
Ω_{obj}	Object solid angle
Ω_s	Source solid angle

Electromagnetic Spectrum

The **electromagnetic spectrum** is the distribution of **electromagnetic radiation** according to energy, frequency, or wavelength. Electromagnetic radiation can be described as a stream of **photons**, which are particles traveling in a wavelike pattern, moving at the speed of light.

Type of Radiation	Frequency Range	Wavelength Range
Gamma rays	$>3 \times 10^{20}$	<1 fm
X rays	3×10^{17}–3×10^{20}	1 fm–1 nm
Ultraviolet	7.5×10^{14}–3×10^{17}	1 nm–400 nm
Visible	4×10^{14}–7.5×10^{14}	0.4 μm–0.75 μm
Near-infrared	10^{14}–7.5×10^{14}	0.75 μm–3.0 μm
Midwave infrared	5×10^{13}–10^{14}	3.0 μm–6 μm
Longwave infrared	2×10^{13}–5×10^{13}	6.0 μm–15 μm
Extreme infrared	3×10^{11}–2×10^{13}	15 μm–1 mm
Micro- and radio waves	$<3 \times 10^{11}$	>1 mm

Frequencies in the visible and infrared spectral bands are measured in the millions of megahertz, commonly referred to as wavelengths rather than frequencies. Wavelength can be measured interferometrically with great accuracy and is related to the optical frequency by the universal equation

$$c = \lambda \nu$$

where λ is the wavelength, ν is the optical frequency, and c is the speed of light in free space (3×10^8 m/sec).

The difference between the categories of electromagnetic radiation is the amount of energy found in their photons. The energy of a photon is inversely proportional to the wavelength and is given by

$$\mathcal{E} = h\nu = \frac{hc}{\lambda}$$

where h is Planck's constant (6.62×10^{-34} J · sec).

Radio waves have photons with very low energies, while gamma rays are the most energetic of all. The electromagnetic spectrum is classified based on the source, detector, and materials technologies employed in each of the spectral regions.

Infrared Concepts

Infrared-imaging systems are often used to form images of targets under nighttime conditions. The target is seen because of **self-radiation** rather than the reflected radiation from the sun. Self-radiation is a physical property of all objects that are at temperatures above absolute zero (i.e., $0 \text{ K} = -273.15 \text{ °C}$).

In order to make this radiation visible, the infrared system depends on the interaction of several subsystems.
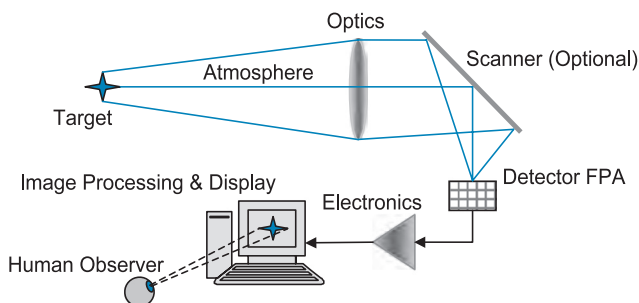
The self-radiation signature is determined by the **temperature** and the surface characteristics of the target. Gases in the atmosphere limit the frequencies at which this radiation is transmitted. The configuration of the optical system defines the **field of view (FOV)**, the **flux collection efficiency**, and the **image quality**. These parameters, along with the detector interface, impact the radiometric accuracy and **resolution** of the resulting image. The detector is a transducer that converts the optical energy into an electrical signal, and electronics amplify this signal to useful levels.

For typical terrestrial and airborne targets, **Planck's equation** dictates that, within the range of temperatures from 300 K to 1000 K, emission of radiation occurs primarily in the infrared spectrum. However, the background is self-luminous as well, causing terrestrial targets to compete with background clusters of similar temperature. Infrared images have much lower **contrast** than corresponding visual images, which have orders of magnitude higher reflectance and emittance differences.

Imaging Concepts

An object is a collection of independent source points, each emitting light rays into all forward directions. When refracted by a lens (i.e., according to Snell's law), rays that diverge from each object point intersect at corresponding image-plane points. The image is built on a point-by-point basis. The power at any image location is proportional to the strength of the corresponding object point, causing a geometrical distribution of power.

The symmetry line that contains the centers of curvature of all optical surfaces is called the **optical axis**. Three ray-trace rules are used to find the image position with respect to the object:

1. Rays entering parallel to the optical axis exit through the back focal point F_B.
2. Rays entering the lens through the front focal point F_F exit parallel to the optical axis.
3. Rays entering through the center (chief rays) of the lens do not change direction.

To determine the image-plane location and size, a thin lens and small-angle or **paraxial approximation** is used, which linearizes the ray-trace equations that determine the ray paths through the optical system (i.e., $\sin \theta \approx \tan \theta \approx \theta$).
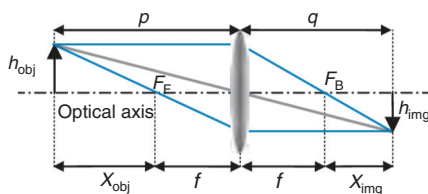
Gaussian lens equation: $\dfrac{1}{f} = \dfrac{1}{p} + \dfrac{1}{q}$

Newtonian lens equation: $x_{\mathrm{obj}}\, x_{\mathrm{img}} = f^2$

A **thin lens** has a thickness that is considered negligible in comparison with its focal length.

Magnification Factors

As the object is placed farther from the front focus of the lens, the image distance gets closer to f ($p \to \infty$, $q \to f$); as the object is placed closer to the front focus of the lens, the image gets farther away ($p \to f$, $q \to \infty$).

The **lateral** or **transverse magnification** of an optical system is given by

$$\mathcal{M} = -\frac{q}{p} = \frac{h_{\text{img}}}{h_{\text{obj}}}$$

By using the Gaussian lens equation, it can be verified that the minimum distance between a real object and its corresponding image is $4f$ (i.e., $p = q = 2f$, in which case $\mathcal{M} = -1$).
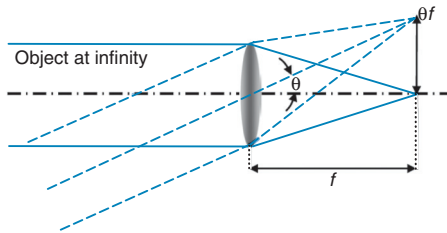
When an off-axis source is located at an infinite distance from the lens, an angle θ [rad] exits between the direction of the collimated rays and the optical axis. The ray focuses at a distance θf away from the optical axis.

Squaring the lateral magnification, the **area** or **longitudinal magnification** is obtained by

$$\mathcal{M}^2 = \frac{A_{\text{img}}}{A_{\text{obj}}} = \left(-\frac{q}{p}\right)^2$$

which is used extensively in radiometric calculations.
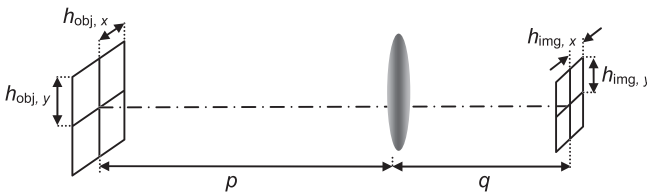
Thick Lenses

When the thickness of a lens cannot be considered negligible, the lens is treated as a thick lens. F_F and F_B are the **front** and **back focal points**, and when these focal points are
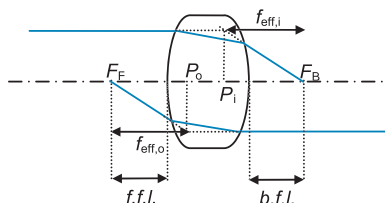
measured from the lens vertices, they define the **front focal length (f.f.l.)** and the **back focal length (b.f.l.)** of the optical element. A diverging ray from F_F emerges parallel to the optical axis, while a parallel incident ray is brought to F_B. In each case, the incident and emerged rays are extended to the point of intersection between the surfaces.

Transverse planes through these intersections are termed the **primary and secondary principal planes** and can lie either inside or outside the lens. Points where these

planes intersect the optical axis are known as the **first and second principal points** P_o and P_i. Incoming and outgoing chief rays that extend until they cross the optical axis locate the **nodal points** N_o and N_i. These six points (two focal, two principal, and two

R_1 and R_2 are the lens radii, and n is the index of refraction of the lens material.

nodal) are named the **cardinal points** of the optical system.

The **effective focal lengths** $f_{eff,o}$ and $f_{eff,i}$ are measured from the foci to their respective principal points and are identical if the medium on each side has the same refractive index:

$$\frac{1}{f_{eff}} = (n-1)\left[\frac{1}{R_1} - \frac{1}{R_2} + \frac{(n-1)t}{n}\frac{1}{R_1 R_2}\right]$$

A rule of thumb for ordinary glass lenses immersed in air is that the separation between the principal points roughly equals one-third of the lens thickness t.

Stops and Pupils

Aperture stop (AS): the physical opening that limits the angle over which the lens accepts rays from the axial object point.

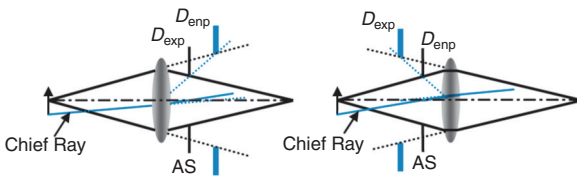**Entrance pupil** D_{enp}: the image of the AS as seen from the axial point on the object plane through the optical elements preceding the stop. If there are no elements between the object and the AS, the latter operates as the entrance pupil.

Exit pupil D_{exp}: the image of the AS as seen from the axial point on the image plane through those optical elements that follow the stop. If there are no elements between the AS and the image, the former serves as the exit pupil.

Axial ray: a ray that starts at the axial object point and ends on the axial image point.

Marginal ray: a special axial ray that starts at the axial object point, goes through the edge of the entrance pupil, and ends on the axial image point. The marginal ray is used to define the *F*/# and the numerical aperture.

Chief ray: a ray that starts at the edge of the object, passes through the center of the entrance pupil, and defines the height of the image.

Telecentric stop: an aperture stop that is located at a focal point of the optical system. It is used to reduce the magnification error in the size of the projected image for a small departure from best focus.

Telecentric system: a system with its entrance or exit pupil located at infinity.

For any point in the object, the amount of radiation accepted by and emitted from the optical system is determined by the sizes and locations of the pupils. The location of the AS is determined by that stop or image of a stop that subtends the smallest angle as seen from the object axial point. An analogous procedure can be carried out from the image plane.

F-number and Numerical Aperture

The **F-number *F*/#** is the parameter used to describe the ratio between the f_{eff} of an optical system and the **diameter** of the entrance pupil. It describes the image-spaced cone for an object at infinity:

$$F/\# \equiv \frac{f_{\text{eff}}}{D_{\text{enp}}}$$
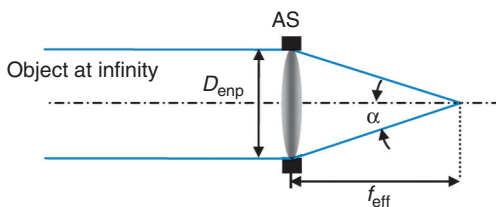
Although the $F/\#$ also exists in image space as q/D_{enp} for finite conjugate systems, the **numerical aperture (NA)** is the parameter that is normally used in these cases.

The refractive index n in air is approximately 1. The numerical aperture is the axial cone of light in terms of the marginal ray angle α and is defined as $\text{NA} \equiv \sin \alpha$.

The NA and the $F/\#$ are related as follows:

$$\text{NA} \equiv \sin\left(\tan^{-1}\frac{1}{2(F/\#)}\right) \quad \text{or} \quad F/\# = \frac{1}{2\tan(\sin^{-1}\text{NA})}$$

Assuming paraxial approximation, $\sin \alpha \approx \alpha$, yielding

$$F/\# \approx \frac{1}{2\text{NA}}$$

Example: If an $F/3$ system has its aperture made larger or smaller by 50% in diameter, what are the new $F/\#$s?

If $D\uparrow \Rightarrow F/\#\downarrow$; $F/\#_{\text{new}} = f_{\text{eff}}/1.5D = 2/3(F/\#) = 2$, resulting in faster optics.

If $D\downarrow \Rightarrow F/\#\uparrow$; $F/\#_{\text{new}} = f_{\text{eff}}/0.5D = 2(F/\#) = 6$, resulting in slower optics.

Field of View

The **field of view (FOV)** is the angular coverage of an optical system. It can be defined either in full or half angles. Using the half-angle principle,

$$\text{FOV}_{\text{half-angle}} = \theta_{1/2} = \left| \tan^{-1} \frac{h_{\text{obj}}}{p} \right| = \left| \tan^{-1} \frac{h_{\text{img}}}{q} \right|$$

The element that limits the size of the object to be imaged is called the **field stop**, which determines the system's FOV. In an infrared camera, it is the edge of the detector array itself that bounds the image plane and serves as the field stop.

For an object at infinity, the full-angle FOV is determined by the ratio between the detector size and the system's focal length:

$$\text{FOV} = \theta = \frac{d}{f}$$

The detector has a **footprint**, the image of the detector projected onto the object plane. The footprint defines the area of the object that contributes flux onto the detector. Given the focal length and size of the detector, the resolution element at the object plane can be determined.

A smaller FOV is attained by increasing the focal length, causing an increment in the **magnification**; a shorter focal length widens the FOV but decreases the magnification.

The *F*/# and FOV are inversely proportional and are affected by both **flux transfer** and **optical aberra-**

tions. There is a tradeoff between the amount of light that reaches the detector and the **image quality**. A system with a small *F*/# and large FOV has high flux-transfer efficiency, but the image quality worsens. A large *F*/# and small FOV restrict the system's flux, but the quality of the image is improved.
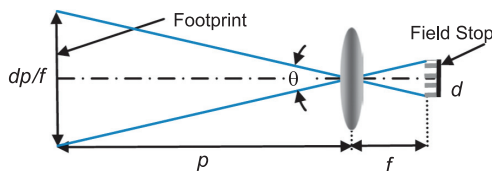
Depth of Focus and Depth of Field

If an optical system is to be used over a range of object distances, it might be necessary to include a mechanical device for changing the focus. For example, the secondary mirror of a two-mirror afocal telescope must be displaced along the optical axis to focus the image on the detector as a function of range. The amount of focusing motion required is found by using the Newtonian lens equation. Hence, for object distances ranging from infinity to 1 km with optics having an EFL of 30 cm, the image will move

$$x_{\text{img}} = \frac{(\text{EFL})^2}{x_{\text{obj}}} = \frac{(30)^2}{10^4} = 90\,\mu\text{m}$$

The **depth of focus** is the extent of the region around the detector plane in which the image is still considered to be in focus. The limits are established by the largest diameter circular spot we are willing to tolerate on our detector system [i.e., the circle of confusion (CoC)]. The depth of focus can be calculated by

$$\delta' = \pm 2\lambda(F/\#)^2$$

The change in object distance that shifts the image by a distance equal to the depth of focus is called the **depth of field**, which can be found by combining the depth of focus and the Newtonian lens equations:

$$\delta = \pm \frac{(\text{EFL})^2}{2\lambda(F/\#)^2} = \pm \frac{D_{\text{enp}}^2}{2\lambda}$$

The depth of field δ and depth of focus δ' are related by the longitudinal magnification of the optical system such that

$$\delta' = \mathcal{M}^2\delta$$

Hyperfocal Distance
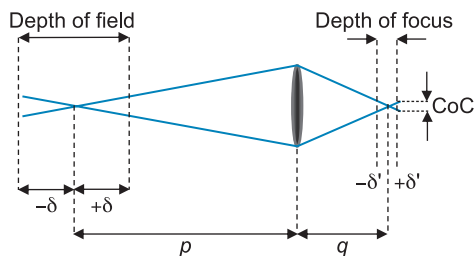
Both depth of field and depth of focus are strongly dependent on changes in the system's aperture and working distance.

For an optical system focused at infinity, the depth of field extends from infinity inward to a finite distance called the **hyperfocal distance (HFD)**. This distance is entirely dependent on whatever level of sharpness is considered to be acceptable. The criterion for the desired acceptable sharpness is identified through the circle of confusion (CoC) limit. Targets that are beyond the hyperfocal distance will require active focusing.

The hyperfocal distance is illustrated in the figure. When the optical system is focused at the hyperfocal distance, p_f becomes infinity, and p_n becomes one-half of the hyperspectral distance. Thus, the image on the detector will appear sharp from p_n to infinity.
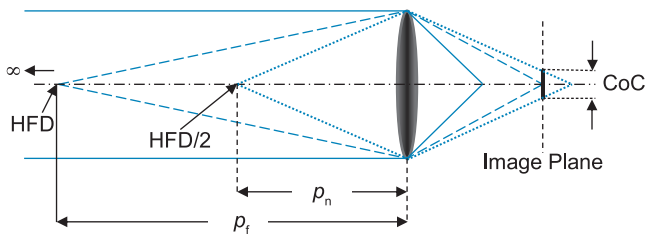
The hyperfocal distance is defined as

$$\text{HFD} = \frac{\text{EFL}(\text{EFL} + 1)}{(F/\#) \cdot \text{CoC}} \cong \frac{(\text{EFL})^2}{(F/\#) \cdot \text{CoC}}$$

> **Example**: Using a circle of confusion of 20 µm, what is the hyperfocal distance of an *F*/2.5 optical system with a 100-mm focal length lens?
>
> $$\text{HFD} = \frac{0.1^2}{2.5 \cdot 20 \times 10^{-6}} = 200 \text{ m}$$
>
> Therefore, any target positioned from 100 m to infinity will have sharp imagery.

Combination of Lenses

Consider two lenses separated by a distance d.

The f_{eff} of this optical system is given by the expression

$$\frac{1}{f_{\text{eff}}} = \frac{1}{f_1} + \frac{1}{f_2} - \frac{d}{f_1 f_2}$$
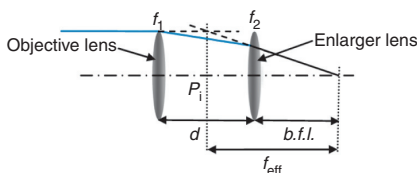
where f_1 and f_2 are the focal lengths of the **objective** and **enlarger lenses**, respectively. An enlarger lens has the ability to move back and forth along the optical axis. The back focal length is the distance from the last surface of the enlarger lens to the focal plane of the system and is given by

$$b.f.l. = \frac{f_2(d - f_1)}{d - (f_1 + f_2)}$$

When the two lenses are placed in contact (i.e., $d \to 0$), the combination acts as a single lens, yielding

$$\frac{1}{f_{\text{eff}}} = \frac{1}{f_1} + \frac{1}{f_2}$$

A special configuration of the two-lens combination system is the so-called relay lens pair. In this case, a source is placed at the front focal point of the optical system; the objective lens projects this source to infinity, and the source is then imaged by the enlarger lens.
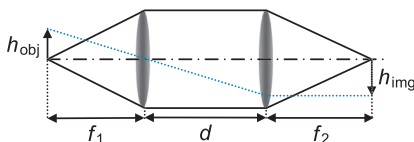
$$\mathcal{M} = \frac{h_{\text{img}}}{h_{\text{obj}}} = -\frac{f_2}{f_1}$$

The separation of the lenses affects the location of the principal planes and thereby affects the effective focal length of the system. Furthermore, as the lenses move apart, the size the detector lens must be increased to avoid vignetting.

Afocal Systems and Refractive Telescopes

Afocal systems do not have focal lengths. Telescopes are afocal systems with their object and image located at infinity. Their primary function is to enlarge the apparent size of a distant object. There are three main types of refractive telescopes, as defined below.

Astronomical (or **Keplerian**) **telescopes** comprise two convergent lenses spaced by the sum of their focal lengths. The objective is usually an achromatic doublet forming a real invert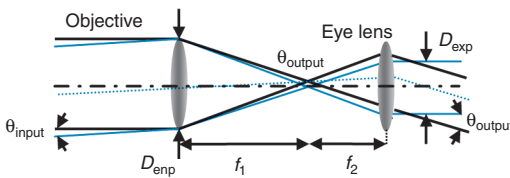ed and reverted image at its focal point; the eye lens then reimages the object at infinity, where it may be erected by the use of an auxiliary lens. The aperture stop and the entrance pupil are located at the objective to minimize its size and cost.

Galilean telescopes comprise a positive objective and a negative eye lens, where spacing is the difference between the absolute values of the focal lengths since f_2 is negative. There is no real internal image, and a reticle or crosshair
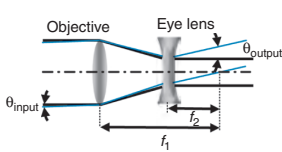
cannot be introduced into the optical system. The final image is erect. The aperture stop is usually the pupil of the viewer's eye, which is also the exit pupil.

Terrestrial (or **erecting**) **telescopes** are astronomical telescopes with an erecting system inserted between the eye lens and objective so that the final image is erected.

The **angular magnification** of these afocal systems is given by the ratio between the angle subtended by the image and the angle subtended by the object:

$$\mathcal{M}_{\text{angular}} = \frac{\theta_{\text{output}}}{\theta_{\text{input}}} = \left| \frac{f_2}{f_1} \right|$$

Afocal Reflective Telescopes

Reflective telescopes do not suffer from chromatic aberrations because the law of reflection is independent of wavelength. Fewer optical elements are typically required for equivalent optical performance, which leads to a lower number of tolerances in both fabrication and alignment. The overall package size and element mass can be effectively reduced because reflective systems naturally fold around themselves. **Afocal reflective telescopes** are limited in field angle and usually require tight tolerances.

The Mersenne afocal telescope is a two-mirror (primary and secondary) combination of confocal parabolas (i.e., the mirrors share their foci), which are utterly corrected for all orders of spherical aberration. An eccentric pupil (off-axis) can be considered as an aperture stop that has been moved perpendicular to the optical axis, thus creating an unobscured clear aperture in an otherwise obscured reflector.
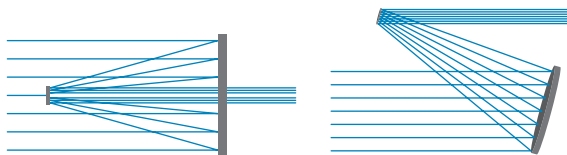
The **three-mirror anastigmat** (TMA) is a mirror system corrected for spherical aberration, coma, and astigmatism. It is primarily used to enable wider FOVs than possible with just two mirrors. The standard three-mirror sequence is parabola/hyperbola/parabola.
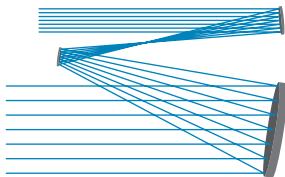
When the TMA consists of two-mirror objectives and a one-mirror relay, the alternative TMA (ATMA) comprises a one-mirror objective and a two-mirror relay. This difference allows the ATMA to operate over a larger ($\approx 50\%$) FOV, but at a lower pupil magnification (≈ 2–$3\times$). Typical surface curves are parabola/hyperbola/parabola but can vary.

Cold-Stop Efficiency and Field Stop

To reduce **thermal noise**, infrared photon detectors are cooled to **cryogenic temperatures**. The detector is housed in a vacuum bottle called a **dewar**. An aperture stop is adjacent to the detector plane, which prevents **stray radiation** from reaching the detector. This **cold shield** is located inside the evacuated dewar and limits the angle over which the detector receives radiation.

The **cold-stop efficiency** is the percentage of the total scene source power reaching the detector. The perfect **cold stop** is defined as one that limits the reception of background radiation to the cone established by the $F/\#$ (i.e., 100% cold-stop efficiency). This is achieved when the cold shield is located at the aperture stop of the optical system (i.e., $F/\#_{optics} = F/\#_{cold\ shield}$).
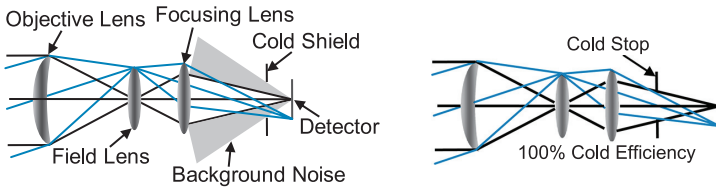
The FOV of an optical system may be increased without increasing the diameter of the detector lens by placing a **field lens** at the internal image of the system. This lens redirects ray bundles (that would otherwise miss the detector) back toward the optical axis. The insertion of this lens has no effect on the system's magnification. This arrangement is good for flux-collection systems (i.e., search systems), but not for imaging systems since the object is not imaged onto the detector, but rather into the field lens.

If the field lens is moved to the detector plane, it becomes an **immersion lens**, and the numerical aperture is increased by a factor of the **index of refraction** of the lens material, without modifying the characteristics of the system. This configuration allows the object to be imaged onto the detector array.
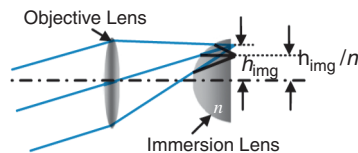
The Warm Shield Concept

In order to reduce the dewar mass and the power needed to cool the overall **integrated detector cooler assembly (IDCA)**, the aperture stop of the optical system needs to be close to the detector. The proximity of the aperture stop to the detector **infrared focal plane array (IRFPA)** is a huge constraint in the effort to reduce off-axis aberrations during the design/optimization of the optical system, and it also increases the size/mass of the optics.
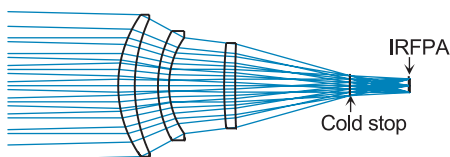
The infrared lens system shown below has the same optical specifications as the triplet above. The difference is that the aperture stop has been moved away from the IRFPA, while the aperture of the cold shield has remained in its original position but has been made larger to avoid vignetting. In this case, the IRFPA would see not only the scene radiation but also the background radiation seen within angle θ.
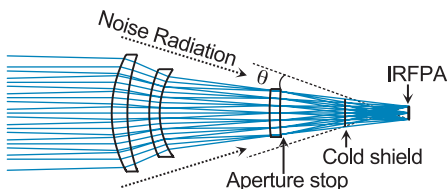
The solution to eliminate the noise radiation seen by the detector through angle θ is adding a **warm shield**. The warm shield is a highly reflective low-emissivity coating surface that reflects photons outside the aperture stop to the cold space.
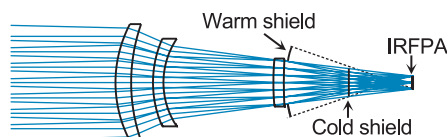
The Warm Shield Concept (cont.)

A warm shield is designed to reflectively block any outside single-bounce rays from reaching the focal plane directly. Scattering effects from the warm shield reflecting surface must be minimized as well. One or more warm shields in series can completely eliminate single-bounce paths to the IRFPA. Aggressive **warm-shielded imagers** are a generic way of producing optical designs that have less optical aberration, a reduction in the size/mass of the optics due to an increase in the *F*/# of the optics with respect to the *F*/# of the cold shield, and better system transmittance through fewer components. Moving the aperture stop away from the detector plane also reduces cosine-fourth law effects, thus improving illumination uniformity.

A complete warm shield eliminates the cold shield used in the current standard photon detector technology, thus producing extremely low **size, weight, and power (SWaP)** infrared sensor devices. In a 100% warm-shielded system, all of the rays from the focal plane emitted into a hemi-sphere need to be returned to the cold focal plane. A hemispheric warm shield structure located at the detector plane accomplishes this task. A hemisphere images a point back on the same plane on the opposite side of the center of curvature of the sphere. If the center of curvature of the sphere is in the middle of the focal plane, all of the light comes back to the cryogenically cooled detector IRFPA.

Hemispheric Warm Shield →

← IRFPA
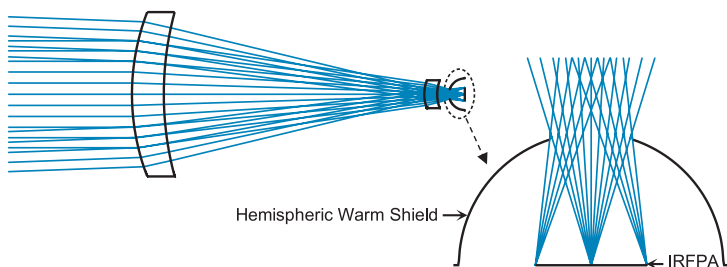
Warm shields are geometry dependent and are unique for each optical design. **Stray light analysis** is critical to optimize the efficiency of warm-shielding systems.

Image Quality

The assumption thus far has been that all points in object space are mapped to points in image space. However, more detailed information such as the size of the image and its energy distribution is required to properly design an optical system. Due to effects of **diffraction** and **optical aberrations**, point sources in the object are seen in the image as **blur spots**, producing a blurred image.

Point Source

p q d_{diff}

Better quality is achieved for smaller blur spots.
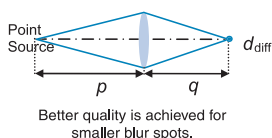
Diffraction is a consequence of the wave nature of radiant energy. It is a physical limitation of the optical system over which there is no control. On the other hand, optical aberrations are image defects that arise due to the deviation from of the paraxial approximation; therefore, they can be controlled through proper design.

Even in the absence of optical aberrations, diffraction phenomena still cause a point to be imaged as a blur circle. Such an optical system is said to be **diffraction limited** and represents the best in optical performance.

The diffraction pattern of a point source appears as a bright central disk surrounded by several alternative bright and dark rings. The central disk is called the Airy disk and contains 84% of the total flux.

Spot profile [W/cm^2]

$\rho = \dfrac{\text{radial distance}}{\lambda(F/\#)}$

$2.44\lambda(F/\#)$

1.22
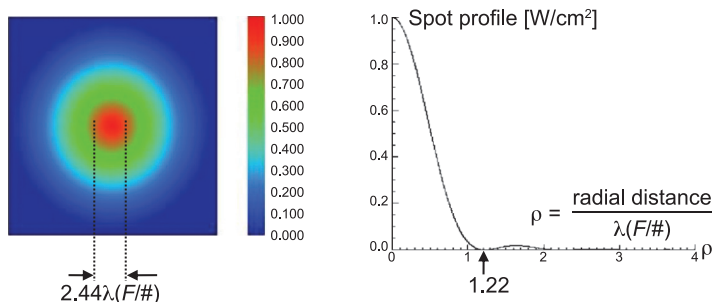
The linear diameter of the diffraction-limited blur spot is given by

$$d_{\text{diff}} = 2.44\lambda(F/\#)$$

Image Quality (cont.)

The effects of diffraction may also be expressed in angular terms. The **full-angular blur** β is the diameter of the diffraction spot divided by f_{eff}, yielding

$$\beta = 2.44 \cdot \frac{\lambda}{D}$$

It can also be defined as the angular subtense of the minimum resolution feature in the object space viewed from the entrance pupil.
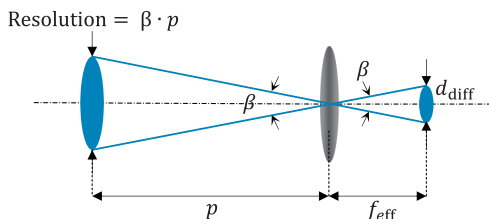
> The size of the blur spot depends on the *F*/# and the spectral band in which the imaging system operates.

Low-*F*/# systems have the smallest diffraction-limited spot sizes, and thus have the best potential performance. However, the aberration effects generally become worse as the *F*/# decreases. Therefore, low-*F*/# systems are harder to correct to diffraction-limited performance. Alternatively, longer-wavelength systems have larger diffraction spots and are easier to correct to a diffraction-limited level of performance compared to shorter-wavelength systems.

For example, an *F*/1 diffraction-limited system operating at 10 μm forms a spot diameter of 24.4 μm. The same system operating at *F*/7 forms a spot diameter of 170.8 μm. The same *F*/1 system operating in the visible spectrum at 0.5 μm forms a spot diameter of 1.22 μm, while the *F*/7 system produces a diffraction spot of 8.5 μm in diameter.

There are additional criteria that can be used to determine the aberration-related quality of an optical system (e.g., wavefront error, peak-diffraction intensity or Strehl ratio, as well as the modulation transfer function).

Understanding Optical Aberrations

Departures from the idealized conditions of paraxial conditions are known as **optical aberrations**. These aberrations depend on the refractive index and dispersive effects of the optical materials and on the geometrical arrangement of the optical surfaces. There are two main groups of aberrations, monochromatic and chromatic. The former can be divided into two subcategories: (1) aberrations that deteriorate the image, making it blurred (e.g., spherical, coma, and astigmatism) and (2) aberrations that distort the image, such as Petzval curvature and distortion. The latter takes place in polychromatic images, in which each color of light transverses a system along different optical paths. An expansion of the Maclaurin theorem yields

$$\sin \theta = \theta - \frac{\theta^3}{3!} + \frac{\theta^5}{5!} - \frac{\theta^7}{7!} + \frac{\theta^9}{9!} + \ \cdots$$

where, for paraxial angles or first-order approximation, $\sin \theta = \theta$. If the first two terms of the expansion are retained, we obtain the so-called third-order theory of aberrations. When the higher terms are included, we proceed to fifth-order aberrations, seventh-order aberrations, and so on. The effect of the higher-order aberrations diminishes as a function of the exponent; therefore, in most cases, the third-order contributions yield a fair estimate of system performance. Even for complex optical systems where higher orders are required to fully describe the overall correction of an optical system, the third-order approximation may dictate what design parameters should be modified to achieve full performance.

The **wavefront** is a surface over which an optical wave has a constant phase. The direction of propagation of the wave is at all times normal to the surface of the wavefront at each point. The **meridional** or **tangential plane** is in the direction of the optical axis. The plane perpendicular to the meridional plane is known as the **sagittal plane**. In a symmetrical optical system, **skew rays** are neither parallel nor do they intersect the optical axis. Skew rays are rays that are not meridional.

Wavefront and Transverse Ray Aberrations
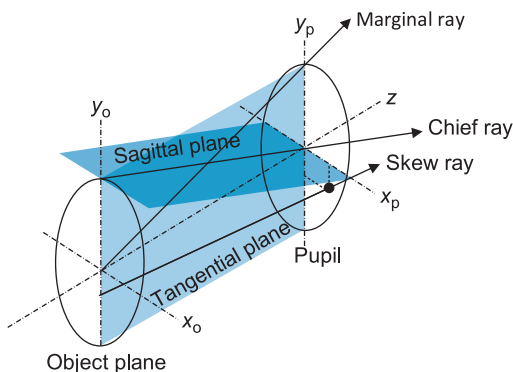
The **optical path difference (OPD)** is defined as the difference between a real **aberrated wavefront** W_{abr} and an ideal **reference wavefront** W_{ref}. The latter is usually designated as the near best fit of the aberrated wavefront, and its radius is centered on the image plane. The departure of the actual wavefront W_{abr} from its ideal shape W_{ref} is a measure of the **wavefront error (WFE)** of the system. The chief ray intersection with the image plane is called the **geometrical image point**. If the aberrated wavefront trails behind the reference ideal wavefront, the OPD is negative, and vice versa.
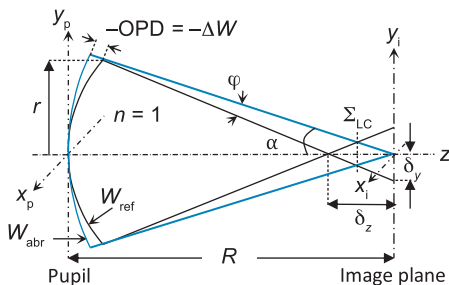
The OPD is a rather small quantity; therefore, the **angular aberration** φ can be defined as the change in wavefront ΔW with respect to a change in height:

$$\varphi = -\frac{\partial \Delta W}{\partial y_p}$$

Wavefront and Seidel Aberrations

The distance between the two focal distances is known as the **longitudinal aberration** δ_z, and the intercept of the axial ray with the image plane is called **transverse** or **lateral aberration** δ_y. It is often useful to express the aberrations as a function of the normalized exit pupil coordinates at the edge of the pupil (marginal ray). The relationships between the ray intercept errors and the WFE along the pupil coordinates x_p and y_p are written as

$$\delta_x = -\frac{R}{r} \cdot \frac{\partial \Delta W}{\partial x_p} \quad \text{and} \quad \delta_y = -\frac{R}{r} \cdot \frac{\partial \Delta W}{\partial y_p}$$

where R is the exit pupil-to-image distance, and r is the geometrical pupil radius.

Consider an optical system with absolute rotational symmetry about the optical axis. Assume that a meridional ray from an object point (x_o, y_o) propagates through a normalized polar pupil point (ρ, θ) and intersects the image surface at (x_i, y_i). The selected object point is at $(0, h)$, where h is the normalized field position.

$$x_p = \rho \cdot \sin\theta$$
$$y_p = \rho \cdot \cos\theta$$
$$\rho^2 = x_p^2 + y_p^2 \text{ and } \theta = \tan^{-1}(x_p / y_p)$$
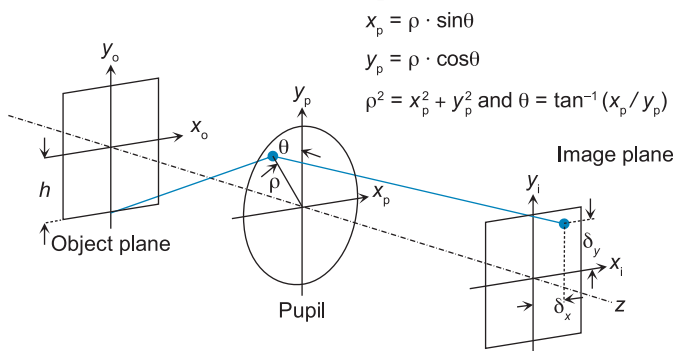
The condition of symmetry is satisfied if ΔW does not change when the meridional plane is rotated about the optical axis. This requirement is met if ΔW is a function of h^2, ρ^2, and $h\rho \cos\theta$. The wavefront error can then be specified as a power series of the form

$$\Delta W(h^2, \rho^2, h\rho \cos\theta) = \sum_{i,j,k} a_{lmn} h^l \rho^m \cos^n \theta$$

where $l = 2i + k$, $m = 2j + k$, and $n = k$.

Wavefront and Seidel Aberrations (cont.)

Due to symmetry, certain coefficients are excluded from the polynomial:

$$\Delta W(h, \rho, \theta) = a_{020}\rho^2 + a_{111}h\rho\cos\theta + a_{040}\rho^4 + a_{131}h\rho^3\cos\theta$$

$$+ a_{222}h^2\rho^2\cos^2\theta + a_{220}h^2\rho^2 + a_{311}h^3\rho\cos\theta + \cdots +$$

Furthermore, inherent third-order aberrations in the performance of the system with spherical surfaces can be written as five sums, S_1 to S_5, referred to as the Seidel sums. Each sum represents one of the five primary third-order defects: S_1 = spherical, S_2 = coma, S_3 = astigmatism S_4 = field curvature, and S_5 = distortion. The wavefront associated with the Seidel coefficients is given by

$$\Delta W(h, \rho, \theta) = \frac{1}{8}S_1\rho^4 + \frac{1}{2}S_2h\rho^3\cos\theta + \frac{1}{2}S_3h^2\rho^2\cos^2\theta$$

$$+ \frac{1}{4}(S_3 + S_4)h^2\rho^2 + \frac{1}{2}S_5h^3\rho\cos\theta$$

The wavefront and Seidel coefficients are summarized in the following table.

i	j	k	l	m	n	Wavefront Coefficient	Seidel Coefficient	Expansion Terms	Aberration
0	1	0	0	2	0	a_{020}		ρ^2	Focal Shift
0	0	1	1	1	1	a_{111}	N/A	$h\rho\cos\theta$	Tilt
1	0	0	2	0	0	a_{200}		h^2	Piston
							Third Order		
0	2	0	0	4	0	a_{040}	$S_1/8$	ρ^4	Spherical
0	1	1	1	3	1	a_{131}	$S_2/2$	$h\rho^3\cos\theta$	Coma
0	0	2	2	2	2	a_{222}	$S_3/2$	$h^2\rho^2\cos\theta$	Astigmatism
1	1	0	2	2	0	a_{220}	$(S_3 + S_4)/4$	$h^2\rho^2$	Field Curvature
1	0	1	3	1	1	a_{311}	$S_5/2$	$h^3\rho\cos\theta$	Distortion
							Fifth Order		
0	3	0	0	6	0	a_{060}		ρ^6	Spherical
0	2	1	1	5	1	a_{151}		$h\rho^5\cos\theta$	Linear Coma
1	0	2	4	2	2	a_{422}		$h^4\rho^2\cos^2\theta$	Astigmatism
2	1	0	4	2	0	a_{420}		$h^4\rho^2$	Field Curvature
2	0	1	5	1	1	a_{511}	N/A	$h^5\rho\cos\theta$	Distortion
1	2	0	2	4	0	a_{240}		$h^2\rho^4$	Sagittal SA
0	1	2	2	4	2	a_{242}		$h^2\rho^4\cos^2\theta$	Tangential SA
1	1	1	3	3	1	a_{331}		$h^3\rho^3\cos\theta$	Cubic Coma
0	0	3	3	3	3	a_{333}		$h^3\rho^4\cos^3\theta$	Linear Coma
						Higher Orders...			

Spherical Aberration

Spherical aberration (SA) corresponds to a dependence of focal length on aperture for nonparaxial rays. For optical components with spherical surfaces, collimated rays at different heights from the optical axis fail to converge at the same point.
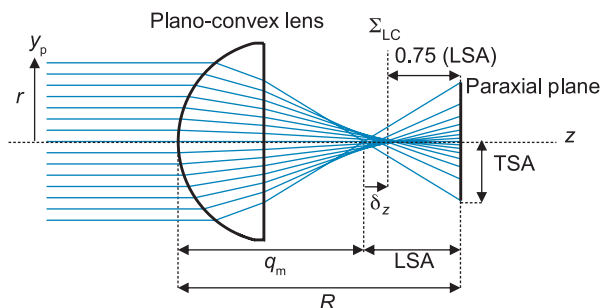

The distance between the marginal and paraxial planes is known as the **longitudinal spherical aberration (LSA)**, and the intercept of the marginal ray with the paraxial plane is called **transverse spherical aberration (TSA)**:

$$\text{LSA} = R - q_{\mathrm{m}} \quad \text{and} \quad \text{TSA} = (\text{LSA})\tan\alpha$$

Notice that the TSA corresponds to the transverse ray aberration equations stated previously:

$$\delta_x = -\frac{R}{r} \cdot \frac{\partial}{\partial x_{\mathrm{p}}} a_{040}(x_{\mathrm{p}}^2 + y_{\mathrm{p}}^2)^2 = -\frac{4R}{r} a_{040} x_{\mathrm{p}}(x_{\mathrm{p}}^2 + y_{\mathrm{p}}^2)$$

$$\delta_y = -\frac{R}{r} \cdot \frac{\partial}{\partial y_{\mathrm{p}}} a_{040}(x_{\mathrm{p}}^2 + y_{\mathrm{p}}^2)^2 = -\frac{4R}{r} a_{040} y_{\mathrm{p}}(x_{\mathrm{p}}^2 + y_{\mathrm{p}}^2)$$

or in polar coordinates, $\delta_{\mathrm{r}} \equiv \delta_x = \delta_y = -\dfrac{4R}{r} a_{040}\rho^3$

When aberrations are present in an optical system, a judicious shift in focal plane can considerably improve the image quality by introducing the appropriate amount of δ_z to balance the wavefront error. In this case, the combined aberrated wavefront is given by

$$\Delta W_{\mathrm{comb}} = a_{040}\rho^4 + a_{020}\rho^2$$

Spherical Aberration (cont.)

The combined ray intercept error can then be written as

$$\delta_y = -\frac{R}{r}(4a_{040}\rho^3 + 2a_{020}\rho)$$

Referring to the transverse ray aberration diagram (page 20), it can be seen that the defocus δ_z is related to the transverse aberration δ_y by

$$\frac{\delta_z}{\delta_y} = \frac{R - \delta_z}{r}$$

Since $R \gg \delta_z$, the longitudinal shift is approximately

$$\delta_z \approx \frac{R}{r}\delta_y = -\frac{R^2}{r^2}(4a_{040} + 2a_{020})$$

where the pupil coordinates have been normalized such that $\rho = 1$ at the edge of the pupil. Assuming that the optical system is free of spherical aberrations (i.e., $a_{040} = 0$), the focal shift is given by

$$\delta_z = -8(F/\#)^2 a_{020}$$

where $F/\# = R/2r$. If we use the **Rayleigh criterion limit** (i.e., $a_{020} = \lambda/4$), the standard equation for the depth of focus is obtained:

$$\delta_z \equiv \delta_f = \pm\frac{\lambda}{2\sin^2\alpha} = \pm 2\lambda(F/\#)^2$$

At the marginal focus $a_{020} = 0$, the focal shift becomes

$$\delta_z = -16(F/\#)^2 a_{040} = \text{LSA}$$

The aberrated spot is minimized if the marginal plane is moved to the position labeled Σ_{LC}, where the marginal ray crosses the caustic. This spot is known as the circle of least confusion and is, in most cases, the best location at which to observe the image. At this particular spot, the resulting aberrated wavefront is given by

$$\Delta W_{\text{comb}} = a_{040}(\rho^4 - 1.5\rho^2)$$

which occurs when the focal shift is $\delta_z = 0.75(\text{LSA})$. At midfocus $a_{020} = -a_{040}$, the focal shift is $\delta_z = 0.5(\text{LSA})$.

Raytracing software offers a number of plots for analyzing the aberrations and performance of an optical system.

Coma

Aberration curves can be stated in terms of the ray intercept errors or the OPD. **Transverse ray fans (TRFs)** and OPD curves are plotted as a function of the relative height of the ray in the entrance pupil.

Transverse ray fan and OPD curves for undercorrected SA of the plano-convex lens.
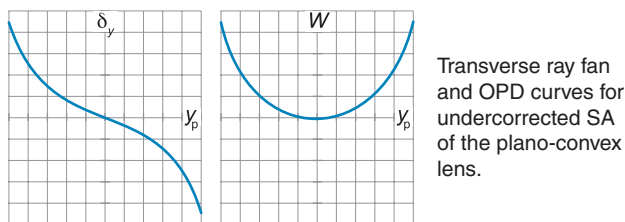
Transverse spherical aberrations are cubic functions; therefore, they have typical s-shaped curves. The OPD plot represents the area under a ray intercept plot and is rather convenient for near-diffraction-limited systems.

The shapes of the intercept curves are useful in establishing the types of aberrations present in an optical system as well as the amount of image blur. Spherical aberrations in optical systems can be corrected by splitting the power of a single lens into multiple lenses, employing materials with higher indices of refraction, varying the size of the pupil aperture, or modifying some of the optical surfaces to be aspheric.

Coma or **comatic aberration** is an off-axis aberration that causes a field point in object space to appear as a comet-like blur in image space. Marginal rays traversing an optical component are imaged at a different height than paraxial rays passing through it. Thus, it appears that the magnification varies as a function of the position of the entrance pupil. An optical component with substantial coma produces a sharp image in the center of the field, but becomes gradually blurred toward the edges. When the marginal rays focus farther from the optical axis, the coma is said to be positive; conversely, negative coma happens when the smallest magnification is associated with the marginal rays.

For coma, different points on the pupil are mapped into circles at the image plane, as illustrated on the next page.

Coma (cont.)
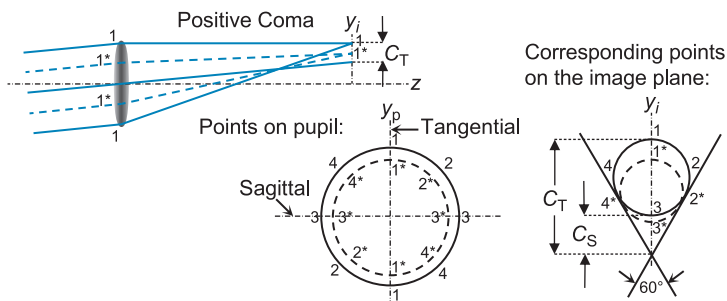
The ray intercept errors for coma are given by

$$\delta_x = -\frac{2R}{r}a_{131}hx_p y_p = -\frac{R}{r}a_{131}h\rho^2\sin 2\theta$$

$$\delta_y = -\frac{R}{r}a_{131}h\rho^2(2+\cos 2\theta)$$

which show that $C_T = 3C_S$, and 55% of the energy in the coma patch is concentrated in C_S. Coma does not have a longitudinal measure.

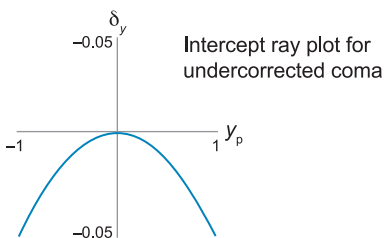The **optical sine theorem** is defined as

$$n_o y_o \sin\alpha_o = n_i y_i \sin\alpha_i$$

where the subscripts o and i indicate object and image space, respectively.

A necessary criterion for the absence of comatic aberration is that the marginal and paraxial magnifications are equal. This statement is correct if the **sine condition** is met:

$$\frac{\sin\alpha_o}{\sin\alpha_i} = \frac{\alpha_o}{\alpha_i} = \text{constant}$$

Intercept ray plot for undercorrected coma

Coma may be eliminated by placing a stop on the proper location within the optical system.

An optical system free of both spherical aberrations and coma is said to be **aplanatic**.

Astigmatism and Field Curvature

Astigmatism is referred to as the third Seidel sum that causes the sagittal and tangential rays to propagate and focus at different distances along the chief ray axis. The extent of the aberrated wavefront depends on the square of the field angle. Astigmatism also occurs in non–rotationally symmetric optical systems due to the misalignment of optical components, or when presumably perfect spherical surfaces are fabricated slightly cylindrically.

Positive astigmatism
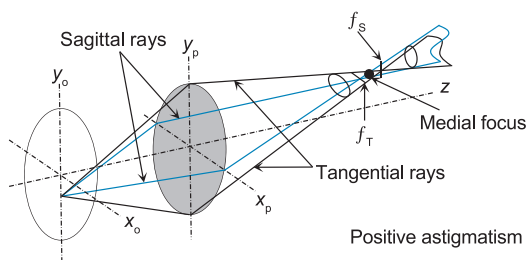
Field (or **Petzval**) **curvature** has the same pupil dependence as defocus, but it also depends on the square of the field height. Field curvature is fundamentally the longitudinal departure from the focal plane that causes a planar object to be projected as a curved nonplanar image. The center of the field appears to be in sharp focus, while the edges seem rather blurred.
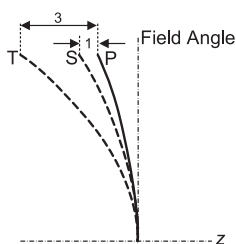
Astigmatism and field curvature are closely related and can be estimated from field plots that display these aberrations over the entire field. When no astigmatism is present in the optical system, the tangential and sagittal surfaces lie on the Petzval curvature surface.

Astigmatism, Petzval, and focal shift interrelate with each other. The resulting aberrated wavefront comprises two different radii of curvature along the tangential and sagittal planes. Across the tangential plane ($\theta = 0$), the WFE is given by

$$\Delta W_T = a_{020}\rho^2 + h^2\rho^2(a_{222} + a_{220})$$

Astigmatism and Field Curvature (cont.)

Forcing $a_{222} = -a_{220} \Rightarrow \Delta W_\text{T} = a_{020}\rho^2$. The WFE at the sagittal plane takes the form

$$\Delta W_\text{S} = a_{020}\rho^2 + h^2\rho^2(a_{222}\cos\theta + a_{220})$$

Therefore, the cumulative ray intercept errors are calculated as

$$\delta_x = -\frac{R}{r}\cdot\frac{\partial\Delta W}{\partial x_\text{p}} = -\frac{2R}{r}(a_{220} + a_{020}h^2)\rho\sin\theta$$

$$\delta_y = -\frac{R}{r}\cdot\frac{\partial\Delta W}{\partial y_\text{p}} = -\frac{2R}{r}\left[a_{020} + (a_{222} + a_{220})h^2\right]\rho\cos\theta$$

With positive astigmatism, the cross-section of the aberrated wavefront gradually becomes elliptical with the major axis in the sagittal plane until it forms a line image at the **tangential focus** f_T. As the wavefront propagates farther, it again deforms into a line at the **sagittal focus** f_S. The best image occurs at the **medial focus**, which is located halfway between the two astigmatic foci, and must satisfy the condition $a_{020} = -(a_{222}/2 + a_{220})h^2$. In this case, the ray intercept errors are reduced to

$$\delta_x = -\frac{2R}{r}a_{222}h^2\rho\sin\theta, \quad \delta_y = -\frac{2R}{r}a_{222}h^2\rho\cos\theta$$

$$\delta_\text{r} = \sqrt{\delta_x^2 + \delta_y^2} = -\frac{2R}{r}a_{222}h^2\rho$$

The longitudinal displacement at the medial focus is

$$\delta_z = -\frac{2R}{r}a_{222}h^2 = -4(F/\#)^2 a_{222}h^2$$

The longitudinal displacement at the tangential focus is $\delta_z = -8(F/\#)^2 a_{222}h^2$, and at the sagittal focus, $\delta_z = 0$.
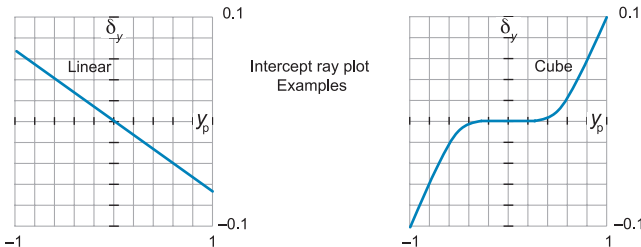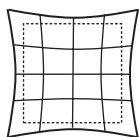
Distortion

Distortion is the last Seidel aberration and occurs when the transverse magnification is a function of the off-axis image distance. The transverse ray errors are given by

$$\delta_y = -\frac{R}{r}a_{311}h^3 \quad \text{and} \quad \delta_x = 0$$

Since distortion is independent of ρ, it does not affect the image quality. In the absence of any of the other Seidel sums, this aberration manifests as a misshaping of the entire image.

Positive or **pincushion distortion** occurs when the magnification increases with the axial distance; each point of the image is pulled radially outward from the optical axis.

Negative or **barrel distortion** occurs when the magnification decreases with the axial distance; each point of the image is pushed radially inward to the optical axis.
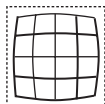
Distortion interacts with tilt such that the combined wavefront error can be written as

$$\Delta W = (a_{111}h + a_{311}h^3)y_{\text{p}}$$

When $a_{111} = -a_{311}h^2$, the wavefront error is nullified.

Distortion is minimized by the proper positioning of the aperture stop in the system. There is no distortion when the incoming and outgoing segments of the chief ray are parallel (i.e., in an orthoscopic system).

The percentage of distortion is plotted as a function of the field angle.
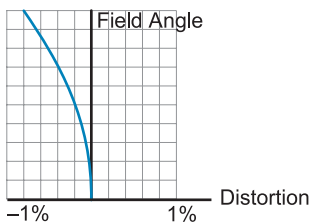
Diffraction of the Aberrated Wavefront

The diffraction pattern of an aberrated wavefront converging into a focal point can be evaluated using scalar diffraction theory. The optical system is assumed to be illuminated with a uniform monochromatic plane wavefront of radiant flux φ. The irradiance distribution or **point spread function (PSF)** of the aberrated wavefront at the image plane is given by

$$E(\xi, \eta) = \frac{A_{\mathrm{p}}\phi}{\lambda^2 f_{\mathrm{eff}}^2}\left| \int\int e^{-j2\pi\Delta W(x_{\mathrm{p}}, y_{\mathrm{p}})}e^{-j2\pi(\xi x_{\mathrm{p}} + \eta y_{\mathrm{p}})}dx_{\mathrm{p}}dy_{\mathrm{p}}\right|^2$$

where A_{p} is the area of the pupil, and f_{eff} is the effective focal length of the optical system. The wavefront error ΔW, conveyed in units of wavelength, is revealed as a phase factor in the pupil of the system. This integral is simply the Fourier transform of the aberrated aperture distribution evaluated at spatial frequency coordinates $\xi = x_{\mathrm{i}}/\lambda f_{\mathrm{eff}}$ and $\eta = y_{\mathrm{i}}/\lambda f_{\mathrm{eff}}$. In most cases, this integral is computed using **fast Fourier transform (FFT)** algorithms.

The irradiance distribution in the image plane for a circular pupil can be written as

$$E(\xi_{\mathrm{r}}, \theta_{\mathrm{i}}) = \frac{\pi\phi}{4\lambda^2(F/\#)^2}\left| \int_{\rho=0}^{1}\int_{\theta=0}^{2\pi} e^{-j2\pi\Delta W(\rho,\theta)}e^{-j\pi\xi_{\mathrm{r}}\rho(\cos\theta-\cos\theta_{\mathrm{i}})}\rho\,d\rho\,d\theta\right|^2$$

$$E(\xi_{\mathrm{r}}) = \frac{\pi\phi}{\lambda^2(F/\#)^2}\left| \int_{\rho=0}^{1} e^{-j2\pi\Delta W(\rho,\theta)}J_0(\pi\xi_{\mathrm{r}}\rho)\rho\,d\rho\right|^2$$

where J_0 is the zero-order Bessel function, and $\xi_{\mathrm{r}} = r_{\mathrm{i}}/\lambda(F/\#)$.
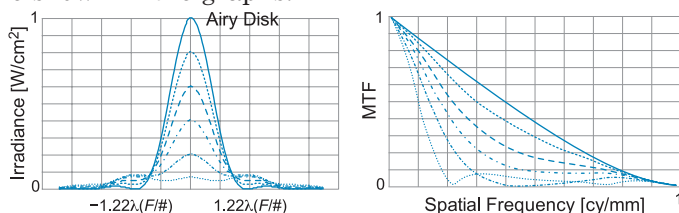
The **modulation transfer function (MTF)** (explained in detail in the Infrared Systems section of FG40), is an additional tool that is used quantitatively to analyze the image quality of an optical system.

The relationship between MTF and PSF is given by

$$\mathrm{MTF}(\xi, \eta) = \frac{|\mathcal{F}\{E(\xi, \eta)\}|}{|\mathcal{F}\{E(\xi, \eta)\}|_{\xi=\eta=0}}$$

Aberration Tolerance

The PSF and MTF for different amounts of defocus a_{020}/λ are shown in the graphs.

The **Rayleigh criterion** states that the optical performance of an imaging system will not be impaired as long as the maximum WFE resulting from the multiple optical aberrations does not exceed one-quarter wavelength ($\lambda/4$). When the WFE exceeds the Rayleigh limit, a significant amount of energy is transferred from the central disk of the Airy disk to its side rings.

There are two ways to quantify wavefront errors: **root sum square** ω or **peak-to-valley** W_{PV}. The former specifies the standard deviation from the reference sphere, while the latter indicates its maximum positive and negative OPD deviation from the paraxial wavefront.
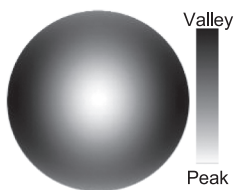
W_{PV} does not correlate well with image quality because it only takes two points into consideration and ignores everything else that lies between them. Consequently, an optical system having large W_{PV} could perform better than a system having a small W_{PV}. Alternatively, ω is a more reliable indicator of wavefront quality because it estimates the statistical OPD deviation averaged over the entire wavefront. Both W_{PV} and ω are expressed in units of wavelength.

The variance or mean square of the wavefront error is

$$\sigma^2 = \overline{(\Delta W - \overline{\Delta W})^2} = \overline{\Delta W^2} - (\overline{\Delta W})^2$$

where the overbars indicate average values. The RMS wavefront error is the square root of the variance:

$$\omega = \left[\overline{\Delta W^2} - (\overline{\Delta W})^2\right]^{1/2}$$

Strehl Ratio

Example: Let's say that we measured the wavefront error at three distinctive points: 0.7λ, 0.5λ, and 0.1λ. The average of their square values is $\overline{\Delta W^2} = 0.25\lambda^2$, and the square of their average values is $(\overline{\Delta W})^2 = 0.188\lambda^2$. The RMS WFE is then $\omega = (0.25\lambda^2 - 0.188\lambda^2)^{1/2} = 0.249\lambda$.

Generally, W_{PV} and ω are related by

$$\frac{W_{\mathrm{PV}}}{\omega} = 3.5$$

However, sometimes this ratio fluctuates between 4 and 5 due to high-order aberrations or manufacturing errors.

The **Strehl ratio (SR)** is often used to determine image degradation. It is defined as the ratio of the peak-diffraction intensity with aberrations to that without aberrations, thus it is constrained as $0 \leq \mathrm{SR} \leq 1.0$. The Strehl ratio can be written in terms of the MTF as well (see the FG40 section on Infrared Systems).
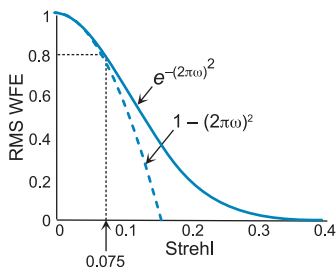
The standard expression of the Strehl ratio in terms of the RMS wavefront error is given by

$$\mathrm{SR} = e^{-(2\pi\omega)^2}$$

For well-corrected imaging systems ($\mathrm{SR} \geq 0.8$), the above equation may be approximated by

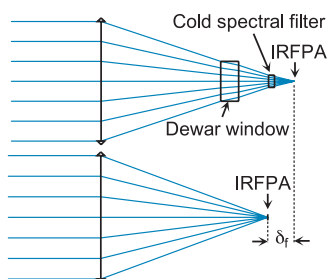$$\mathrm{SR} \approx 1 - (2\pi\omega)^2$$

which is valid for ω values of $\leq 0.075\lambda$. However, the SR becomes increasingly inaccurate with larger wavefront errors.

An uncorrected aberration is called a **zonal** or **residual wavefront error**.

Plane-Parallel Surfaces: Optical Windows

An IDCA often comprises a dewar window and a cold spectral filter.


If these components are inserted into the image-forming optical path of an optical system, with their **plane-parallel surfaces** perpendicular to the optical axis, the axial location of the image is shifted away from the focusing component.

The shift in focus for paraxial incidence is given by

$$\delta_f = \frac{(n_w - 1)t_w}{n_w} + \frac{(n_s - 1)t_s}{n_s}$$

where n_w, t_w and n_s, t_s are the refractive index and thickness of the window and spectral filter, respectively.

Optical windows are also used in telescope systems for protection from the environment. In some applications, these windows are tilted so that they can be mounted into gimballed turrets, and to prevent back reflections into the field of view.
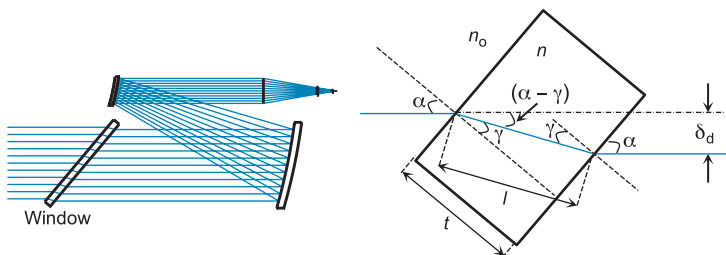
If a collimated beam is incident on an optical window at an angle α, a lateral displacement occurs, given by

$$\delta_d = l \cdot \sin(\alpha - \gamma) = l(\sin\alpha\cos\gamma - \sin\gamma\cos\alpha)$$

$$\delta_d = t\left(\sin\alpha - \frac{\sin\gamma\cos\alpha}{\cos\gamma}\right)$$

Plane-Parallel Surfaces: Optical Windows (cont.)

Applying Snell's law ($n_o \sin \alpha = n \sin \gamma$), we obtain

$$\delta_d = t \cdot \sin \alpha \left(1 - \frac{n_o}{n} \frac{\cos \alpha}{\cos \gamma} \right)$$

Knowing that $\cos \gamma = \sqrt{1 - (n_o/n)^2 \sin^2 \alpha}$, the lateral displacement may be written as

$$\delta_d = t \cdot \sin \alpha \left(1 - \sqrt{\frac{1 - \sin^2 \alpha}{n^2 - \sin^2 \alpha}} \right)$$

For paraxial approximation, this equation is reduced to

$$\delta_d = \frac{(n-1)t\alpha}{n}$$

If the light incident on the window is collimated, the refractive wavefront is free of aberrations; however, optical aberrations will occur if the window is introduced into a converging or diverging beam (i.e., the rays enter and exit at dissimilar angles).
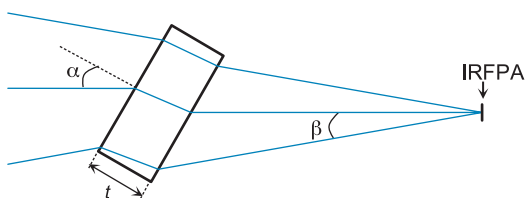
The table displays the degree to which the three relevant Seidel aberrations are introduced by a window under these settings.

| Aberration	Formula
Spherical	$\delta_z = \frac{t\beta^2(n^2-1)}{2n^3} = \frac{t(n^2-1)}{8(F/\#)^2 n^3}$
Astigmatism	$\delta_z = \frac{t\alpha^2(n^2-1)}{2n^3}$
Sagittal Coma	$\delta_y = \frac{t\alpha\beta^2(n^2-1)}{2n^3} = \frac{t\alpha(n^2-1)}{8(F/\#)^2 n^3}$

Chromatic Aberrations

Chromatic aberration in optical systems arises from the wavelength dependence of the refractive index. **Axial color aberration (ACA)** is the variation of focal length with wavelength along the optical axis. Alternatively, off-axis polychromatic light leads to **lateral color aberration (LCA)**, which is related to the difference in transverse magnification. A chromatic uncorrected optical component shows the so-called **primary spectrum**, where the far ends of the spectrum focus at different positions.
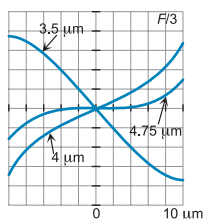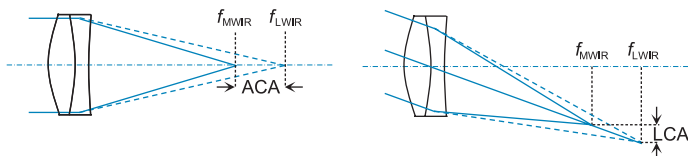
Another important aspect of chromatic aberration is the wavelength dependence of monochromatic aberrations. For example, the meridional ray intercept curves of a corrected MWIR optical system with optical aberrations is plotted for three different colors.

An **achromatic** design is accomplished by forcing the two foci of the far ends of the spectrum to coincide. However, the intermediate wavelengths will still be focused farther from the two selected colors.
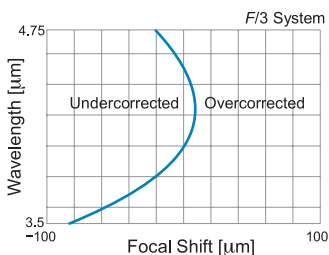
This difference in focal distance is called the **secondary spectrum**. The variation of SA with wavelength is referred to as **spherochromatism** or the **tertiary spectrum**.

An **apochromatic** lens corrects for both primary and secondary spectrums. Reflective components do not suffer from chromatic aberrations.

Aspheres

Aspheric optical components or **aspheres** are lenses or mirrors with complex curved surfaces, whose profiles differ from plain spherical or cylindrical curves. Unlike conventional spheres, aspheres gradually change their radius of curvature as a function of the distance from the optical axis. They provide flexible ways to minimize optical aberrations, thus allowing the design of fast optical systems with good image quality and fewer components.
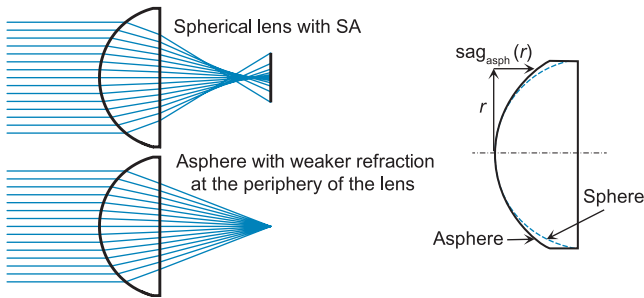

Even aspheres are defined by the following sag equation:

$$\mathrm{sag}_{\mathrm{asph}}(r) = \frac{cr^2}{1 + \sqrt{1 - (k+1)c^2r^2}} + \sum_i \alpha_{2i} r^{2i}$$

where $\mathrm{sag}_{\mathrm{asph}}(r)$ is the sagittal surface parallel to the optical axis, c is the surface curvature at the vertex R^{-1}, r is the radial distance from the optical axis, k is the conic constant, and α_{2i} are the aspheric deformation coefficients.

If $\alpha_{2i} = 0$, the resulting surface is characterized solely by k. The deviation of a specific conic from the circular form is known as the eccentricity ε, where $k = -\varepsilon^2$.
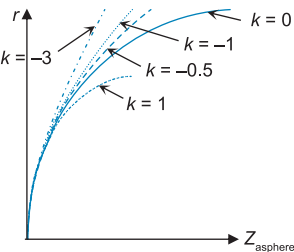
| Conic Section	k	ε
Sphere	$k = 0$	$\varepsilon = 0$
Parabola	$k = -1$	$\varepsilon = 1$
Prolate Ellipse	$-1 < k < 0$	$0 < \varepsilon < 1$
Oblate Ellipse	$k > 0$	$\varepsilon > 0$
Hyperbola	$k < -1$	$\varepsilon < 1$

Kinoforms

A **kinoform** lens element is a **diffractive optical element (DOE)** whose phase-controlling surface is super-imposed directly onto an asphere. Diamond turning is commonly employed to simultaneously manufacture this refractive/diffractive high-efficiency hybrid lens component. These diffractive structures may also be produced on chalcogenide glasses by diamond turning the mold insert. The smoothly varying profile of the kinoform can be approximated into a multilevel **binary** surface by breaking it down into a series of discrete steps. Binary surfaces are primarily produced by microlithographic processes.

Kinoform with quadratic blazed profile

Zones   0   1 2 3 4 5

Four-level binary profile
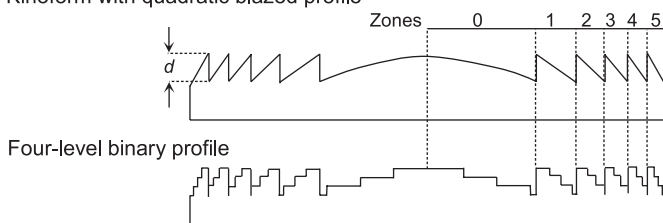
The inclusion of DOE surfaces in refractive paths enables both achromatic and athermal solutions, and allows for the desensitization of alignment tolerances. DOEs can yield designs with unique performance while reducing size and cost. However, stray radiation is a concern in these systems and must be properly analyzed. Kinoforms are primarily used in infrared systems. The long spectral bands assure that the required feature sizes are sufficiently large for the diamond-cutting tool radius. Surface roughness, effective transmittance loss, diffraction efficiency, and machining time depend on the radius of this tool.

The ideal kinoform looks like a Fresnel lens composed of a multitude of zones with a constant grating groove depth of

$$d = \frac{\lambda_o}{n(\lambda_o) - 1}$$

where λ_o is the primary wavelength. The phase shift transition between zones is exactly 2π.

Kinoforms (cont.)

The diffraction efficiency of a kinoform structure is 100% for the principal wavelength and declines for any additional wavelengths within the spectral band:

$$\eta_{\text{kino}} = \text{sinc}^2\left[\pi\left(\frac{\lambda_o}{\lambda}\right) - 1\right]$$

The diffraction efficiency of a binary structure with N discrete levels can be calculated by $\eta_{\text{bin}} = \text{sinc}^2(\pi/N)$.

The phase profile of a diffractive surface in radians can be written as the following polynomial expansion:

$$\varphi(r) = \frac{2\pi}{\lambda_o}\sum_i C_{2i}r^{2i}$$

where C_{2i} are the phase coefficients. If r is defined as the overall lens radius ($r = D_{\text{lens}}/2$), the number of zones can be computed by

$$m = \frac{1}{\lambda_o}\sum_i C_{2i}r^{2i}$$

The form of the diffraction sag varies in accordance with

$$\text{sag}_{\text{diff}} = \frac{1}{n(\lambda_o) - 1}\sum_i C_{2i}r^{2i} + \frac{\lambda_o}{n(\lambda_o) - 1}\left(\text{int}\frac{1}{\lambda_o}\sum_i C_{2i}r^{2i}\right)$$

where int denotes the integration operation. Given that the number of zones m has been identified, this equation can be written as

$$\text{sag}_{\text{diff}} = \frac{\sum_i C_{2i}r^{2i} + \lambda_o(m - 1)}{n(\lambda_o) - 1}$$

$$\Rightarrow \text{sag}_{\text{total}} = \text{sag}_{\text{asph}} + \text{sag}_{\text{diff}}$$
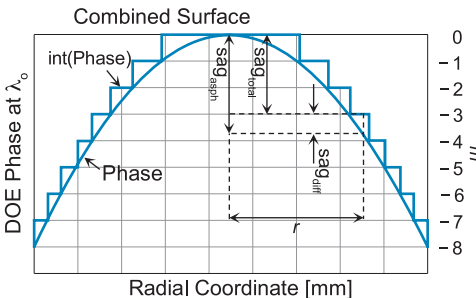

Combined Surface

Image Anomalies in Infrared Systems

Three common image anomalies are associated with IR systems.

Shading: the gradual fall off in the scene radiance toward the edges of the detector, caused by $\cos^4\theta$ dependence of the effective exitance of a uniform source. Shading is controlled by optical design techniques that keep the angle of the chief ray small in image space.

Scan noise: the amount of self-radiation reaching the detector due to both room-temperature internal housing and optical elements as a function of scan position. Scan noise can also be caused by vignetting in an image-side scanner (e.g., rotating polygon). There is a final

Since $\alpha < \beta$, the mirror in position 1 has less scan-noise contribution than the mirror in position 2.

FPA

1   2

displacement d from the center of the facet in the direction normal to the initial position. Then the interactive scanning moves in and out, and the exit beam wanders left and right, causing vignetting.

Direction of facet rotation

d

Detector

Beam wander

Colder area
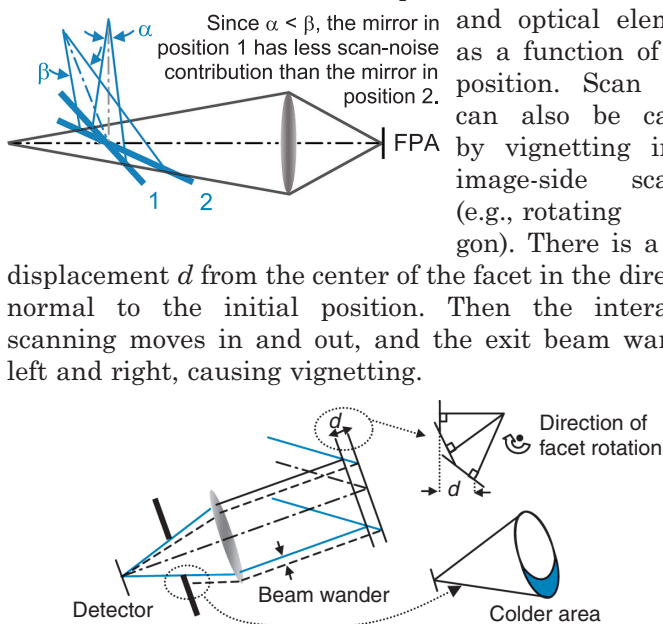
The **narcissus effect**: the result of a cold reflection of the detector array into itself, which appears as a dark spot at the center of the scan. It is controlled by using the appropriate antireflective coatings on the optical elements, and by optical design techniques that ensure that the cold-reflected image is out of focus at the detector plane. Its magnitude is often expressed as a multiple of the system's noise level.
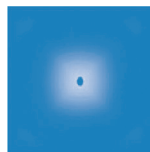
Optical Properties of Specular Light

The choice of infrared materials is dictated by the application; consequently, their optical, mechanical, and thermal properties are of utmost importance. Some of these properties include **transmittance range**, **absorptance**, **reflection loss**, **strength and hardness**, **thermal expansion**, **thermal conductivity**, **fracture toughness**, **water erosion resistance**, etc.

The **refractive index** n is defined as

$$n = \frac{c}{\upsilon}$$

where c is the speed of light (3×10^{-10} cm/sec) in free space, and υ is the speed of light in the medium.

Whenever a ray crosses a boundary between two materials of different refractive indexes, there is some power transmitted, reflected, and absorbed (i.e., conservation of energy):

$$\phi_i = \phi_t + \phi_r + \phi_a; \quad \phi \equiv \text{power [W]}$$

The direction of the transmitted light is given by **Snell's law**, and the direction of the reflected beam is determined by the law of reflection.
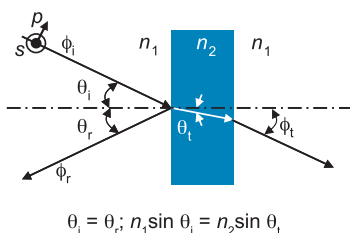
$$\theta_i = \theta_r; \; n_1 \sin \theta_i = n_2 \sin \theta_t$$

The distribution of power between the transmitted and reflected components from a single surface is determined by the **Fresnel equations**:

s-polarization,

$$\rho_s = \frac{(n_1 \cos \theta_i - n_2 \cos \theta_t)^2}{(n_1 \cos \theta_i + n_2 \cos \theta_t)^2} \quad \text{and} \quad \tau_s = \frac{4 n_1 n_2 \cos \theta_i \cos \theta_t}{(n_1 \cos \theta_i + n_2 \cos \theta_t)^2}$$

p-polarization,

$$\rho_p = \frac{(n_2 \cos \theta_i - n_1 \cos \theta_t)^2}{(n_2 \cos \theta_i + n_1 \cos \theta_t)^2} \quad \text{and} \quad \tau_p = \frac{4 n_1 n_2 \cos \theta_i \cos \theta_t}{(n_1 \cos \theta_t + n_2 \cos \theta_i)^2}$$

and at normal incidence,

Optical Properties of Specular Light (cont.)

$$\rho_n = \left(\frac{n_2 - n_1}{n_2 + n_1}\right)^2 \quad \text{and} \quad \tau_n = \frac{4n_1 n_2}{(n_1 + n_2)^2}$$

where

$$\rho = \frac{\phi_r}{\phi_i} \quad \text{and} \quad \tau = \frac{\phi_t}{\phi_i}$$

The absorption is fundamentally a quantum process where the molecules absorb energy from incident photons. It takes power out of the beam radiation, raising the temperature of the material, and can be written as

$$\phi(z) = \phi_i e^{-\alpha z}$$

where α is the **absorption coefficient** [cm^{-1}], and z is the propagation distance within the material.

The **internal transmittance** is defined as the transmittance through a distance in the medium, excluding the Fresnel reflection loss at the boundaries:

$$\tau_{\text{internal}} = \frac{\phi(z)}{\phi_i} = e^{-\alpha z}$$

Conversely, the **external transmittance** is the transmittance through a distance in the medium that includes the Fresnel loss at the boundaries:

$$\tau_{\text{external}} = \tau^2 e^{-\alpha z} = \tau^2 \tau_{\text{internal}}$$

When examining material specifications from a vendor, it is necessary to take into account the distinction between internal and external transmittances.

The overall **reflectance** and/or **transmittance** of a plane-parallel plate with smooth surfaces results from the multiple transmitted and reflected components of the surfaces. Assuming normal incidence, the total reflectance can be written as

$$\phi_r = \phi_{r1} + \phi_{r2} + \phi_{r3} + \phi_{r4} + \cdots +$$

$$\phi_r = \rho\phi_i + \rho\tau^2 e^{-2\alpha d}\phi_i + \rho^3\tau^2 e^{-4\alpha d}\phi_i + \rho^5\tau^2 e^{-6\alpha d}\phi_i + \cdots +$$

Using infinite geometric progression, **total reflectance** is given by

Optical Properties of Specular Light (cont.)
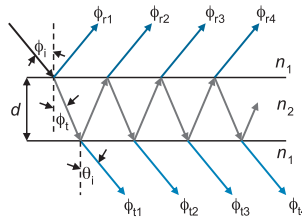
$$\rho_{total} = \frac{\phi_r}{\phi_i} = \rho + \frac{\rho(1-\rho)^2 e^{-2\alpha d}}{1 - \rho^2 e^{-2\alpha d}}$$

Similarly, the **total transmittance** is given by

$$\tau_{total} = \frac{\phi_t}{\phi_i} = (1-\rho)^2 e^{-\alpha d}(1 + \rho^2 e^{-2\alpha d} + \rho^4 e^{-4\alpha d} + \rho^6 e^{-6\alpha d} + \cdots)$$

$$= \frac{(1-\rho)^2 e^{-\alpha d}}{1 - \rho^2 e^{-2\alpha d}}$$

The **absorptance** is then obtained by

$$a = 1 - \rho_{total} - \tau_{total} = \frac{(1-\rho)(1 - e^{-\alpha d})}{1 - \rho e^{-\alpha d}} \equiv \varepsilon$$

Kirchhoff's law states that the integrated absorptance is identical to the integrated emittance ε. For a transparent window with low absorptance,

$$a \equiv \varepsilon \cong 1 - e^{-\alpha d} \cong \alpha d$$

For opaque materials, $\rho_{total} = \rho$, and $a = 1 - \rho$. For lossless media ($e^{-2\alpha d} \approx 1$),

$$\tau_{total} = \frac{1-\rho}{1+\rho} \quad \text{and} \quad \rho_{total} = \frac{2\rho}{1+\rho}$$

Real materials are not perfect insulators and exhibit dielectric losses. Therefore, it is sometimes convenient to define a complex refractive index as

$$n_{complex} = n \pm ik$$

where n indicates the phase velocity as presented in the previous equations, and k is the extinction coefficient that specifies the amount of absorption loss or gain (i.e., sign convention) when the electromagnetic wave propagates within the material.

Regions of Strong Absorption in Infrared Materials

The absorption and extinction coefficients are linked by

$$\alpha = \frac{4\pi k}{\lambda}$$

The attenuation coefficient δ [dB$\cdot$cm^{-1}] is also related to the absorption coefficient by

$$\delta = \frac{10}{\ln 10} \cdot \alpha$$

The absorptance in infrared materials is mainly governed by two processes: **intraband** (or **free-carrier**) **absorption** and **lattice vibrations**. The former occurs when the material absorbs high-frequency photons (i.e., ultraviolet absorption edge), and carriers are excited to higher-state energy levels. The latter takes place where the frequency of the incoming electromagnetic radiation is resonant with that of the lattice dipole (i.e., infrared absorption edge).

For a diatomic molecule, the electronic states can be represented by plots of potential energy as a function of the internuclear distance. Vibrational transitions occur between different vibrational levels of the same electronic state.
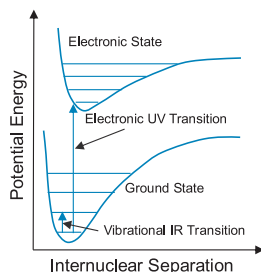
The absorbed energy is converted into quantum vibrational motion or phonons, thus increasing the temperature of the material. De Broglie's particle–wave duality states that

$$p_{\mathrm{m}} = \frac{h}{\lambda}$$

where p_{m} is the momentum of a photon, h is Planck's constant, and λ is the wavelength. When $\lambda = a_{\mathrm{lattice}}$, where a_{lattice} is the lattice constant, the momentum between the incident photon and the thermal phonon is conserved; therefore, complete absorption of the radiation by the crystal structure ensues.

Spectral Transmittance: Origin and Model

Between the electronics and vibrational resonances lies the transparent region of the material. The level of absorption in this see-through window depends on the impurities, crystal defects, and extrinsic scattering. The **spectral transmittance** of some of the most common infrared materials is shown in the table.

Material	λ_{cuton} [μm]	λ_{cutoff} [μm]
AgCl − Silver Chloride	0.42	23
Al_2O_3 − Sapphire	0.15	5.5
$Al_{23}O_{27}N_5$ − ALON	0.23	5.0
As_2S_3 − Arsenic Sulfide	0.5	11
BaF_2	0.14	12.2
CaF_2	0.13	9.4
Calcium Aluminate	0.4	5.5
CdS	0.52	14.8
CdTe	0.85	29.9
CsBr − Cesium Bromide	0.23	43.5
CsI − Cesium Iodide	0.25	55
Diamond*	0.25	>100
GaAs	0.9	17.3
GaP	0.54	10.5
Ge	1.8	18
GeAsSe − Chalcogenide	1.0	12.0
InP − Indium Phosphate	0.93	20
KBr − Potassium Bromide	0.2	30.2
KCl − Potassium Chloride	0.18	23.3
KI − Potassium Iodide	0.25	38.5
LiF	0.15	5.7
$MgAl_2O_4$ − Spinel	0.2	5.8
MgF_2 − Single Crystal	0.121	7.7
MgF_2 − Hot Pressed	0.7	9.0
MgO	0.35	6.8
NaCl	0.17	18.2
PbF_2 − Lead Fluoride	0.29	12.5

Spectral Transmittance: Origin and Model (cont.)

Material	λ_{cuton} [μm]	λ_{cutoff} [μm]
Si	1.1	8.0
SiC	0.5	4.8
Si_3N_4	0.3	4.5
SiO_2 − Fused Silica	0.15	4.5
TiO_2 − Rutile	0.43	5.5
TlBr/TlI − KRS-5	0.6	40.0
TlBr-TlCl − KRS-6	0.4	30.0
Y_2O_3	0.29	8.0
Y_2O_3:Ln^{3+}	0.25	8.0
ZnS (standard)	1.0	12
ZnS (multispectral)	0.4	12
ZnSe	0.6	18.0
ZrO_2:Y_2O_3 − Zirconium Oxide	0.38	6.0

Diamond* − Excludes 3–5 μm.

The material's cutoff frequency is determined by the vibrational frequency of its diatomic molecules. A chemical bond acts like a spring, where a force F_s is required to either extend or compress the spring by a distance x:

$$F_s = \pm\, k_s \cdot x$$

where k_s is the spring stiffness.
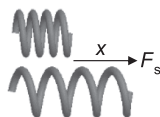
Effect of Temperature on Emittance

The discrete vibrational energy levels within the material are obtained by solving the **Schrödinger wave equation**:

$$\mathcal{E}_n = \left(i + \frac{1}{2}\right) h \nu_{\mathrm{v}} = \left(i + \frac{1}{2}\right) \frac{h}{2\pi} \sqrt{\frac{k_{\mathrm{s}}}{m^*}}$$

where i is a quantum integer number, ν_{v} is the vibrational frequency, and m^* is the effective atomic mass. The transition from an energy level i to an energy level $i + 1$ may be written as

$$\Delta \mathcal{E} = h \nu_{\mathrm{v}} = h \nu \equiv \frac{hc}{\lambda_{\mathrm{cutoff}}}$$

which states that, due to the absorption of a photon, the vibrational frequency equals the photon frequency, and thus is inversely proportional to the **cutoff wavelength**.

From the above equations, the following can be inferred:

➢ Since $\mathcal{E}_n \propto \sqrt{k_{\mathrm{s}}}$, weak bonds have lower energies.
➢ Since $\mathcal{E}_n \propto \sqrt{m^{*-1}}$, lighter atoms have higher energies.
➢ The cutoff wavelength is determined by the excited energy states because $\Delta \mathcal{E} \propto \lambda_{\mathrm{cutoff}}^{-1}$.
➢ MWIR transmitting materials have lighter atoms and strong bonds, while LWIR transparent materials comprise heavier atoms with weak bonds.
➢ With the exception of diamond, longwave materials are more fragile and brittle than midwave materials.

The absorption coeffient is a function of both wavelength and temperature. As the absorption coefficient increases, so does the integrated **emittance**. At high temperatures, the intensified emittance of an optical window or dome may block the radiation from an intended target. This stray light increment reduces the **signal-to-noise ratio (SNR)** of an infrared system as well. Assuming that the main noise contribution from the IRFPA is due to the shot noise generated by the infrared material, the SNR can be approximated by

$$\mathrm{SNR} \approx \varepsilon_{\mathrm{target}} \phi_{\mathrm{signal}} \sqrt{\frac{\eta \tau_{\mathrm{int}}}{\varepsilon_{\mathrm{material}} \phi_{\mathrm{material}}}}$$

Birefringence

The last equation on page 46 shows that the degradation of the SNR in an infrared system is clearly contingent on the emittance and temperature of its optical components.

Furthermore, a LWIR system can tolerate much greater emittance than a MWIR system. For example, the table below shows that a rise of 300 K in a zinc sulfide (ZnS) window operating at 10.5 μm is not quite as significant as the same change in temperature of a sapphire (Al_2O_3) window operating at 4 μm.

Material	$\varepsilon(\lambda, T) \cdot M(\lambda, T)$ [W/cm^2]		
Thickness = 1 cm	$T = 300$ K	$T = 600$ K	Factor
Al_2O_3 (4 μm)	1.07×10^{-6}	7.98×10^{-4}	745.8
ZnS (10.5 μm)	5.51×10^{-7}	1.19×10^{-5}	21.6

Most infrared materials such as ZnS are optically isotropic, meaning that the index of refraction is equal in all directions throughout the crystalline lattice. Conversely, anisotropic crystals (such as sapphire) have crystallographically distinct axes and interact with light by a mechanism that is dependent on the orientation of the crystalline lattice with respect to the polarization and propagation direction of light.

When a beam of light enters the optical axis of anisotropic crystals, the waves are split into two orthogonal polarized ray components—termed ordinary and extraordinary—that travel through the molecular lattice along slightly different optical paths, depending on their orientation with respect to the crystalline optical axis.

This phenomenon is termed **birefringence** and is quantified as the maximum difference between the refractive indices exhibited by the **birefractive material**: $\Delta n = n_e - n_o$

Dispersion is the variation in the index of refraction with wavelength ($dn/d\lambda$) and is an important material property when considering large-spectral-bandwidth optical systems.

Material Dispersion

The dispersion is greater at short wavelengths and decreases at longer wavelengths; however, for most materials, it increases again when approaching the LWIR absorption band. The index of refraction lowers with increasing wavelength as well.

For historical reasons, dispersion is often quoted as a unitless ratio called the **reciprocal relative dispersion** or **Abbe number**, defined by

$$V = \frac{n_{\mathrm{mean}} - 1}{\Delta n} = \frac{n_{\mathrm{mean}} - 1}{n_{\mathrm{final}} - n_{\mathrm{initial}}}$$

where n_{initial} and n_{final} are the initial and final index of refraction values of the spectral band of interest, respectively, and n_{mean} is the mean center value. Δn is basically the measured value of the dispersion, and $n_{\mathrm{mean}} - 1$ specifies the refractive power of the material. The smaller the Abbe number the larger the dispersion. For example, the V number for a germanium lens in the 8- to 12-μm spectral band is

$$V = \frac{n(10\,\mu\mathrm{m}) - 1}{n(12\,\mu\mathrm{m}) - n(8\,\mu\mathrm{m})} = \frac{4.0038 - 1}{4.0053 - 4.0023} = 1001.27$$

Another useful definition is the **relative partial dispersion**, given by

[adapted from Wolfe & Zissis, *The Infrared Handbook* (1989)]

$$P = \frac{n_{\mathrm{mean}} - n_{\mathrm{initial}}}{n_{\mathrm{final}} - n_{\mathrm{initial}}}$$

which is a measure of the rate of change of the slope of the refractive index versus wavelength $dn^2/d\lambda^2$. The chart shows the dispersion of the most common IR materials.
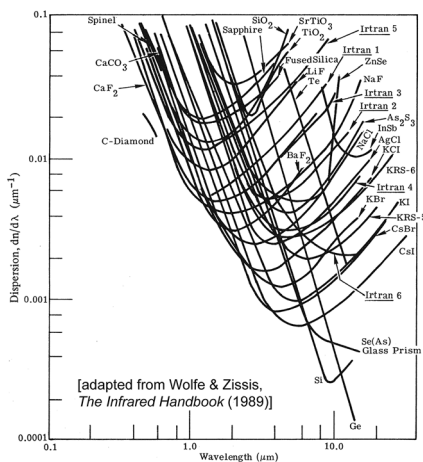
Optical Scatter

Optical scatter is an interaction between EM radiation and matter. It redirects the light by mechanisms other than specular and is affected by surface topography, index fluctuations, surface contamination, bulk particulates such as bubbles, and inclusions that are large compared to the wavelength. Scatter phenomena are rather complex, and analytical solutions are often difficult to develop; therefore, stray light computer models are frequently used for optical scatter analysis.
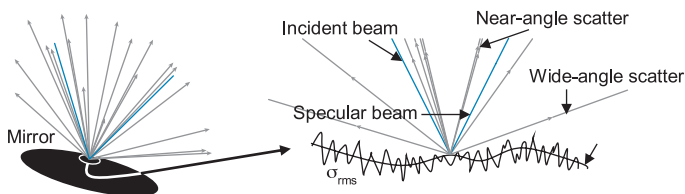
The fundamental radiometric equation (see page 81) can be written as

$$\partial^2 \phi_d = \frac{L_{out}}{E_{inc}} E_{inc} \partial A_{inc} \cos\theta \partial\Omega_d = \mathrm{BSDF}(\theta, \varphi)\phi_{inc}\cos\theta\partial\Omega_d$$

The term **bidirectional scatter distribution function (BSDF)** converts the incoming irradiance to outgoing radiance and is commonly used to describe scatter light patterns. The BSDF may be written as

$$\mathrm{BSDF} \equiv \frac{L_{out}}{E_{inc}} = \frac{\phi_{out}}{\phi_{inc}\Omega_d}\,[\mathrm{sr}^{-1}]$$

Using spherical coordinates, the detector solid angle can be expressed as

$$\partial\Omega_d = \frac{dA_d}{r^2} = \sin\theta\partial\theta\partial\varphi$$

The ratio of the outbound scatter flux to the incident specular flux is called the **total integrated scatter (TIS)** and is obtained by integrating the BSDF over the solid-angular subtense of a unit hemisphere:

$$\mathrm{TIS} = \frac{\phi_d}{\phi_{inc}} = \int_{\varphi=0}^{2\pi}\int_{\theta=0}^{\pi/2}\mathrm{BSDF}(\theta, \varphi)\sin\theta\cos\theta d\theta d\varphi$$

Optical Scatter (cont.)

The fraction of the total radiant flux remaining in a specular beam after reflectance or transmittance from moderately rough surfaces is given by

$$\text{TIS} = 1 - \exp\left[-\left(\frac{2\pi n \cos\theta\sigma_{\text{rms}}}{\lambda}\right)^2\right]$$

where n is the refractice index, and σ_{rms} specifies the standard deviation or root-mean-square **surface roughness**, calculated by

$$\sigma_{\text{rms}} = \sqrt{\frac{1}{N}\sum_{i=1}^{N}(y_i - \overline{y})^2}$$

where N is the number of equally spaced measurements of the surface elevation profile y_i, and $\overline{y}$ is mean elevation.
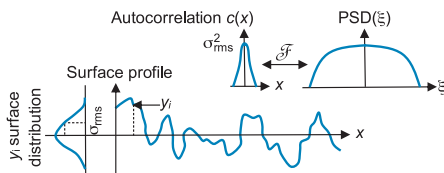
In most cases, y_i is obtained from measured data from either a profilometer or a white light interferometer.

For a smooth, clean surface, where $\sigma_{\text{rms}} \ll 1$, the TIS equation can be simplified to

$$\text{TIS} \cong \left(\frac{2\pi n \cos\theta\sigma_{\text{rms}}}{\lambda}\right)^2$$

Whether modeled or measured, TIS is constrained between zero and unity. TIS values in glasses such as fused silica are ordinarilly near 0.1%, while in single crystals such as sapphire and calcium fluoride are on the order of 0.01–0.1%. In polycrystalline materials (e.g., magnesium fluoride, spinel, and ALON), TIS varies between 0.5 and 5%.

The BSDF can be plotted either as a function of scatter angle or versus the difference between the inplane specular and scatter directions (i.e., $|\beta - \beta_0|$), where $\beta = \sin(\theta_{\text{scatter}})$ and $\beta_0 = \sin(\theta_{\text{specular}})$.

Optical Scatter (cont.)

All of the Lorentzian curves shown on the left plot below are superpositioned onto the $|\beta - \beta_0|$ curve. This is convenient because scatter from smooth optical surfaces can be modeled as the superposition of phase gratings on a surface (i.e., according to the grating equation: $\beta - \beta_0 = m\lambda/d$).
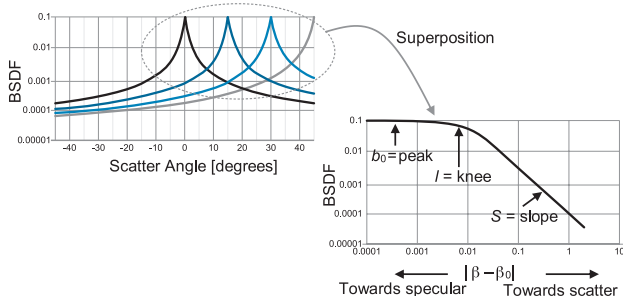
To better understand the $|\beta - \beta_0|$ plot, let's assume that the incident beam is normal to the surface, so $\beta_0 = 0$. At the limit where θ_{scatter} approaches 0 deg, $|\beta - \beta_0| \to 0$, near-angle scatter occurs. At the other limit, where $\theta_{\text{scatter}} = 90$ deg, $|\beta - \beta_0| = 1$, wide-angle scatter takes place.

Light scattering is commonly characterized by the **Harvey–Shack empirical model**,

$$\text{BSDF}(\beta, \beta_0) = b_0 \left[1 + \left(\frac{\beta - \beta_0}{l}\right)^2\right]^{S/2}$$

where the parameters b_0, l, and S are shown in the above $|\beta - \beta_0|$ plot. In standard measured surfaces, the values of the slope S are between –0.5 and –2. The knee l is often difficult to view because it is too close to specular, but a reasonable assumption is that it varies between 0.0001 and 0.01. The specular peak b_0 can be calculated by

$$b_0 = \left(\frac{nB}{\lambda^2}\right)^2 \frac{2\pi\sigma_{\text{rms}}^2}{\ln\left(1 + \frac{B^2}{\lambda^2}\right)}$$

where 100 μm $< B <$ 500 μm. B is normally 200 μm for standard optical surfaces.

Mechanical Properties

The tension test consists of a cylinder anchored at one end and subjected to an uniaxial load P. As the load increases, the axial deflection δl of the loaded end will increase as well. When the **stress** exceeds the **strength** of the material, the material fractures into two or more pieces.

At the moment of failure, the **ultimate tensile stress (UTS)** is given by

$$\sigma_f = \frac{P_f}{A_0} \ [\text{Pa or psi}]$$

where P_f is the load at fracture, and A_0 is the original cross-sectional area.

If the specimen is loaded by an axial force $P < P_f$, the stress is defined by analogy as

$$\sigma' = \frac{P}{A_0}$$

The **strain** is defined as the fractional increase in length:

$$\varepsilon' = \frac{\delta l}{l}$$

The slope of the stress versus strain is the modulus of elasticity, or **Young's modulus**, and is given by

$$E' = \frac{\sigma'}{\varepsilon'}$$

The greater the value of E' the stiffer the material; therefore, a greater stress is required to produce a given strain.
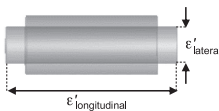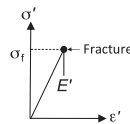
The ratio between the longitudinal and lateral tensile strains is called the **Poisson ratio** and is designated by

$$\nu' = -\frac{\varepsilon'_{\text{lateral}}}{\varepsilon'_{\text{longitudinal}}}$$

A positive tensile strain in the longitudinal direction contributes to a negative compressive strain in the lateral direction, and vice versa.

Stress Concentration

Stiffness is a measure of the load required to induce a given deformation within the material, while the strength refers to the material's resistance to failure. Stiffness is usually measured by applying moderate loads, short of fracture.

If a specimen is subjected to a shearing stress, where the load P is applied transversely to the length over which it is distributed, the shear stress yields a shear strain.

The angular distortion or change in the right angle is denoted by

$$\frac{\delta}{h} = \tan\beta' \approx \beta'$$
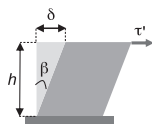
The majority of infrared-transmissive materials are either single crystals, polycrystalline, or amorphous glasses (i.e., ceramic structures). Ceramic materials are held together by covalent and/or ionic bonds, which tend to brittle fracture before any elastic deformation takes place. Moreover, microscopic imperfections in these materials act as **stress concentrators**, decreasing their toughness and reducing their tensile strength, thus causing the material to shatter.

An optical window is strongest when force is evenly distributed over its area, so a reduction in area by a crack would set off a localized increase in stress. For example, the stress concentration in an elliptical crack of length $2a$ and width $2b$ is given by the Inglis equation:

$$\sigma'_{\text{localized}} = \sigma'_{\text{load}}\left(1 + 2\sqrt{\frac{a}{\rho}}\right)$$
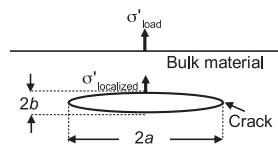
where $\rho = b^2/a$ is the radius of curvature. As ρ approaches zero, $\sigma_{\text{localized}}$ tends to infinity.

The perceived fracture strength is two orders of magnitude lower than the theoretical cohesive strength. This discrepancy is explained by the Griffith theory of brittle fracture.

Hardness

The **Griffith equation** states that crack propagation occurs when the released elastic strain energy is at least equal to the energy required to generate a new crack surface. The stress required to create the new crack surface is given by
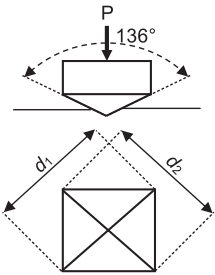
$$\sigma_f = \sqrt{\frac{2E' \cdot \gamma}{\pi d}}$$

where E' is Young's modulus, γ is the surface energy density of the material, and d is the flaw length.

Hardness is the resistance of a material to permanent localized deformation, usually by indentation, due to a constant compression load from a sharp object. Hardness measurements are used extensively for quality control because they are considered to be nondestructive, speedy tests where the indentations are created using light loads.

Vickers and Knoop indenters are commonly used for determining the hardness of brittle materials and thin film coatings. The **Vickers test** uses a square pyramidal indenter that is prone to crack the materials, while the **Knoop test** uses a rhombic-based pyramidal indenter, which produces longer but shallower indentations.
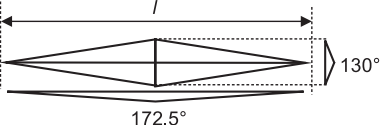

Vickers Indentation

Knoop Indentation

$$H_{Vickers} = \frac{2P \sin\left(\frac{136°}{2}\right)}{d^2}$$

$$\overline{d} = \frac{d_1 + d_2}{2}$$

$$H_{Knoop} = \frac{P}{C_k l^2}$$

Ideally, the correction factor C_k related to the shape of the indenter is 0.07079.

Fracture Toughness and Weibull Statistics

The **fracture toughness** or **stress-intensity factor** indicates the amount of stress required to propagate a preexisting flaw and is calculated by

$$K_{\mathrm{Ic}} = Y\sigma_{\mathrm{f}}\sqrt{\pi d} \quad [\mathrm{MPa}\sqrt{\mathrm{m}}]$$

where d is either the length of a surface crack or one-half of the length of an internal crack, and Y is a dimensionless geometry factor on the order of 1. The Roman numeral subscript I in K_{Ic} indicates an uniaxial opening as the mode of fracture (II–sliding, III–tearing), while the subscript c stands for critical.
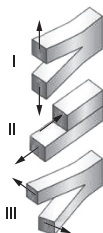
Mode I fracture occurs when the crack plane is normal to the direction of largest tensile loading. This is the most commonly encountered mode and is a condition called **plane strain**. K_{Ic} is the uppermost value of stress intensity that a material under this specific condition can withstand without fracture. Under this condition, materials behave essentially as elastic until the fracture stress is reached, and then sudden fracture occurs. Since little or no plastic deformation is perceived, mode I fracture is termed brittle fracture.

The strength in brittle materials is statistical in nature because it depends on the probability of finding a flaw that exceeds a certain critical size (i.e., failure due to the weakest link of a chain). This unpredictability is based on the **Weibull distribution**, which is an indicator of the variability of strength of materials resulting from a distribution of flaw sizes.

Consider a ceramic window of surface A with a certain distribution of flaws and subjected to a stress σ'. If we presume that the window is divided into n differential surface elements δA such that the total volume is $A = n\delta A$, the probability that the window will fracture under the applied stress is given by

$$P_{\mathrm{failure}} = 1 - \exp\{-[kA(\sigma'/\sigma_0)]^m\}$$

where σ_0 is a scaling factor (often assumed to equal the average strength), the product kA is the effective area, and m is the **Weibull modulus**.

Safety Factor

> ➢ A higher Weibull modulus m infers a more reproducible strength.
> ➢ If the applied stress σ' is uniform, $k = 1$.
> ➢ If the failure occurs within the bulk of the material, the surface A may be substituted by the volume V.

Since the strength in ceramic materials of seemingly identical samples is highly variable, the mean strength is defined as the average value obtained from different tensile stress tests of a large number of samples of the same kind. With standard deviations of more than 15%, it is advisable to add a **safety factor (SF)** to reduce the risk and to avoid the possibility of a catastrophic failure.

The maximum stress allowed can be calculated by

$$\sigma_{max} = \frac{\overline{\sigma}_f}{SF}$$

where $\overline{\sigma}_f$ is the mean strength.

Depending on the system's reliability, the safety factor ranges between 2 and 20; however, a safety factor of 4 is the standard value used for windows and domes. The way the stress is applied also affects the SF selection, as seen in the table.

Manner of Loading	SF
Static – Stress is applied slowly and remains applied or is infrequently removed.	4–6
Repeated – Fatigue failure may occur at stresses lower than static load failure.	>10
Impact – High initial stress develops.	>15

Safety factors are also required to account for the following:

> ➢ imperfections and material degradation,
> ➢ unexpected stress,
> ➢ erosion,
> ➢ environmental conditions, radiation, chemicals, etc.
> ➢ thermal shock induced by a high-energy laser or aerothermal heating, and
> ➢ cost and loss of life.

Thermal Properties

The rate of heat transfer by conduction in the x direction through a finite area A_x in which T is only a function of x is given by the **Fourier law of conduction**:

$$q = -k'A_x \frac{\partial T}{\partial x}$$

where A_x is normal to the direction of the transfer, and k' is the **thermal conductivity**. k' is a thermophysical property of the medium that represents the rate of heat transfer in $W/m \cdot K$. The higher the thermal conductivity the faster the heat propagation across the optical component.
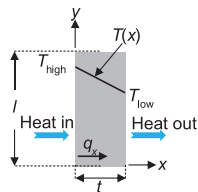
The **thermal diffusivity** is a material-specific property that defines the speed of heat propagation by conduction during changes of temperature. It is the measure of thermal inertia and is expressed by

$$\kappa' = \frac{k'}{\rho' C_p} \ [\mathrm{m^2/sec}]$$

where $\rho' C_p$ is the volumetric heat capacity $[\mathrm{J/m^3 \cdot K}]$. κ' simply describes how quickly a material reacts to a change in temperature.

The fractional change in size per degree change in temperature at a constant pressure can be written as

$$\alpha' = \frac{1}{l}\frac{\partial l}{\partial T} \quad \text{so} \quad \varepsilon' = \frac{\partial l}{l} = \alpha' \partial T$$

where α' in K^{-1} is defined as the **coefficient of thermal expansion (CTE)**.

Infrared ceramic materials are good insulators of heat and electricity, and are rather stable at high temperatures; some types such as chalcogenide glasses are able to progressively decrease their viscosity when heated. This plastic deformation is ideal for replicating complex molding. Nevertheless, the strength of most of these optical materials decreases at high temperatures. ZnS and GaP are an exception to this rule, given that they strengthen as the temperature rises.

Thermal Shock

Thermal shock damage occurs when components are subjected to sudden and large temperature gradients. For example, resistance to failure by thermal shock induced by severe aerothermal heating is one of the critical requirements for optical domes as seekers accelerate to their programmed velocity. A rapid increase in the component's front surface temperature due to air friction may cause it to shatter.

Because of the significant stress between the external (expanded) an internal (unexpanded) surfaces, thermal shock failure may occur at either surface at different stages of the flight.
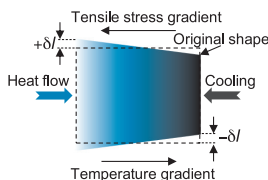
Thermal shock resistance (TSR) is a performance measure influenced by both intrinsic properties (e.g., thermal conductivity) and extrinsic properties (e.g., strength) of the material, and it is best analyzed by using finite-element thermal stress computer models. However, in the absence of state-of-the-art software, an analytical indication of relative performance can be attained by means of the Hasselman parameters (see next page).

The ratio between the heat-transfer resistances within the bulk and at the surface of a component is given by the **Biot number** Bi:

$$\text{Bi} = \frac{\overline{h}t}{k'}$$

where t is the material thickness, and $\overline{h}$ is the mean coefficient of heat transfer in $W/m^2 \cdot K$.

$\text{Bi} \gg 1$ indicates a thermally thick substance, which infers that the heat conduction inside the bulk of a window component is much slower than the heat convection away from its surface; therefore, thermal shock is likely to occur. Conversely, $\text{Bi} \ll 1$ labels a substance as thermally thin, which implies slow thermal heating that is synonymous to mild thermal shock.

Thermal Shock (cont.)

If the surface temperature of a body is rapidly changed from T_0 to T_1, the stress generated at the surface is

$$\sigma' = \frac{\alpha' E'(T_0 - T_1)}{1 - \nu'} = \frac{\alpha' E' \Delta T}{1 - \nu'}$$

In the limit of severe thermal shock, Hasselman's basic thermal shock parameter is defined as

$$R = \frac{\sigma_\mathrm{f}(1 - \nu')}{\alpha' E'} \quad [\mathrm{K}]$$

where R indicates the maximum ΔT before cracks form.

If the surface of the component is exposed to slow thermal heating, the **Hasselman parameter** incorporates the effect of thermal conductivity:

$$R' = Rk' = \frac{\sigma_\mathrm{f} k'(1 - \nu')}{\alpha' E'} \quad [\mathrm{Jcm^{-1}s^{-1}}]$$

where R' specifies the maximum heat flux for steady flow.

For constant heating rates, the volumetric heat capacity is also taken into account:

$$R'' = \frac{R'}{\rho' C_\mathrm{p}} = \frac{\sigma_\mathrm{f} k'(1 - \nu')}{\rho' C_\mathrm{p} \alpha' E'} \quad [\mathrm{cm^2\,Ks^{-1}}]$$

where R'' states the maximum allowable rate of surface heating.

R, R', and R'' can be used for assessing and selecting optical ceramic components for use under the given thermal conditions. The higher the value of these parameters the greater the resistance to crack initiation.

Some properties and conditions leading to good TSR are

- ➢ low and linear expansion coefficients to reduce the stress associated with temperature gradients,
- ➢ high thermal conductivity to conduct heat away and minimize temperature gradients,
- ➢ high fracture toughness to improve resistance to crack propagation,
- ➢ small size components, and
- ➢ slow heating rate and uniform heating.

Infrared Material Properties at 300 K

Mechanical and thermal properties of some of the most versatile infrared optical materials are specified in the following table.

Material	CTE ($\alpha' \times 10^{-6}$ K^{-1})	ρ' [g/cm^3]	E' [Gpa]	H [Gpa]	k' [W/m·K]	C_p [J/g·K]	ν	$\overline{\sigma}_f$ [MPa]
Al_2O_3 − Sapphire	7.0	3.98	345	220.6	46	0.76	0.23	400
$Al_{23}O_{27}N_5$ − ALON	5.6	3.71	323	181.4	12.6	0.83	0.24	317
GaAs	5.7	5.32	82.7	71.7	55	0.34	0.31	116
$La_2O_3Y_2O_3$	6.6	5.13	170	75	5.3	0.48	0.30	160
LiF	34.4	2.6	64.7	9.8	11.3	1.62	0.33	110
$MgAl_2O_4$ − Spinel	6.97	3.58	193	161.3	25	0.82	0.26	276
MgF_2	13.7	3.18	138.5	49	14.5	0.24	0.28	137
MgO	10.5	3.58	300	66.2	45	0.95	0.18	310
Si	2.6	2.33	131	112.8	163.3	0.71	0.26	162
SiC	2.9	2.95	344	249	151	0.67	0.21	600
SiO_2 − Fused Silica	0.59	2.65	70.5	72.6	1.46	0.73	0.17	95
Y_2O_3	7.1	5.13	164	70.6	13	0.46	0.29	150
BaF_2	19.9	4.89	53	8	11.7	0.45	0.34	66
CaF_2	18.9	3.18	76	16.7	9.7	0.91	0.29	110
CsI	48.1	4.51	5.3	1.96	110	0.2	0.26	18
NaCl	41.1	2.16	40	1.6	6.5	0.87	0.25	37
GaAs	5.7	5.37	83	69.6	48	0.325	0.31	138
GaP	4.65	4.14	103	73.5	110	0.43	0.31	140
Ge	5.7	5.32	102.6	67.8	59	0.31	0.27	93
TiO_2 − Rutle	7.1	4.25	259	86.2	9	0.69	0.27	293
TlBr/TlI − KRS-5	58	7.37	15.8	3.9	54.4	0.2	0.37	26
TlBr-TlCl − KRS-6	50	7.18	20.7	3	70	0.19	0.22	21
ZnS (standard)	6.8	4.08	74.5	22.5	16.7	0.469	0.27	103.4
ZnS (multispectral)	6.5	4.09	85.5	10.5	27	0.527	0.27	68.9
ZnSe	7.57	5.27	67.2	11.3	18	0.356	0.28	55.1
Diamond	0.8	3.51	1143	882.6	2000	0.52	0.07	200

○ MWIR ◉ MWIR & LWIR ● LWIR
H = Hardness (1 GPa = 0.09807 Kg/mm^2)

Infrared Material Trade Names

Trademark names applied to well-known infrared materials are provided in the following table.

Trade name	Composition	Chemical Name
Irtran® 1	MgF_2	Magnesium Fluoride
Irtran® 2	ZnS	Standard Zinc Sulfide
Irtran® 3	CaF_2	Calcium Fluoride
Irtran® 4	ZnSe	Zinc Selenide
Irtran® 5	MgO	Magnesium Oxide
Irtran® 6	CdTe	Cadmium Telluride
Cleartran®	ZnS	Multispectral Zinc Sulfide
Waterclear®	ZnS	Multispectral Zinc Sulfide
Elemental®	ZnS	Elemental Zinc Sulfide
AMTIR® 1	GeAsSe	Germanium Arsenic Selenium
AMTIR® 2	AsSe	Arsenic Selenium
AMTIR® 3	GeSbSe	Germanium Antimony Selenium
AMTIR® 4	AsSe	Arsenic Selenium
AMTIR® 5	AsSe	Arsenic Selenium
AMTIR® 6	AsS	Arsenic Sulfide
AMTIR® 7	–	–
GASIR® 1	GeAsSe	Germanium Arsenic Selenium
GASIR® 5	AsSe	Arsenic Selenium
KRS® 5	Tl(Br,I)	Thallium Bromide Iodide
KRS® 6	Tl(Br,Cl)	Thallium Bromide Chloride
Corning 9754®	$GeO_2Al_2O_3$	Germanate Glass
Corning 7972® ULE	$TiSiO_2$	Titania Silicate Oxide Glass Ultra Low Expansion
N-BK®-7	BK-7	Borosilicate Crown Glass
IRG® 11	MgO	Magnesium Oxide
BS®37A & 39B	CaAl	Calcium Aluminate Glass
Ceralloy® 398J	Y_2O_3	Yttrium Oxide
Ceralloy® 408	ZrO_2	Zirconium Oxide
Tuftran®	ZnSe/ZnS	ZnSe/ZnS Composite
Suprasil® 300 Series	SiO_2	Fused Silica
Suprasil® 311 & 312	SiO_2	Fused Silica
Suprasil® 3000 Series	SiO_2	Fused Silica
lnfrasil® 301 & 302	SiO_2	Fused Silica

Irtran® – Eastman Kodak
Cleartran® or Waterclear® – CVD, Inc.
Elemental® – Raytheon
AMTIR® – Amorphous Materials
GASIR® – Umicore Electro-Optic Materials
BS® – Barr & Stroud
BK® & IRG® – Schott Glasses Technologies
Ceralloy® – Ceradyne, Inc.
Tuftran® – Rohm and Haas
Suprasil® & lnfrasil® – Heraeus Quartz

Zinc Sulfide and Zinc Selenide

Zinc sulfide (ZnS) and **zinc selenide (ZnSe)** are best made by **chemical vapor deposition (CVD)** processes.

ZnS comes in three different varieties called standard grade, multispectral ZnS (also known as Cleartran™ or Water-clear®), and elemental. The standard-grade material has a milky yellow to amber opaque color that has relatively poor transmittance in the visible and MWIR spectral regions.

Post-deposition **hot isostatic pressing (HIP)** transforms the standard grade into a crystalline lattice with virtually no defects, yielding a water-clear material with low scatter and superior transmittance from 0.4 to 12 μm.

Nevertheless, the intense heat and high pressure of the HIP process causes the grain of CVD-made ZnS to increase in size by one to two orders of magnitude, thus causing a $\sim$30% decrement in the material's mean strength.

Zinc Sulfide (ZnS)
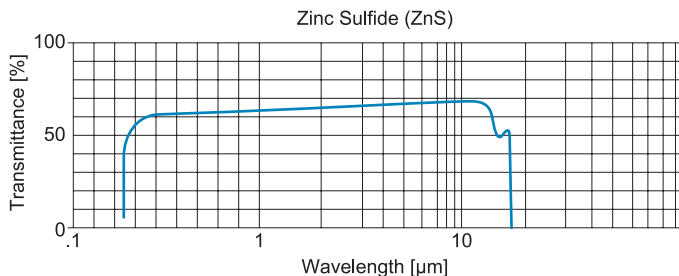
Elemental ZnS is a light yellow material with strength and hardness comparable to the standard grade, but with transmittance similar to that of Cleartran™.

ZnS provides low emissivities at high temperatures, reasonable hardness, and fairly good resistance to failure by thermal shock. Its high resistance to rain erosion, high-speed dust, and particulate abrasion makes it suitable for field applications. Oxidation-resistance coatings should be used to protect the material from reaction with air at very high temperatures.

Measured values of heat capacity and thermal conductivity of Cleartran® as a function of temperature are shown below.

Zinc Sulfide and Zinc Selenide (cont.)
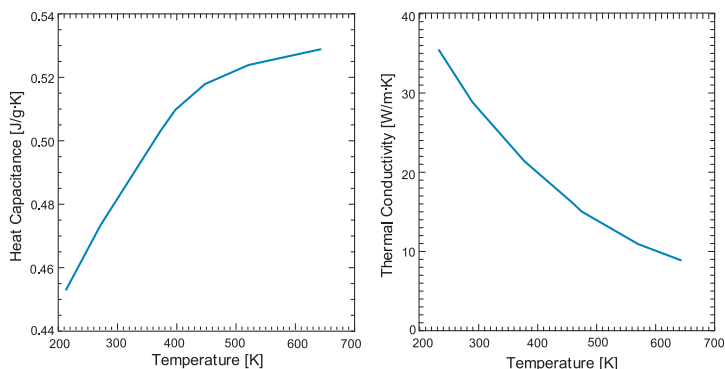
The emittance of unpolarized light at normal incidence at different spectral lines on a 5-mm thick Cleartran® window is depicted below. The emissivity increases as a function of both temperature and wavelength. Its strength increases with increasing temperature.
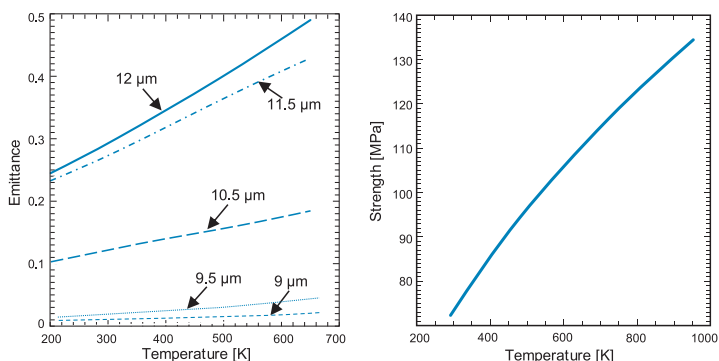
Because of its excellent optical properties, ZnS is one of the most widely used infrared materials.

ZnSe is a preferred material for the manufacture of broadband optical components such as windows, lenses, beam splitters, and optical couplers.

Its optical quality surpasses that of any of the ZnS grades, but ZnSe is softer and more brittle than ZnS. Thick coatings are required to protect this material against dust and rain at supersonic speeds.

Tuftran™

Because of its low absorptance and wide transmission range (i.e., 0.5–18 µm), ZnSe CVD is an excellent material used in many thermal imaging as well as in medium- and high-power CW CO_2 (10.6 µm) laser systems. ZnSe is non-hygroscopic and chemically stable unless treated with strong acids. It is frequently used in most industrial, field, and laboratory environments.

Zinc Selenide (ZnSe)
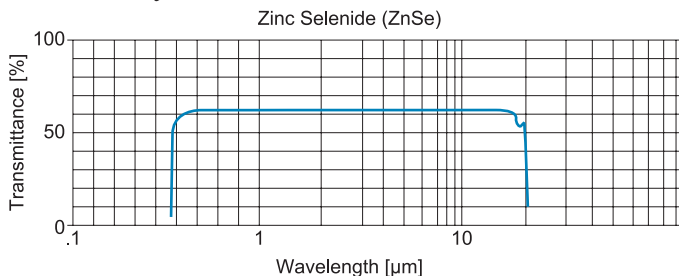
ZnSe optics are consistently made in diameters of 5–300 mm; however, customized large-size optics (e.g., >1 m in diameter) can be fabricated as well.

Tuftran™ is an infrared material comprising a polished ZnSe window over which a 1-mm coating layer of ZnS is chemically vapor deposited. This hybrid optical component features the mechanical toughness of ZnS while conserving the wide spectral waveband of ZnSe.

ZnSe window = 5 mm; ZnS coating = 1 mm
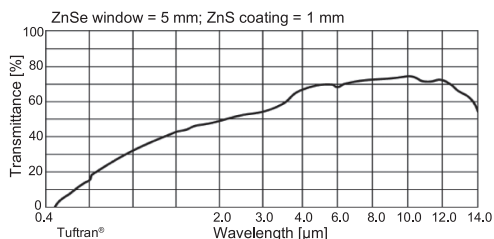
The thick ZnS coating protects the ZnSe window and enhances the material's environmental durability, making it better able to resist rain, dust, and dirt. The resulting material offers high physical hardness, non-hygroscopicity, and excellent optical characteristics. Tuftran™ components have been produced in plates up to 60 cm in diameter.

Sapphire

Chemically, **sapphire** is single-crystal **aluminum oxide (Al_2O_3)**; its transmittance extends from 0.15 to 5.5 μm. Sapphire optical components (e.g., windows, wafers, flats, and waveplates) provide exceptional surface hardness, high melting point, and excellent thermal stability. Sapphire is also a great thermal conductor and a superior dielectric material; its high dielectric constant makes it inert and insoluble in water, common acids, and alkalis. Due to its high modulus of elasticity and high tensile strength, synthetic sapphire is extremely durable and impact resistant.

Nevertheless, given the extreme hardness of this material (i.e., second only to diamond), sapphire is difficult and expensive to cut, grind, and polish into a final optical component. Moreover, sapphire is a birefringent material.

Synthetic sapphire can be grown in all common crystal orientations, including the *a*, *c*, *r*, and *m* planes, as shown in the center diagram below. For optical applications requiring low birefringence, the single crystal is specified as zero degree, or c-cut, meaning that the optical axis of the material should be perpendicular to the plane of the window.
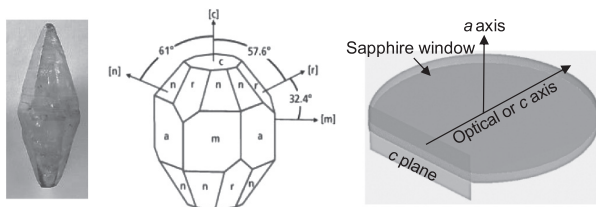
Conversely, when making sapphire waveplates, the single-crystal boule is grown and cut at an orientation that maximizes the birefringence.
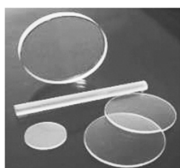
There is no universal grading system used by manufacturers of synthetic sapphire. Therefore, its quality is graded by the application requirements and specifications.

ALON and Spinel

Aluminum oxynitrite (Al$_{23}$O$_{27}$N$_5$) termed **ALON** and **magnesium aluminate (MgAl$_2$O$_4$)**, commonly known as **spinel**, are transparent polycrystalline ceramic materials with physical properties similar to sapphire. Their advantage is that these isotropic cubic crystal structures are nonbirefringent and have a high degree of temperature stability. Their transmission window spans the near ultraviolet to ∼6 μm.
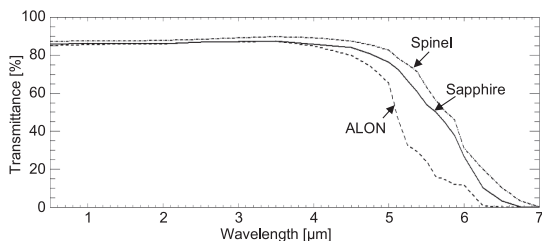
Unlike sapphire, ALON and spinel can be fabricated using sinter/HIP and LiF-doped/HIP. These materials are not limited by slow growth, and large-sized (>50 cm) and/or complex shapes are attainable.

The temperature and wavelength dependence of sapphire, ALON, and spinel versus the absorption coefficient α is shown below. The emittance is directly proportional to α.
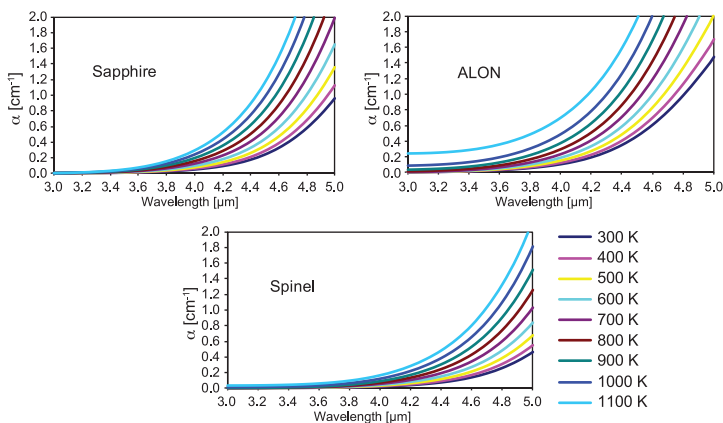
Yttria

Yttria (Y_2O_3) has excellent optical performance from 0.29 to 8.0 µm at both ambient and elevated temperatures. This material shows a weak absorption band around 2.75 µm.
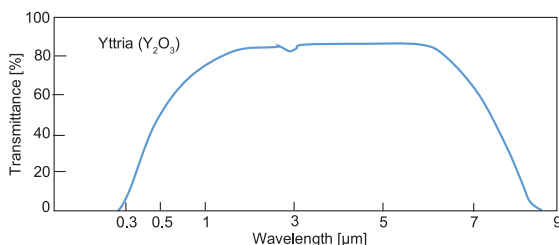
Transparent yttria ceramics are produced with high optical quality and tested as windows and domes. Conventional yttria has a mean strength of 150 MPa. Although conventional yttria's strength and hardness are lower than the more durable but less transmitting MWIR materials (sapphire, ALON, spinel), its thermal shock performance is similar. Substantial strengthening of this infrared material will enable additional DoD applications.

With a melting point of 2430 °C, yttria is an oxide that wears down the diamond point too rapidly to be diamond-turned. Its erosion resistance is considered to be intermediate among the oxides, but outstanding compared to non-oxide infrared transmitting materials. Yttria exhibits very low emissivity, which limits background radiation upon heating.
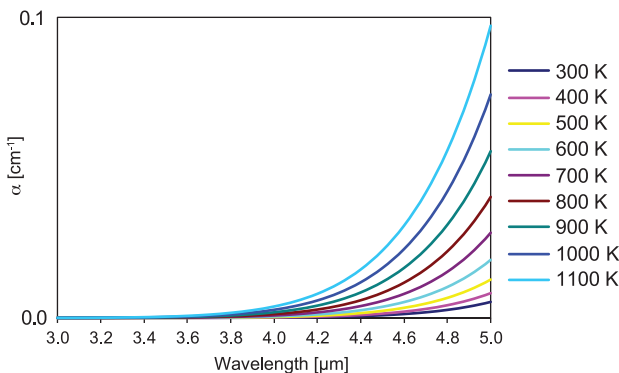
Silicon and Germanium

Silicon (Si) is a very useful material in the 1- to 8-μm and 48- to 100-μm (astronomical applications) spectral bands. Optical-grade polycrystalline silicon is used to make lenses, domes, and windows. Due to its high thermal conductivity, it is a very good substrate for high-power lasers. Silicon has modest rain erosion resistance and inferior sand erosion resistance.
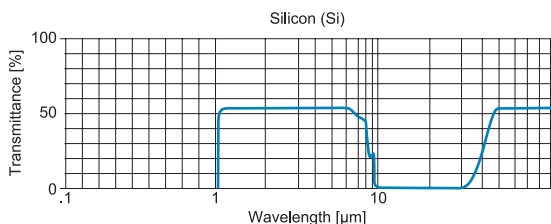
Germanium (Ge) is a multipurpose IR material that provides excellent transmittance in the 1.8- to 18-μm spectral range. It has the highest index of refraction of any commonly used IR material, which results in high Fresnel losses and less than 50% transmittance without the use of AR coatings. Standard optical-grade Ge has an absorption coefficient no greater than 0.035 cm^{-1} at 10.6 μm at 25 ˚C.
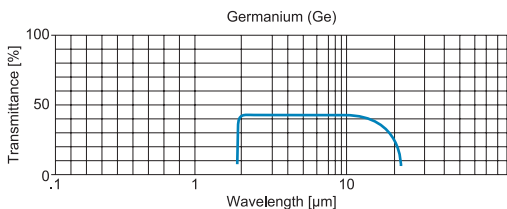
The upper operating temperature of Ge is about 100 ˚C and is limited by intraband absorption. Ge is non-hygroscopic and has good thermal conductivity, excellent surface hardness, and good strength. Its high index of refraction (e.g., 4.0038 at 10.6 μm) makes it useful in lens design. Ge has a large thermo-optic coefficient (dn/dT), causing large focal shifts with temperature that can make athermalization of an optical system difficult. The high refractive indices of both Si and Ge require the use of AR coatings.

Gallium Arsenide

Gallium arsenide (GaAs) optical-grade material has a low absorption coefficient (less than 0.02 cm^{-1}) from 0.9 to 17.3 µm. It is particularly useful in applications where toughness and durability are important. The material is non-hygroscopic, safe to use in laboratories and field applications, and chemically stable except when in contact with strong acids. The use of GaAs will extend optics lifetime in cases where frequent cleaning by wiping is required.

Gallium Arsenide (GaAs)
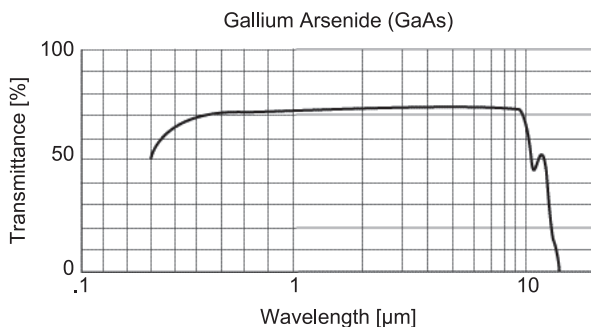
GaAs hardness and strength are similar to those of Ge. Like Ge and Si, GaAs is rather reflective (e.g., $n_{GaAs} = 3.303$ at 4 µm) and requires AR coatings.

When an optical component such as a cold filter is exposed to cryogenic temperatures, GaAs is sometimes preferred over Si because it has a better CTE match to the coating materials, thus reducing the risk of the coating cracking. Furthermore, GaAs has a higher bandgap than Si; therefore, it can be used in higher temperatures (460 °C versus 250 ˚C) without significant free-carrier absorption. GaAs also provides an alternative to ZnSe in medium- and high-power laser systems for lenses and beam splitters. GaAs optical-grade material is generally more expensive than Ge and ZnSe.

Single-point diamond turning is an effective technique to polish and shape materials such as ZnS, ZnSe, Si, Ge, and GaAs. Nevertheless, sapphire, spinel, ALON, and yttria are not diamond-turnable materials because they wear out the diamond-turning tools at a much faster rate, thus making it more difficult and costly to produce and polish aspheric and other complex optical surfaces.

CVD Diamond

Synthetic monocrystalline and polycrystalline diamond prepared by CVD techniques has excellent transparency from the ultraviolet to the far infrared. It exhibits absorption in the MWIR, thus limiting its usefulness in this spectral region as a thin protective film.
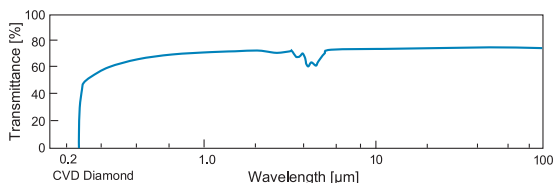
CVD diamond exhibits low thermal expansion, unsurpassed hardness, exceedingly high thermal conductivity, and thermal shock resistance. It is not affected by any acid or other chemicals and can handle extreme thermal and/or thermomechanical loads. Furthermore, its large bandgap (5.45 eV) allows the material to remain transparent at elevated temperatures.
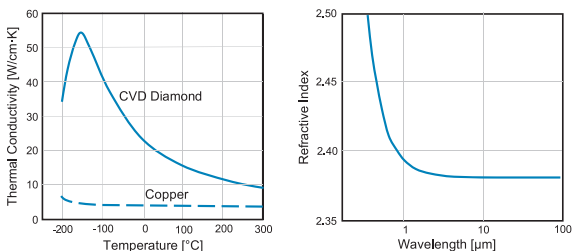
Diamond's exceptional properties derive from its strong tetrahedral covalent bonding between its four nearest neighbors, linked in a highly dense cubic lattice (1.76×10^{23} atoms/cm^3). The grain size in optical diamond windows is in the submicron range at the beginning of diamond growth. As the optical element increases in thickness, the grains grow larger. The mechanical strength is inversely proportional to the square root of the grain size. Optical-grade CVD diamond is typically grown at a rate of 3 μm/h.

Chalcogenide Glasses

The word **amorphous** is used to indicate the noncrystalline nature of IR glasses. **AMTIR** is the acronym for **amorphous material transmitting IR radiation**.

AMTIR began as a development in molding technology, where it was required to produce infrared lenses from chalcogenide glasses. When heated, **chalcogenide glasses** behave like plastics, (i.e., their viscosity progressively decreases). At certain temperatures, the viscosity is ideal for these glasses to precisely duplicate the surface of a mold. Spherical, aspherical, and diffractive optical surfaces can be produced by conventional grinding and polishing, single-point diamond turning, or molding.

The superb optical transmittance, small thermal change in refractive index, and low dispersion of these glasses enable the design of color-corrected optical systems without thermal defocusing. Other trademark names for infrared chalcogenide glasses are GASIR®, OPTIR®, and Schott IRG and IG. The CTEs of AMTIR-5, GASIR-5, IG-6, IRG-26, and IRG-27 are rather similar to that of aluminum, thus keeping athermal performance while reducing system complexity and cost.
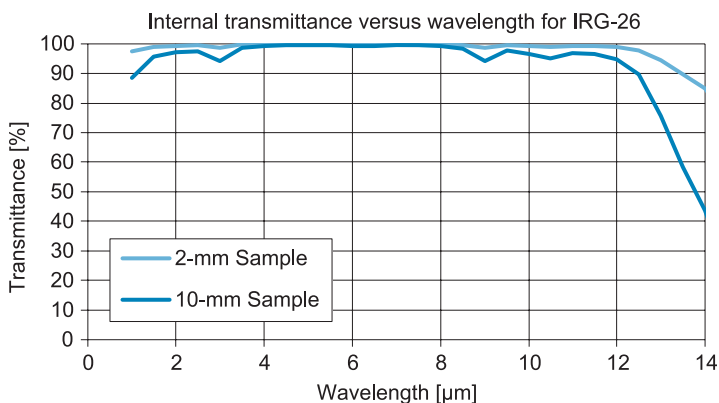
Figure adapted from Schott North America, Inc. https://www.us.schott.com/

Chalcogenide Glasses (cont.)

Property	AMTIR-1	AMTIR-2	AMTIR-3	AMTIR-4	AMTIR-5	AMTIR-6	C1
Composition	GeAsSe	AsSe	GeSbSe	AsSe	AsSe	AsS	AsSeTe
Transmittance Range [μm]	0.7–12	1–14	1–12	1–12	1–12	0.6–8	1.2–14
Refractive Index @ 10 μm	2.4981	2.7703	2.6027	2.646	2.7423	2.3807	2.8051
$dn/dT \times 10^{-6}$ @ 10 μm [°C^{-1}]	72	30.7	91	–19	20	<1	31
Knoop Hardness – H [Gpa]	170	110	150	84	87	109	110
CTE ($\alpha' \times 10^{-6}$ K^{-1})	12	22.4	14	27	23.7	21.6	23
k' [W/m·K]	25.12	22.19	22.19	22.19	23.86	16.75	21.77
C_p [J/g·K]	0.3	0.28	0.27	0.36	0.32	0.46	0.26
ρ' [g/cm^3]	4.4	4.66	4.67	4.49	4.51	3.2	4.69
$\bar{\sigma}_f$ [Mpa]	18.6	17.2	17.2	16.2	16.5	16.5	17.2
E [Gpa]	22.1	38.6	21.4	15.2	17.6	15.8	12.4
ν	0.27	0.29	0.26	0.297	0.279	0.24	0.29
Transition Temperature [°C]	405	188	295	131	170	210	154

Table adapted from Amorphous Material, Inc. www.amorphousmaterials.com/products/

Antireflection Coatings on High-Index Substrates

The simplest form of **antireflection (AR)** coating is a single homogeneous quarter-wave layer.

$$\rho_a = \left(\frac{n_0 - n_{f1}}{n_0 + n_{f1}}\right)^2$$

$$\rho_b = \left(\frac{n_{f1} - n_s}{n_{f1} + n_s}\right)^2$$
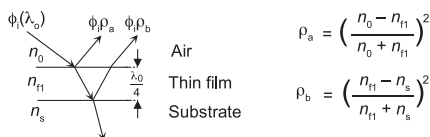
Zero reflectance occurs when the intensities of the light reflected at the upper and lower boundaries of the thin film are identical, which implies that

$$\frac{n_{f1}}{n_0} = \frac{n_s}{n_{f1}} \quad \text{or} \quad n_{f1} = \sqrt{n_0 n_s}$$

The quarter-wave-layer optical thickness ensures that the relative phase shift between the two reflected beams is 180 deg, thus causing destructive interference. The limitation of a single-layer coating is that it produces zero reflectance at merely λ_0.

A **high-efficiency broadband AR (HEBBAR)** coating requires a multilayer coating. For example, a three-layer coating must satisfy these constraints:

$$n_{f1} = \sqrt[4]{n_0^3 n_s}, \;\; n_{f2} = \sqrt[4]{n_0^2 n_s^2}, \quad \text{and} \quad n_{f3} = \sqrt[4]{n_0 n_s^3}$$

where $n_0 < n_{f1} < n_{f2} < n_{f3} < n_s$, and each layer is $\lambda_0/4$.

The tensile or compressive stress caused by the CTE mismatch between the substrate and coating is given by

$$\sigma_f' = \frac{E_f'(\alpha_f' - \alpha_s')(T - T_0)}{1 - \nu}$$

where T is the stress-free condition temperature, T_0 is the operational temperature, and α_f' and α_s' are the CTEs of the thin film and substrate, respectively. The stress-induced deflection of a circular substrate disk with diameter D and thickness t is

$$\Delta x = \frac{3(1 - \nu_s')\delta_f D^2 \sigma_f'}{4 E_s' t^2}$$

where δ_f is the thickness of the thin film coating.

AR Surfaces Based on Nanostructure Arrays

An AR coating based on a **nanostructure array (NSA)** enthused by "moth's eye" structures provides another way of reducing reflectance. A subwavelength-size NSA leads to a gradient in refractive index between the air and the substrate surface, which is optically equivalent to a laterally nonstructured thin film with a gradual change of the refractive index in depth.
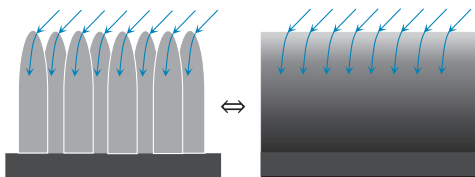
This periodical structure of protuberances can realize broadband, omnidirectional, and polarization-insensitive AR performance. NSAs can be lithographically patterned with distinctive refractive index profiles, such as linear, parabolic, cubic, exponential, exponential-sinusoidal, etc., thus exhibiting different AR performances. Numerical computation based on effective medium theory (EMT) or alternatively, rigorous coupled-wave analysis (RCWA), are essential to conducting the optimization of AR structures and coatings.

AR coatings can be developed to protect against erosion and particle impact at high speeds. They provide scratch resistance and can sometimes enhance the mechanical strength of substrates. For example, diamond-like carbon (DLC) and germanium-carbon are used for protection against abrasion, and they adhere well to Si, Ge, and ZnS. Boron with gallium phosphide (BP/GaP) is an excellent erosion-resistant thin film composite material but has high emittance at elevated temperatures. A sputtered layer of ZnS on a bulk ZnS substrate is called a REP coating, which stands for rain erosion protection. Diamond is unarguably the best erosion-resistant coating material as it can be grown directly on Si by CVD and can be attached to ZnS and ZnSe using optical brazing processes.

Pressure Windows: Calculation

The diameter-to-thickness ratio of a circular optical window is given by

$$\frac{t_c}{D} = \frac{1}{2}\sqrt{\frac{\chi\sigma'_f}{\sigma_{max}}}$$

where χ is an empirical constant that takes a value of 0.75 for a clamped window and 1.125 for an unclamped window (i.e., 50% greater).

For a rectangular window, the diameter-to-thickness ratio becomes

$$\frac{t_r}{L} = \sqrt{\frac{\chi\sigma'_f}{2\sigma_{max}[1 + (L/W)^2]}}$$

where L and W are the length and width of the window, respectively.

The unclamped condition may be used if soft gaskets are employed within the clamped mounting structure. The CTE mismatch between the materials must be taken into consideration.

Examples: Determine the thicknesses of a multispectral ZnS-clamped window and a sapphire-infrared-clamped window. Both circular windows are 25 mm in diameter and must endure a stress of 10 MPa. Use SF = 4.

$\overline{\sigma}_{f\text{-mean\_ZnS}} = 70$ MPa for ZnS
$\overline{\sigma}_{f\text{-mean\_sapphire}} = 400$ MPa for sapphire

$$t_{c\_ZnS} = \frac{25}{2}\sqrt{\frac{4 \cdot 0.75 \cdot 10}{70}} = 8.2 \text{ mm}$$

$$t_{c\_sapphire} = \frac{25}{2}\sqrt{\frac{4 \cdot 0.75 \cdot 10}{400}} = 3.4 \text{ mm}$$

Mirrors

Mirrors are characterized by their surface reflectivity and polish, as well as by the properties of the substrates on which these polishes are established. In general, mirrors are fabricated by applying a reflective coating to a suitable substrate. High-quality mirror surfaces must have a high degree of flatness and surface roughness smaller than the radiation wavelength. They must also provide durable, stable, and easy-to-clean surfaces.

Plots of reflectance versus wavelength for commonly used metallic coating materials are shown. Aluminum is widely used because it offers an average reflectance of 96% throughout the visible, near infrared, and near-ultraviolet regions of the spectrum. Alternatively, silver exhibits higher reflectance (98%) throughout most of the visible and IR spectrum. However, it oxidizes faster; reducing its reflectance and causing light to scatter. On the other hand, bare gold combines good tarnish resistance with consistently high reflectance (99%) through the near, middle, and far-infrared regions. All of the metals exhibit higher reflectance at long wavelengths.
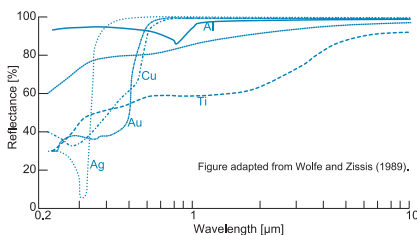
Figure adapted from Wolfe and Zissis (1989).

Metallic reflective coatings are delicate and require care during cleaning. Therefore, metallic coatings that are overcoated with a single, hard dielectric layer of half-wave optical thickness improve abrasion and tarnish resistance. Depending on the dielectric used, such coatings are referred to as **durable**, **protected**, or **hard coated**. The reflectance of metallic coatings can also be increased over the desired spectral range or for different angles of incidence by overcoating it with a quarter-wave stack of multilayer dielectric film, said to be **enhanced**.

Metallic coatings can have inconsistent thickness variation, which distorts the wavefront of the reflected beam.

Mirrors (cont.)

Moreover, CTE differences between the substrate and coating materials affect the mirrors' permanence.

Modern polishing techniques can yield a precision-quality surface finish of less than 20 Å rms on pure metal substrates, thus eliminating the need for metallic coatings. Pure metal optics mirrors offer a hard, scratch-resistant surface with little thermal distortion. For high-energy laser (HEL) applications, a mirror's ability to conduct heat is an essential property.

Mirror substrates include glass, ceramic, metals, metal alloys, and composites. A list of materials and properties of common mirror substrates is provided in the table.

Material	CTE $(\alpha' \times 10^{-6} \, \text{K}^{-1})$	$\rho'[\text{g/cm}^3]$	$E'[\text{Gpa}]$	$k'[\text{W/m} \cdot \text{K}]$	$C_p[\text{J/g} \cdot \text{K}]$	ν
Glasses and Crystalline Ceramics						
Borosilicate	3.2	2.23	68	1.13	0.105	0.2
Cer-Vit	0.05	2.53	91.0	1.61	0.82	0.24
Fused Silica	0.5	2.65	70.5	1.46	0.73	0.17
N-BK7	7.1	2.51	82	1.11	0.86	0.206
Single-Crystal Si	2.6	2.33	131	156	0.71	0.42
Soda-Lime Flat	8.6	2.44	74	0.94	0.21	0.22
ULE®	0.03	2.21	67	1.3	0.77	0.17
ZERODUR®	0.05	2.53	90.3	1.46	0.8	0.24
Metals, Metal Alloys, and Composites						
Aluminum	23.0	2.7	72.0	227	0.87	0.34
Aluminum SXA™	12.4	2.91	117.0	123	0.87	0.29
Beryllium I-70	11.3	1.85	287	216	1.92	0.043
Copper OFHC	16.5	8.94	117	391	0.38	0.34
Copper Glidcop™	16.6	8.84	130	365	0.38	0.33
CFRP	0.2	1.8	105	10.0	0.712	0.32
Electroless Nickel	12.5	8.0	110	7.4	0.46	0.41
Electrolytic Nickel	13.4	8.9	199.5	70	0.46	0.3
Invar 36	0.5	8.05	141	10.4	0.52	0.26
Super Invar	0.05	8.13	148	10.5	0.51	0.26
Molybdenum	4.8	10.22	324.8	142	0.28	0.29
Steel − Stainless	11.0	7.75	210	251	0.502	0.28
SiC CVD	2.4	3.21	461	198	0.73	0.21
SiC RB 30% Si	2.5	2.91	413	155	0.67	0.24
Titanium	12.0	4.65	100	21.9	0.523	0.36

OFHC − Oxygen-free high thermal conductivity
CFRP − Carbon-fiber-reinforced polymer

Solid Angle

The **solid angle** Ω in 3D space measures a range of pointing directions from a point to a surface. It is defined, assuming paraxial approximation, as the element of the area of a sphere divided by the square of the radius of the sphere. The solid angle is dimensionless and measured in square radians or **steradians [sr]**.
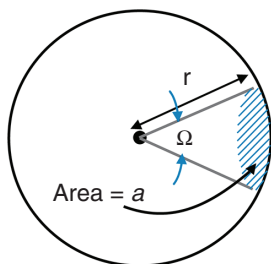
For example, the area of a full sphere is given by $4\pi r^2$; therefore, its solid angle is 4π. A hemisphere contains half as many radians as a sphere (i.e., $\Omega = 2\pi$).

$$\Omega = \frac{a}{r^2} \quad a << r^2$$

When large angles are involved, a more exact definition is required. Using spherical coordinates, the solid-angular subtense can be expressed as a function of a flat disc or planar angle θ as

$$d\Omega = \frac{da}{r^2} = \sin\theta \, d\theta \, d\varphi$$

Integrating over the acceptance cone,
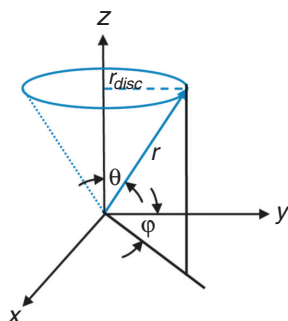
$$\Omega = \int_0^{2\pi} d\varphi \int_0^{\theta_{max}} \sin\theta \, d\theta = 2\pi(1 - \cos\theta_{max}) = 4\pi\sin^2\frac{\theta_{max}}{2}$$

is obtained.

If the disc is tilted at a selected angle γ, its differential solid angular subtense is decreased by a factor of $\cos\gamma$.

$$d\Omega' = d\Omega\cos\gamma$$
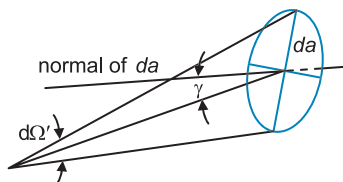
Radiometry

Radiometry is a quantitative understanding of flux transfer through an optical system. Given the radiation from a thermal source transmitted through the optics of an infrared system, the fundamental question is how much of the source power is collected by the infrared sensor. Radiometric calculations predict the system's **signal-to-noise ratio (SNR)**.

Understanding the radiometric terms and their units is the key to performing radiometric calculations.

Symbol	Radiometric Term	Units
Q_e	Radiant energy	Joule
ϕ_e	Radiant power or flux	Watt
I_e	Radiant intensity	Watt/sr
M_e	Radiant exitance	Watt/cm^2
E_e	Irradiance	Watt/cm^2
L_e	Radiance	Watt/cm$^2 \cdot$ sr
Q_p	Photon energy	Photon or quantum
ϕ_p	Photon flux	Photon/sec
I_p	Photon intensity	Photon/sec $\cdot$ sr
M_p	Photon exitance	Photon/cm$^2 \cdot$ sec
E_p	Photon irradiance	Photon/cm$^2 \cdot$ sec
L_p	Photon radiance	Photon/sec $\cdot$ cm$^2 \cdot$ sr

Subscript e = energy-derived units; subscript p = photon rate quantities.

Conversion between the two sets of units is done with the formula that determines the amount of energy carried per photon:

$$\mathcal{E} = \frac{hc}{\lambda}; \ \Rightarrow \ \phi_e[\text{W}] = \phi_p[\text{photon/sec}] \cdot \mathcal{E}$$

where h is Planck's constant, c is the speed of light, and λ is the wavelength. Photon-derived units are useful when considering an infrared sensor (e.g., photovoltaic) that responds directly to photon events rather than to thermal energy (e.g., microbolometer).

The energy carried per photon is inversely proportional to the wavelength; therefore, a short-wavelength photon carries more energy than a long-wavelength photon. The energy carried per photon can also be explained as the number of photons per second it takes to produce 1 W.

Radiometric Terms

Flux: a quantity propagated or spatially distributed according to the laws of geometrical optics.

Both **irradiance** and **exitance** have units of spatial power density; however, the terms have different interpretations. The exitance is the power per unit area leaving a surface, thus describing a self-luminous source. It is defined as the ratio of the differential flux to the source area from which it is radiating as the area is reduced to a point:

$$M = \frac{\partial \phi}{\partial A_s}$$

where the total flux radiated into a hemisphere is given by

$$\phi = \int M \cdot \partial A_s$$
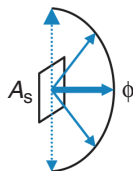
$\phi = MA_s$ for small but final quantities.

Equivalently, irradiance is a measure of the total incident flux per unit area on a passive receiver surface (e.g., sensor). It is defined as the ratio of power to the area upon which it is incident as the area is reduced to a specific position:

$$E = \frac{\partial \phi}{\partial A_d} \quad \Rightarrow \quad \phi = \int E \cdot \partial A_d$$

The **intensity** is the radiant power per unit solid angle as the solid angle is reduced in value to a specific direction.

$$I = \frac{\partial \phi}{\partial \Omega} \quad \Rightarrow \quad \phi = \int I \cdot \partial \Omega$$
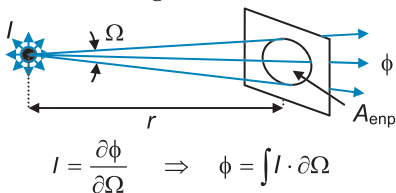
Intensity is used to characterize the amount of flux radiated from a **point source** that is collected by the entrance pupil.

The intensity varies as a function of the view angle and can be written as $I = I_0 \cos \theta$, where I_0 is the intensity in the direction normal to the surface.

Both the flux and the irradiance decrease as "one-over-squared fall off":

$$\phi = I \cdot \Omega = I \frac{A_{enp}}{r^2}; \quad E = \frac{\phi}{A_{enp}} = \frac{I}{r^2}$$

Field Guide to Infrared Optics, Materials, and Radiometry

Radiometric Terms (cont.)

Radiance is the most general term to describe source flux because it includes both positional and directional characterization. It is used to characterize extended sources, i.e., sources that have appreciable area compared to the square of the viewing distance. The visual equivalent of the radiance is the term "brightness."
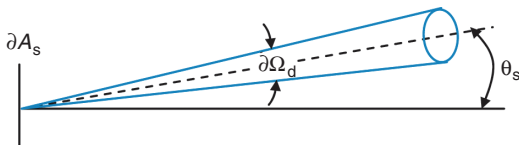
The radiance is defined for a particular ray direction as the radiant power per unit projected source area (perpendicular to the ray) per unit solid angle:

$$L \equiv \frac{\partial^2 \phi}{\partial A_s \cos \theta_s \partial \Omega_d}; \quad \Rightarrow \quad \partial^2 \phi = L \partial A_s \cos \theta_s \partial \Omega_d$$

which is the **fundamental equation of radiation transfer**. The term $\partial^2 \phi$ is the power radiated into the cone and is incremental with respect to both the area of the source and the solid angle of the receiver.

For small but final source area and detector solid angle quantities,

$$\phi \cong L A_s \cos \theta_s \Omega_d$$

A **Lambertian radiator** emits radiance that is independent of angle (i.e., the radiance is isotropic and is equally uniform in each direction within the hemisphere). The transfer equation can be applied to a Lambertian emitter to obtain the relationship between radiance and exitance:

$$M = \frac{\partial \phi}{\partial A_s} = \int_{\Omega_d} L \cos \theta_s \partial \Omega_d = \int_0^{2\pi} d\varphi \int_0^{\pi/2} L \cos \theta_s \sin \theta_s d\theta_s = \pi L$$

Similarly, the intensity can be obtained by integrating the fundamental equation with respect to the source area:

$$I = \frac{\partial \phi}{\partial \Omega_d} = \int_{A_s} L \cos \theta_s dA_s = L A_s \cos \theta_s$$

Flux Transfer

The fundamental equation of radiation transfer states that an element of power is given by the radiance times the product of two projected areas, divided by the square of the distance between them. Assuming normal angles of incidence (i.e., $\theta_s = \theta_d = 0$),

$$A_s \Omega_d = A_d \Omega_s$$
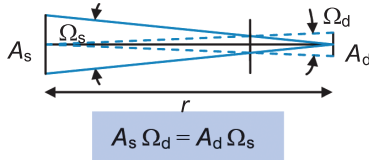
$$\phi = LA_s\Omega_d = L\frac{A_sA_d}{r^2} = L\Omega_sA_d$$

Two equivalent expressions in terms of area solid angle product are obtained by grouping either the source or the detector area with r^2.

This relationship, defined as the so-called **AΩ product**, is completely symmetrical and can be used to calculate the power in either direction of the net power flow. It is also known as the **optical invariant**, **throughput**, or **étendue**.

In the case where the detector is tilted ($\theta_d \neq 0$), the flux decreases by the cosine of the angle:

$$\phi = LA_s\frac{A_d \cos\theta_d}{r^2}$$
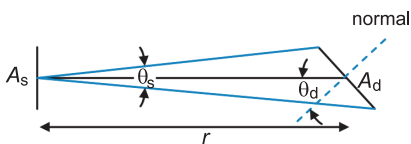
Consider the case for $\theta_s \neq 0$ but $\theta_d = 0$, where the flux decreases in proportion to $\cos^3\theta_s$:
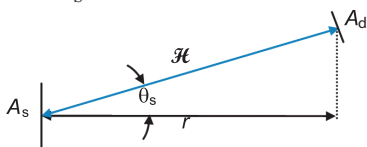
$$\phi = LA_s\cos^3\theta_s\frac{A_d}{r^2}$$

The last case is when $\theta_d = \theta_s \equiv \theta \neq 0$, which leads to the most realistic situation, the so-called **cosine fourth law**:

$$\phi = LA_s\cos^4\theta\frac{A_d}{r^2}$$
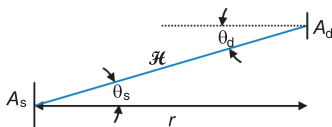
Flux Transfer for Image-Forming Systems

For purposes of simplification, the cosine projections are dropped (i.e., paraxial approximation), in which case the flux transfer is simply described in terms of the $A\Omega$ product.
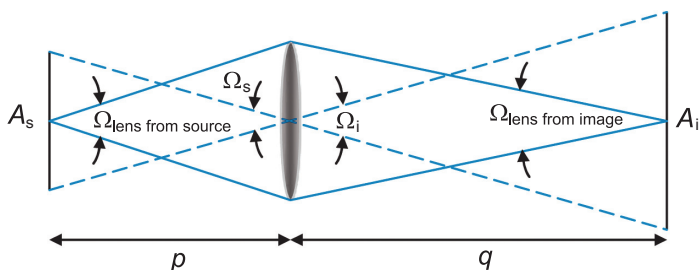
Recalling the area or longitudinal magnification equation, the total flux collected by the optical system may be calculated by one of the following flux-transfer equations:

$$\phi = L_s A_s \Omega_{\text{lens from source}} = L_s A_s \frac{A_{\text{lens}}}{p^2}$$

$$\phi = L_s A_i \Omega_{\text{lens from image}} = L_s A_i \frac{A_{\text{lens}}}{q^2}$$

$$\phi = L_s A_{\text{lens}} \Omega_s = L_s A_{\text{lens}} \frac{A_s}{p^2}$$

$$\phi = L_s A_{\text{lens}} \Omega_i = L_s A_{\text{lens}} \frac{A_i}{q^2}$$

In paraxial approximation, the lens aperture acts as the intermediate receiver. In more complex optical systems, the entrance pupil is the intermediate receiver.

Source Configurations

The source may be idealized as either a **point source** or a uniform **extended-area source**. A point source cannot be resolved by the optical system. It is smaller than the projection of the resolution spot at the object plane. An extended source, on the other hand, has an appreciable area compared to the detector's footprint.
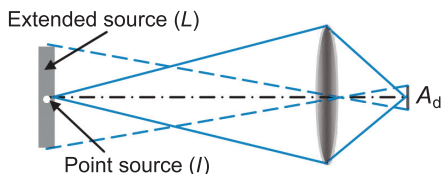
It is appropriate to use **radiance** in characterizing radiant flux from an extended-area source, while it is appropriate to use **intensity** to characterize radiation from a point source.

The source power collected by the lens is imaged onto the detector focal plane. The **image irradiance** for a distant extended-area source can be calculated directly using a large **Lambertian disc**, which can represent the actual extended source or an intermediate source such as a lens.
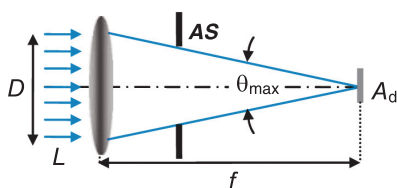
An extended source fills the FOV such that the solid angle is bounded by the marginal rays and limited by the aperture stop.

Using a Lambertian disc, the following relationships are derived:
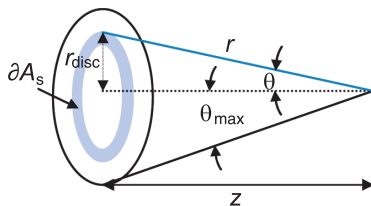
$$r_{\text{disc}} = z\tan\theta \Rightarrow dr_{\text{disc}} = d(z\tan\theta) = z\sec^2\theta\, d\theta = \frac{z}{\cos^2\theta}\, d\theta$$

$$A_{\text{s}} = \pi r_{\text{disc}}^2 \Rightarrow dA_{\text{s}} = 2\pi r_{\text{disc}}dr_{\text{disc}} = 2\pi z^2\tan\theta\,\frac{d\theta}{\cos^2\theta}$$

Field Guide to Infrared Optics, Materials, and Radiometry

Source Configurations (cont.)

The transfer flux is obtained by integrating the fundamental equation of radiation transfer over the source and detector areas:

$$\phi_d = L \iint_{A_s A_d} \partial A_s \cos\theta_s \partial\Omega_d = L \iint_{A_s A_d} \partial A_s \cos\theta_s \frac{\partial A_d \cos\theta_d}{r^2}$$

$$\phi_d = L \iint_{\theta A_d} 2\pi z^2 \tan\theta \frac{d\theta}{\cos^2\theta} \cos^2\theta \left(\frac{\cos^2\theta}{z^2}\right) \partial A_d$$

$$\phi_d = 2\pi L A_d \int_0^{\theta_{max}} \sin\theta\cos\theta d\theta = \pi L A_d \sin^2\theta_{max}$$

The irradiance on a detector from an extended-area source is then obtained by dividing the transferred flux by the area of the detector:

$$E_{\text{extended source}} = \frac{\phi}{A_d} = \pi L \sin^2\theta_{max} = \frac{\pi L}{4(F/\#)^2 + 1}$$

For an extended-area source, the image irradiance depends only on the source radiance and the *F*/# of the optical system.

In the case of a point source, the collected power is defined by the intensity times the solid angle of the optics:

$$\phi = I \cdot \Omega_{\text{opt}} = I \cdot \frac{A_{\text{opt}}}{p^2}$$
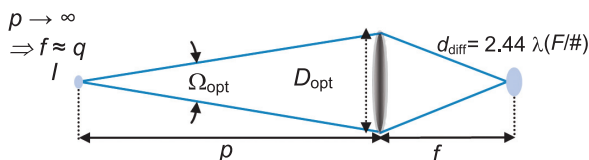
If the optics is diffraction limited, 84% of the flux transfer is concentrated into the image spot; therefore, the average irradiance of a point source at the detector plane is given by

$$E_{\text{point source}} = \frac{\phi}{A_d} \times 0.84 = \frac{0.84 I \Omega_{\text{opt}}}{\frac{\pi}{4} d_{\text{diff}}^2} = \frac{0.84 I \Omega_{\text{opt}}}{\frac{\pi}{4}[2.44\lambda(F/\#)]^2}$$

Blackbody Radiators

Empirically, it is found that solid bodies heated to incandescent temperatures emit radiation primarily in the infrared portion of the spectrum, and these incandescent sources emit their radiation in a continuous wavelength rather than at discrete spectral lines.

To describe radiation that emits a finite total power distributed continuously over wavelength, **spectral radiometric quantities** with units per micron of wavelength interval are used. The weighted spectral quantities are denoted with a subscript λ (e.g., $M_{e,\lambda}$ is the spectral exitance in W/cm^2 μm). In-band nonspectral quantities are obtained by integrating the spectral terms over any spectral interval; for example,

$$L = \int_{\lambda_1}^{\lambda_2} L_\lambda d\lambda, \quad M = \int_{\lambda_1}^{\lambda_2} M_\lambda d\lambda, \quad \phi = \int_{\lambda_1}^{\lambda_2} \phi_\lambda d\lambda$$

The term **blackbody (BB)** is used to describe a perfect radiator (i.e., an idealized thermal source). A blackbody absorbs all of the radiant energy; as a consequence, it is the perfect emitter. BBs have the maximum possible spectral exitance for a body at a specified temperature, either over a particular spectral region, or integrated over all wavelengths. They are a convenient baseline for radiometric calculations because any thermal source at a specified temperature is constrained to emit less radiation than a blackbody source at the same temperature.

BB radiation is also called **cavity radiation**. Virtually any heated cavity with a small aperture produces high-quality radiation. These blackbody simulators are used primarily
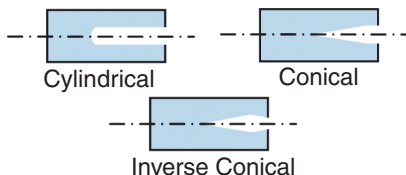
as laboratory calibration standards. The most popular blackbody cavities are cylinders and cones, the latter being the most common.

Cylindrical   Conical

Inverse Conical

The aperture of the cavity defines the area of the source. Some commercial blackbodies have an aperture wheel that allows a choice of source area.

Planck's Radiation Law

The radiation characteristics of ideal blackbody surfaces are completely specified if the temperature is known. Blackbody radiation is specified by **Planck's equation** and defines the spectral exitance as a function of absolute temperature and wavelength:

$$M_{e,\lambda} = \frac{2\pi hc^2}{\lambda^5} \frac{1}{\exp(hc/\lambda kT) - 1}$$

$$= \frac{c_1}{\lambda^5} \frac{1}{\exp(c_2/\lambda T) - 1} \, [\text{W/cm}^2 \cdot \mu\text{m}]$$

where h is Planck's constant: 6.626×10^{-34} J · sec; k is Boltzmann's constant: 1.3806×10^{-23} J/K; T is the absolute temperature in degrees Kelvin [K]; λ is the wavelength in centimeters [cm]; c is the speed of light in vacuum: 2.998×10^{10} cm/sec; c_1 is the first radiation constant: $2\pi hc^2 = 3.7415 \times 10^4$ W/cm^2 · μm^4; and c_2 is the second radiation constant: $hc/k = 1.4382$ cm · K.

Planck's equation generates spectral exitance curves that are quite useful for engineering calculations.
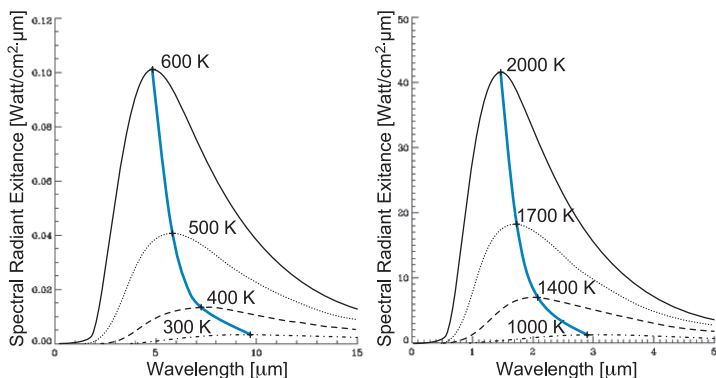
Planck curves illustrate the following characteristics:

➤ The shape of the blackbody curves does not change for any given temperature.
➤ The individual curves never cross one another; the exitance increases rapidly for increased temperatures at all wavelengths.

Planck's Radiation Law (cont.)

➤ The temperature is inversely proportional to wavelength; the peak exitance shifts toward shorter wavelengths as the temperature increases. Therefore, at low temperatures, most of the exitance is at higher wavelengths, while at high temperatures, most of the exitance is at lower wavelengths.

➤ As the temperature increases, the peak of the Planck function is shifted to the left (i.e., Wien's law). This can be seen by the hyperbola passing through the maximum of each of the Planck curves at different temperatures.

➤ The slope of the Planck curve is sharper to the left of the peak exitance than to the right, where the curve becomes more asymptotic. Consequently, the sensitivity (i.e., $\partial M_\lambda / \partial T$) of an infrared system increases at lower wavelengths.

➤ Atmospheric conditions are essential to determine what spectral region should be chosen for a particular application. As the aerosol concentration increases, the particle sizes grow and the transmittance in the MWIR is affected more than in the LWIR (i.e., Raleigh scattering $\propto \lambda^{-4}$). In contrast, water vapor influences primarily the LWIR, while CO_2 is important in the MWIR. Atmospheric self-emission or path radiance must be prevented as well.

➤ Sunglints depend on the target's emittance and are negligible in the LWIR because the solar intensity is an order of magnitude smaller than in the MWIR band.

➤ The size of the optics and spatial resolution in object space are key to determining the system's optimal spectral waveband.

➤ The output of an infrared detector is determined by the overlap of the spectral flux and the detector's spectral responsivity. The detector peak response in the LWIR is about four times lower than in the MWIR.

Planck's radiation formula models system design and analysis problems. For example, the radiant emittance of a blackbody at temperatures from 400 to 900 K includes the temperature of the hot metal tailpipes of jet aircrafts.

Stefan–Boltzmann and Wien's Displacement Laws

The **Stefan–Boltzmann law** relates the total blackbody exitance at all wavelengths to source temperature and is obtained by integrating the wavelength dependence of Planck's radiation law:

$$M_e(T) = \int_0^\infty M_{e,\lambda}(\lambda, T) d\lambda = \int_0^\infty \frac{2\pi h c^2}{\lambda^5} \frac{d\lambda}{\exp(hc/\lambda kT) - 1} = \frac{2\pi^5 k^4 T^4}{15 c^2 h^3}$$

$$M_e(T) = \sigma_e T^4$$

where σ_e is the **Stefan–Boltzmann constant** and has a value of 5.7×10^{-12} W/cm^2 K^4. The Stefan–Boltzmann law only holds for exitance integrated from zero to infinity over the interval of the wavelength.

The total exitance at all wavelengths multiplied by the source area results in the total power radiated, which increases as the fourth power of the absolute source temperature in Kelvin. For example, at room temperature (300 K), a perfect blackbody of an area equal to 1 cm^2 emits a total power of 4.6×10^{-2} W. Doubling the temperature to 600 K, the total power increases 16 fold to 0.74 W.

The derivative of Planck's equation with respect to wavelength yields **Wien's displacement law**, which gives the wavelength for which the peak of the spectral-exitance function occurs as a function of temperature:

$$\frac{\partial M_{e,\lambda}(\lambda, T)}{\partial \lambda} = 0 \quad \Rightarrow \quad \lambda_{max} T = 2898 \, [\mu m \cdot K]$$

Thus, the wavelength at which the maximum spectral radiant exitance varies is inversely proportional to the absolute temperature. The plot of λ_{max} as a function of temperature is a hyperbola (see plots on page 87).

For example, a blackbody source at 300 K has its maximum exitance at 9.7 µm; however, if the temperature of this source is changed to 1000 K, the maximum value at which the peak exitance occurs is at 2.9 µm. The sun is a blackbody source at approximately 6000 K. Applying Wien's law, it is found that its maximum wavelength occurs at 0.5 µm, which corresponds to the peak response of the human eye.

Rayleigh–Jeans and Wien's Radiation Laws

Two well-known approximations to Planck's radiation law are the Rayleigh–Jeans and Wien's radiation laws. The former applies at long wavelengths:

$$hc/\lambda kT \ll 1 \quad \Rightarrow \quad M_{e,\lambda} \cong \frac{2\pi ckT}{\lambda^4}$$

while the latter is valid only at short wavelengths:

$$hc/\lambda kT \gg 1 \quad \Rightarrow \quad M_{e,\lambda} \cong \frac{2\pi hc^2}{\lambda^2} \exp\left(-\frac{hc}{\lambda kT}\right)$$

As the temperature increases, the peak wavelength decreases (Wien's law) and the area under the Planck curve increases much faster (Stefan–Boltzmann law).

Thermal Equations in Photon-Derived Units

In photon-derived units, Planck's radiation, Boltzmann and Wien's displacement, Wien's radiation, and Rayleigh–Jeans formulae are given by

Planck's radiation equation:

$$M_{p,\lambda} = \frac{2\pi c}{\lambda^4} \frac{1}{\exp(hc/\lambda kT) - 1} \, [\text{photon/sec} \cdot \text{cm}^2 \cdot \mu\text{m}]$$

Stefan–Boltzmann law:

$$M_p(T) = \sigma_p T^3$$

where σ_p has a value of 1.52×10^{-11} photons/sec $\cdot$ cm$^2 \cdot$ K^3

Wien's displacement law:

$$\lambda_{max} T = 3662 \ [\mu\text{m} \cdot \text{K}]$$

Rayleigh–Jeans radiation law:

$$hc/\lambda kT \ll 1 \quad \Rightarrow \quad M_{p,\lambda} \cong \frac{2\pi kT}{\lambda^3 h}$$

Wien's radiation law:

$$hc/\lambda kT \gg 1 \quad \Rightarrow \quad M_{p,\lambda} \cong \frac{2\pi c}{\lambda^4} \exp\left(-\frac{hc}{\lambda kT}\right)$$

Exitance Contrast

In terrestrial infrared systems, the target and background are often of similar temperatures, in which case the target has very low thermal contrast. The proper choice of spectral pass-band wavelength $\Delta\lambda$ becomes essential to maximize the visibility of the target. This pass band should straddle the wavelength for which the exitance changes the most as a function of temperature.

This consideration of exitance contrast involves the following second-order partial derivative, where the system operating within a finite pass band is most sensitive to small changes in temperature:

$$\text{Finds } \lambda_{\text{peak-contrast}} \quad \frac{\partial}{\partial \lambda}\left[\frac{\partial M_\lambda(\lambda,T)}{\partial T}\right]=0 \quad \begin{array}{l}\text{Finds best sensitivity}\\\text{(steepest slope)}\end{array}$$

Carrying out these derivatives yields a constraint on wavelength and temperature in a fashion similar to Wien's displacement law, yielding

$$\lambda_{\text{peak-contrast}}\,T = 2410\ [\mu\text{m}\cdot\text{K}]$$

For a given blackbody temperature, the maximum exitance contrast occurs at shorter wavelengths than the wavelength of the peak exitance. For example, at 300 K the peak exitance occurs at 9.7 μm, while the **peak exitance contrast** occurs at 8 μm.
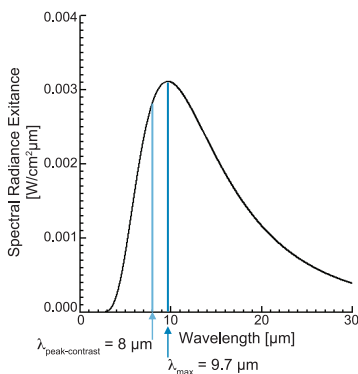
Emissivity

Emissivity is the ratio of the spectral exitance of a real source at a given temperature to that of a blackbody at the same temperature:

$$\varepsilon(\lambda, T) = \frac{M_{\lambda,\text{source}}(\lambda, T)}{M_{\lambda,\text{BB}}(\lambda, T)}$$

The spectral exitance of any real source at a given temperature is bound by the spectral exitance of a perfect radiator at the same kinetic temperature; hence, ε is constrained between zero and unity.

The emissivity characterizes how closely the radiation spectrum of a real heated body corresponds to that of a blackbody. It is a spectrally varying quantity and can be referred to either as a spectral (measured over a finite pass band) or a total (measured over all wavelengths) quantity. This emission efficiency parameter depends also on the surface temperature. However, emissivity data for most materials are typically constants and are seldom given as a function of λ and T unless the material is especially well-characterized.

There are three types of sources that can be differentiated depending on how their spectral emissivity varies: (1) a blackbody or perfect radiator, for which its emissivity equals unity for all wavelengths; (2) a graybody when its emissivity is a constant fraction of what the corresponding blackbody would radiate at the same temperature ($\varepsilon < 1$); its emissivity is independent of wavelength and has the same spectral shape as a blackbody; and (3) a selective radiator, where ε is an explicit function of λ.
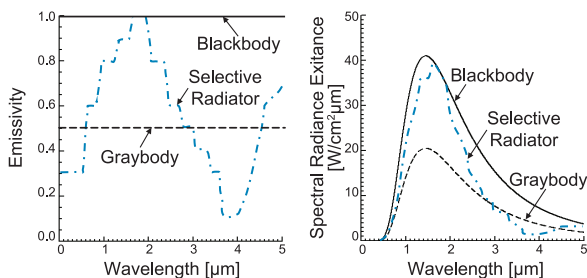
Kirchhoff's Law

If a solid body of a certain mass is located within a colder isothermal cavity, according to the second law of thermodynamics, there will be a net flow of heat from the object to the walls of the hollow space. Once the body reaches thermal equilibrium with its surroundings, the first law of thermodynamics or conservation of energy requires that

$$\phi_{inc} = \phi_{absorbed} + \phi_{transmitted} + \phi_{reflected}$$

where ϕ_{inc} is the incident flux on the solid body. Dividing both sides of the equation by ϕ_{inc} yields

$$1 = a + \tau + \rho$$

where a is the absorptance, τ is the transmittance, and ρ is the reflectance. For an opaque body (i.e., $\tau = 0$), the incident radiation is either absorbed or reflected, yielding

$$a = 1 - \rho$$

which indicates that surfaces with low reflectance are high emitters.

If the body absorbs only a portion of the radiation that is incident on it, then it emits less radiation in order to remain in thermal equilibrium; that is,

$$E = \varepsilon M$$

which leads to **Kirchhoff's law**, which states that the absorptance of a surface is identical to the emittance of that surface. Kirchhoff's law also holds for spectral quantities; it is a function of temperature and can vary with the direction of measurement. This law is sometimes verbalized as "**good absorbers are good emitters**."

Integrated absorptance $= a(\lambda, T) \equiv \varepsilon(\lambda, T) =$ Integrated emittance

For polished metals, the emissivity is low; however, it increases with temperature and may increase substantially with the formation of an oxide layer on the object surface. A thin film of oil and surface roughness can increase the emissivity by an order of magnitude compared to a polished metal surface. The emissivity of nonmetallic surfaces is typically greater than 0.8 at room temperature, and it decreases as the temperature increases.

Emissivity of Various Common Materials

Metals and Other Oxides	Emissivity
Aluminum: Polished sheet	0.05
Sheet as received	0.09
Anodized sheet, chromatic-acid process	0.55
Vacuum-deposited	0.04
Brass: Highly polished	0.03
Rubbed with 80-grit emery	0.20
Oxidized	0.61
Copper: Highly polished	0.02
Heavily oxidized	0.78
Gold: Highly polished	0.21
Iron: Cast-polished	0.21
Cast, oxidized	0.64
Sheet, heavily rusted	0.69
Nickel: Electroplated, polished	0.05
Electroplated, not polished	0.11
Oxidized	0.37
Silver: Polished	0.03
Stainless Steel: Type 18-8 buffed	0.16
Type 18-8, oxidized	0.85
Steel: Polished	0.07
Oxidized	0.79
Tin: Commercial tin-plated sheet iron	0.07

Nonmetallic Materials	Emissivity
Brick: Red common	0.93
Carbon: Candle soot	0.95
Graphite, filed surface	0.98
Concrete	0.92
Glass: Polished plate	0.94
Lacquer: White	0.92
Matte black	0.97
Oil, lubricant (Thin film of nickel base):	
Nickel base alone	0.05
Oil film: 1, 2, 5×10^{-3} in	0.27, 0.46, 0.72
Thick coating	0.82
Paint, oil: Average of 16 colors	0.94
Paper: White bond	0.93
Plaster: Rough coat	0.91
Sand	0.90
Human skin	0.98
Soil: Dry	0.92
Saturated with water	0.95
Water: Distilled	0.96
Ice, smooth	0.96
Frost crystals	0.98
Snow	0.90
Wood: Planed oak	0.90

Data from Wolfe & Zissis, *The Infrared Handbook* (1989).

Radiometric Measure of Temperature

There are many applications in the infrared where the actual kinetic temperature of a distant object must be known. However, infrared systems can only measure the apparent spectral exitance emitted by targets and/or backgrounds, which is a function of both temperature and emissivity. The temperature of the infrared source can be measured if emissivity of the viewing source within the appropriate spectral region is known. Discrepancies in emissivity values produce built-in errors in the calculation of this kinetic temperature.

Three main types of temperature measurements are discussed below.

Radiation temperature T_{rad}: a calculation based on the Stefan–Boltzmann law because it is estimated over the whole spectrum:

$$M_{\mathrm{meas}} = \sigma T_{\mathrm{rad}}^4$$

where M_{meas} is the measured exitance. If the source is a graybody with a known emissivity, then T_{true} can be calculated from T_{rad}:

$$M_{\mathrm{meas}} = \sigma T_{\mathrm{rad}}^4 = \varepsilon \sigma T_{\mathrm{true}}^4 \Rightarrow T_{\mathrm{true}} = \frac{T_{\mathrm{rad}}}{\sqrt[4]{\varepsilon}}$$

Due to its strong dependence on emissivity, T_{rad} cannot be corrected to find T_{true} if ε is an unknown. Similarly, T_{rad} is affected by the attenuation in the optical system, especially in harsh environments where the optical elements might be dirty.

Brightness temperature T_{b}: a measurement performed using Planck's radiation law because it is estimated over a single wavelength λ_0, or in a narrow spectral region ($\Delta\lambda$) around a fixed wavelength λ_0. For a blackbody source, $T_{\mathrm{b}} = T_{\mathrm{true}}$; therefore, Planck's equation can be solved for T_{b}:

$$T_{\mathrm{b}} = \frac{c_2}{\lambda_0 \ln\left\{ 1 + \frac{c_1}{\lambda_0^5 M_\lambda(\lambda_0, T_{\mathrm{b}})} \right\}}$$

where $c_1 = 3.7415 \times 10^4 \ \mathrm{W/cm^2 \ \mu m^4}$, and $c_2 = 1.4382 \ \mathrm{cm \cdot K}$.

Radiometric Measure of Temperature (cont.)

If the source is a graybody with a known emissivity, then T_{true} can be calculated from T_{b} as follows:

$$\frac{c_1}{\lambda_0^5}\frac{1}{\exp(c_2/\lambda_0 T_{\text{b}})-1}=\frac{c_1}{\lambda_0^5}\frac{\varepsilon}{\exp(c_2/\lambda_0 T_{\text{true}})-1}$$

yielding

$$T_{\text{true}}=\frac{c_2}{\lambda_0 \ln\{1+\varepsilon[\exp(c_2/\lambda_0 T_{\text{b}})-1]\}}$$

The exitance levels measured for T_{b} are lower than the levels for T_{rad} because of the narrowband filtering involved. The best sensitivity for this measurement is obtained by choosing λ_0 near the wavelength of the peak exitance contrast, where M_λ changes most with temperature. The absolute background temperature of the universe was determined through this process.

The brightness temperature measures the correct temperature as long as the emissivity is known and there is no spurious attenuation in the optical system. Lack of knowledge of either of these parameters will produce a large error in the radiometric measurement.

Color temperature T_{c}: the temperature of a blackbody that best matches the spectral composition of the target source. This spectral composition is defined as the ratio of the measured spectral exitance at two different wavelengths, given by

$$\frac{M_\lambda(\lambda_1)}{M_\lambda(\lambda_2)}=\frac{\lambda_2^5}{\lambda_1^5}\frac{\exp(c_2/\lambda_2 T_{\text{e}})-1}{\exp(c_2/\lambda_1 T_{\text{e}})-1}$$

Under these circumstances, the emissivity cancels out

because of the ratio, and $T_{\text{c}}=T_{\text{true}}$ for both black and graybodies.
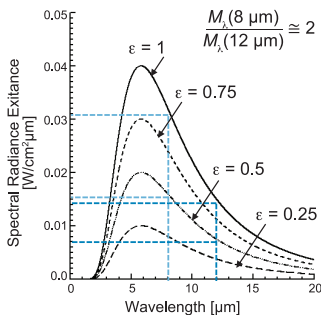
This method is strongly affected when the target source is a selective radiator. In this case, the measurement of the spectral exitance must be performed at many wavelengths.

Collimators

A **collimator** is an optical assembly that places a target at infinity and produces a controllable irradiance that is independent of distance. It is widely used for testing the sensitivity and the resolution of infrared systems.
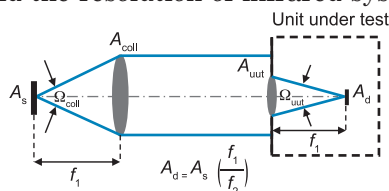
Assuming a Lambertian source that is radiating at all wavelengths, the total flux emitted can be written using the Stefan–Boltzmann law:

$$\phi = L_s A_s \Omega_{\text{coll}} = \frac{\sigma T^4}{\pi} \frac{A_s A_{\text{coll}}}{f_1^2}$$

The source exitance and/or the irradiance falling on the detector surface can be obtained by dividing the radiant flux over the area of the collimator, yielding

$$M = \frac{\sigma T^4}{\pi} \frac{A_s}{f_1^2} = \frac{\sigma T^4}{\pi} \frac{A_d}{f_2^2} = E$$

An extended source placed at the focal plane of a collimator can be seen only in a well-defined region. The maximum distance at which the infrared imaging system can be placed from the collimator is

$$d_{\text{max}} = \frac{f_{\text{coll}}}{t} D_{\text{coll}}$$

If the imaging system is placed at a distance greater than d_{max}, the target's outer edges are clipped, and only the central portion of the target is seen.
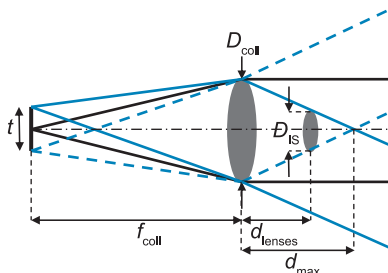
The distance between the collimating and imaging system optical components is

$$d_{\text{lenses}} = \frac{f_{\text{coll}}}{t} (D_{\text{coll}} - D_{\text{IS}})$$

Spectral Atmospheric Transmittance

Absorption losses and light **scatter** along the atmospheric path are critical parameters that must be considered when developing infrared systems. High absorptance takes place in different parts of the spectrum due to molecular motions, rotations, and vibrations of atmospheric constituents, the primary being carbon dioxide (CO_2), water vapor (H_2O), and ozone (O_3). For example, the near-infrared is greatly affected by H_2O, as are the short- and longwave sides of the LWIR spectral window. The MWIR has two dips due to CO_2 and O_3.

There are three main atmospheric windows: the visible to the near-infrared and SWIR (up to 2.2 µm), MWIR (3–5 µm), and LWIR (8–14) µm. Technologies have evolved independently, optimizing the operation in each of these spectral bands.
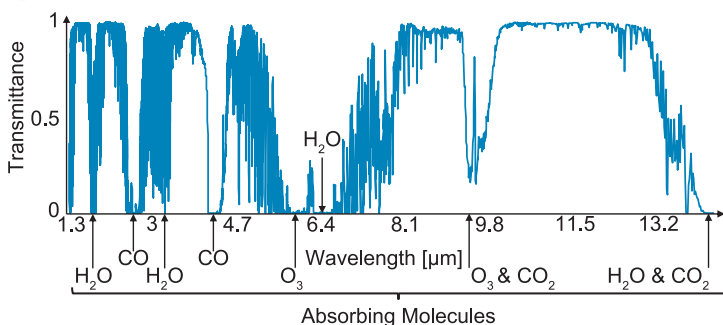
The **spectral atmospheric transmittance** over a path length r for radiation of wavelength λ may be expressed by **Beer's law**:

$$\tau_{atm} = e^{-\sigma \cdot r}$$

where σ is the **extinction coefficient** and is expressed by

$$\sigma = \alpha + \gamma$$

where α and γ are the absorption and scatter coefficients, respectively, and refer to wavelength-dependent attenuation of electromagnetic radiation. Extinction is defined as the attenuation in the amount of radiation passing through the atmosphere and is expressed in units of km^{-1}. The product $\sigma \cdot r$ is known as the **optical depth**.

Spectral Atmospheric Transmittance (cont.)

Absorption is fundamentally a quantum process where the atmospheric molecules absorb energy from incident photons. Conversely, light scatter results from photons colliding with atmospheric particles. Because of the sun's radiation, aerosols and molecular scattering are particularly important background sources in the visible spectrum. However, in the infrared, this effect is minimal because the wavelengths are much longer here.

According to the **Rayleigh principle**, the **scattered flux density** is inversely proportional to the fourth power of the driving wavelength ($\propto 1/\lambda^4$). This rule is utilized provided that the air molecules and haze particles are small compared to the wavelength (i.e., $2\pi a/\lambda < 1$, where a is the radius of the scattering particle). **Mie scatter theory** is applied when the size of the atmospheric particles is $2\pi a/\lambda \geq 2$. The Mie solution to Maxwell's equations describes the scattering of an electromagnetic plane wave incident on a homogeneous sphere.
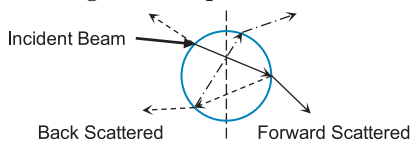
Mie scattering occurs mostly in lower portions of the atmosphere where larger particles are plentiful. Particulate contamination such as smoke, dust, pollen, and microscopic water droplets are classic examples of larger particles. Scattered light entering the **line of sight (LOS)** of an **electro-optical (EO)** system can be quantified using **stray light analysis** programs.

The extinction coefficient due to rain is independent of wavelength because average raindrop diameters (0.1 to 10 mm) are considerably larger than the visible/infrared wavelengths under consideration. Rain attenuation can be estimated by using the Marshall–Palmer raindrop size empirical distribution over the path length:

$$\tau_{\text{atm}-\text{rain}} = e^{-0.365 \cdot d^{0.63} \cdot r}$$

where d is the rain rate in mm/hr, and r is the range.

Path Radiance

The **path radiance**, or **atmospheric noise**, represents the atmospheric self-emission and radiation scattered into the sensor's LOS. In order to acquire a target, one must be able to distinguish that target from the background. The inherent contrast is given by

$$C_0 = \frac{L_{t_0} - L_{b_0}}{L_{b_0}}$$

where L_{t_0} and L_{b_0} are the target and background radiances, respectively, at zero range. The target and background radiances at range r are characterized by

$$L_{t_r} = L_{t_0} \cdot \tau_{atm} + L_{pr}$$

$$L_{b_r} = L_{b_0} \cdot \tau_{atm} + L_{pr}$$

where L_{pr} is the path radiance term. The apparent contrast at range r can be reformulated as

$$C_r = \frac{L_{t_r} - L_{b_r}}{L_{b_r}} = \frac{C_0}{1 + \frac{L_{pr}}{L_{b_0}} \frac{1}{\tau_{atm}}}$$

The L_{pr} parameter is rather difficult to quantify; therefore, solutions with moderate accuracy, such as the **sky-to-ground ratio (SGR)**, are used to determine the reduction in contrast. The SGR is defined as

$$SGR = \frac{L_{pr}}{L_{b_0}} \cdot \frac{1}{(1 - \tau_{atm})}$$

Therefore, the **contrast transmittance** or transference ratio can be calculated by

$$\tau_c = \frac{C_r}{C_0} = \frac{1}{1 + SGR\left(\frac{1}{\tau_{atm}} - 1\right)}$$

One should not try to compare contrast transmittance with atmospheric transmittance. Contrast transmittance is a measure of loss of contrast, while atmospheric transmittance is simply a loss of energy.

Path Radiance (cont.)

A plot of the **contrast transmittance** versus SGR for four different values of **atmospheric transmittance** is shown in the figure.
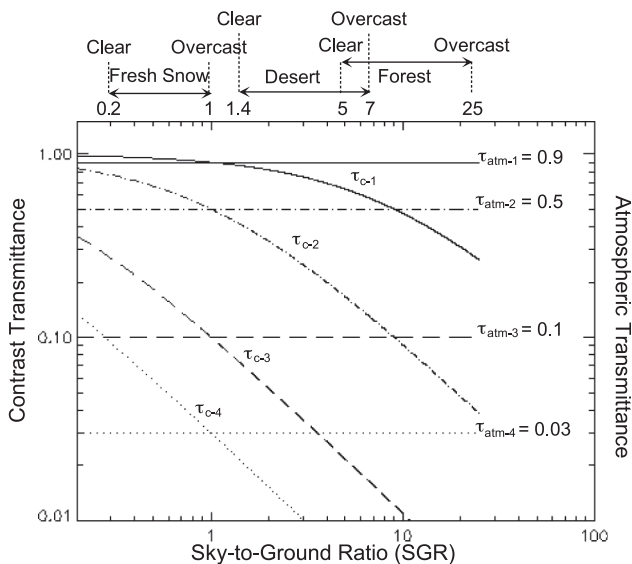
SGR = 1 yields $\tau_c = \tau_{atm}$;
SGR > 1 pertains to bright or hot background scenarios;
SGR < 1 refers to dark or cold background situations.

The fire-induced transmittance and turbulence effects (FITTE) is a computer module that predicts infrared atmospheric path radiance with high accuracy.

LOWTRAN, MODTRAN®, HITRAN, FASTCODE, PcModWin©, and PcLnWin© are standard codes used to compute atmospheric transmittance and radiance along arbitrary paths.

The atmosphere is problematic for high-energy laser systems. Small temperature variations cause random changes in wind velocity or turbulence motion. These changes in temperature give rise to small changes in the index of refraction of air, acting like little lenses that cause intensity variations. These fluctuations distort the laser beam wavefront, producing unwanted effects such as beam wander, beam spreading, and scintillation.

<div align="center">

Equation Summary

</div>

Thin lens equation:

$$\frac{1}{f} = \frac{1}{p} = \frac{1}{q} \quad \text{Gaussian} \qquad x_{\text{obj}} x_{\text{img}} = f^2 \quad \text{Newtonian}$$

Lateral or transverse magnification:

$$\mathcal{M} = -\frac{q}{p} = \frac{h_{\text{img}}}{h_{\text{obj}}}$$

Area or longitudinal magnification:

$$\mathcal{M}^2 = \frac{A_{\text{img}}}{A_{\text{obj}}} - \left(\frac{q}{p}\right)^2$$

Thick lens equation:

$$\frac{1}{f_{\text{eff}}} = (n-1)\left[\frac{1}{R_1} - \frac{1}{R_2} + \frac{(n-1)t}{n}\frac{1}{R_1 R_2}\right]$$

F-number and numerical aperture:

$$F/\# \equiv \frac{f_{\text{eff}}}{D_{\text{enp}}} \qquad \text{NA} \equiv \eta \sin \alpha$$

$$F/\# = \frac{1}{2\tan(\sin^{-1}\text{NA})} \qquad \text{NA} = \sin\left[\tan^{-1}\frac{1}{2(F/\#)}\right]$$

$$F/\# \cong \frac{1}{2\text{NA}} \quad \text{paraxial approximation}$$

Field of view:

$$\text{FOV}_{\text{half-angle}} = \theta_{1/2} = \left|\tan^{-1}\frac{h_{\text{obj}}}{p}\right| = \left|\tan^{-1}\frac{h_{\text{img}}}{q}\right|$$

$$\text{FOV}_{\text{full-angle}} = \theta = \frac{d}{f} \quad \text{paraxial approximation}$$

Depth of focus and depth of field:

$$\delta' = \pm 2\lambda(F/\#)^2$$

$$\delta = \pm\frac{(\text{EFL})^2}{2\lambda(F/\#)^2} = \pm\frac{D_{\text{enp}}^2}{2\lambda}$$

$$\delta' = \mathcal{M}^2\delta$$

Equation Summary

Hyperfocal distance:

$$\text{HFD} = \frac{\text{EFL}(\text{EFL} + 1)}{(F/\#) \cdot \text{CoC}} \cong \frac{(\text{EFL})^2}{(F/\#) \cdot \text{CoC}}$$

Diffraction-limited expressions:

$$d_{\text{diff}} = 2.44\lambda(F/\#) \quad \text{blurs pot}$$

$$\beta = 2.44\frac{\lambda}{D} \quad \text{angular blur}$$

Relationship between RMS and P-V wavefront errors:

$$\frac{W_{\text{PV}}}{\omega} = 3.5$$

Strehl ratio:

$$\text{SR} = e^{-(2\pi\omega)^2}$$

$$\text{If } \text{SR} \geq 0.8 \Rightarrow \text{SR} \approx 1 - (2\pi\omega)^2$$

Shift in focus in an optical window:

$$\delta_f = \frac{(n_w - 1)t_w}{n_w} + \frac{(n_s - 1)t_s}{n_s}$$

Beam displacement:

$$\delta_d = t \cdot \sin\alpha \left(1 - \sqrt{\frac{1 - \sin^2\alpha}{n^2 - \sin^2\alpha}} \right)$$

Paraxial approximation:

$$\delta_d = \frac{(n - 1)t\alpha}{n}$$

Sag equation for even aspheres:

$$\text{sag}_{\text{asph}}(r) = \frac{cr^2}{1 + \sqrt{1 - (k + 1)c^2r^2}} + \sum_i \alpha_{2i}r^{2i}$$

Equation Summary

Kinoform expressions:

$$\eta_{\text{kino}} = \text{sinc}^2 \left\{ \pi \left(\frac{\lambda_o}{\lambda} \right) - 1 \right\}$$

$$\varphi(r) = \frac{2\pi}{\lambda_o} \sum_i C_{2i} r^{2i}$$

$$m = \frac{1}{\lambda_o} \sum_i C_{2i} r^{2i}$$

$$\text{sag}_{\text{diff}} = \frac{\sum_i C_{2i} r^{2i} + \lambda_o(m - 1)}{n(\lambda_o) - 1}$$

$$\text{sag}_{\text{total}} = \text{sag}_{\text{asph}} + \text{sag}_{\text{diff}}$$

Refractive index:

$$n = \frac{c}{v}$$

Law of reflection:

$$\theta_i = \theta_r$$

Snell's law:

$$n_1 \sin \theta_i = n_2 \sin \theta_t$$

Fresnel Equations

s-polarization:

$$\rho_s = \frac{(n_1 \cos \theta_i - n_2 \cos \theta_t)^2}{(n_1 \cos \theta_i + n_2 \cos \theta_t)^2} \quad \text{and} \quad \tau_s = \frac{4 n_1 n_2 \cos \theta_i \cos \theta_t}{(n_1 \cos \theta_i + n_2 \cos \theta_t)^2}$$

p-polarization:

$$\rho_p = \frac{(n_2 \cos \theta_i - n_1 \cos \theta_t)^2}{(n_2 \cos \theta_i + n_1 \cos \theta_t)^2} \quad \text{and} \quad \tau_p = \frac{4 n_1 n_2 \cos \theta_i \cos \theta_t}{(n_1 \cos \theta_t + n_2 \cos \theta_i)^2}$$

Normal incidence:

$$\rho_n = \left(\frac{n_2 - n_1}{n_2 + n_1} \right)^2 \quad \text{and} \quad \tau_n = \frac{4 n_1 n_2}{(n_1 + n_2)^2}$$

Equation Summary

Internal transmittance:

$$\tau_{\text{internal}} = \frac{\phi(z)}{\phi_{\text{incident}}} = e^{-\alpha z}$$

External transmittance:

$$\tau_{\text{external}} = \tau^2 e^{-\alpha z} = \tau^2 \tau_{\text{internal}}$$

Total transmittance:

$$\tau_{\text{total}} = \frac{(1-\rho)^2 e^{-\alpha d}}{1 - \rho^2 e^{-2\alpha d}}$$

Total reflectance:

$$\rho_{\text{total}} = \frac{\phi_{\text{r}}}{\phi_{\text{i}}} = \rho + \frac{\rho(1-\rho)^2 e^{-2\alpha d}}{1 - \rho^2 e^{-2\alpha d}}$$

Absorptance equals emittance:

$$a = 1 - \rho_{\text{total}} - \tau_{\text{total}} = \frac{(1-\rho)(1 - e^{-\alpha d})}{1 - \rho e^{-\alpha d}} \equiv \varepsilon$$

Absorption coefficient:

$$\alpha = \frac{4\pi k}{\lambda}$$

Attenuation coefficient:

$$\delta = \frac{10}{\ln 10} \cdot \alpha$$

Reciprocal relative dispersion or Abbe number:

$$V = \frac{n_{\text{mean}} - 1}{\Delta n} = \frac{n_{\text{mean}} - 1}{n_{\text{final}} - n_{\text{initial}}}$$

Relative partial dispersion:

$$P = \frac{n_{\text{mean}} - n_{\text{initial}}}{n_{\text{final}} - n_{\text{initial}}}$$

Equation Summary

Stress:

$$\sigma' = \frac{P}{A_0}$$

Strain:

$$\varepsilon' = \frac{\delta l}{l}$$

Young's modulus:

$$E' = \frac{\sigma'}{\varepsilon'}$$

Poisson ratio:

$$\nu' = -\frac{\varepsilon'_{\text{lateral}}}{\varepsilon'_{\text{longitudinal}}}$$

Fracture toughness or stress intensity factor:

$$K_{\text{Ic}} = Y\sigma_{\text{f}}\sqrt{\pi d} \quad [\text{MPa}\sqrt{\text{m}}]$$

Probability of failure – Weibull distribution:

$$P_{\text{failure}} = 1 - \exp\left[-\left(kA\frac{\sigma'}{\sigma_0}\right)^m\right]$$

Safety factor:

$$\sigma_{\text{max}} = \frac{\overline{\sigma_{\text{f}}}}{\text{SF}}$$

Fourier law of conduction:

$$q = -k'A_x\frac{\partial T}{\partial x}$$

Thermal diffusivity:

$$\kappa' = \frac{k'}{\rho'C_{\text{p}}} \quad [\text{m}^2/\sec]$$

Equation Summary

Coefficient of thermal expansion:

$$\alpha' = \frac{1}{l}\frac{\partial l}{\partial T} \quad \text{so} \quad \varepsilon' = \frac{\partial l}{l} = \alpha' \partial T$$

Diameter-to-Thickness Ratio of an Optical Window

Circular window:

$$\frac{t_{\mathrm{c}}}{D} = \frac{1}{2}\sqrt{\frac{\chi\sigma_{\mathrm{f}}'}{\sigma_{\max}}}$$

Rectangular window:

$$\frac{t_{\mathrm{r}}}{L} = \sqrt{\frac{\chi\sigma_{\mathrm{f}}'}{2\sigma_{\max}[1 + (L/W)^2]}}$$

Solid angle equations:

$$\Omega = 4\pi\sin^2\frac{\sigma_{\max}}{2}$$

$$\Omega = \frac{a}{r^2} \ \ a \ll r^2 \ \text{paraxial approximation}$$

Intensity:

$$I = \frac{\partial\phi}{\partial\Omega_{\mathrm{d}}} = LA_{\mathrm{s}}\cos\theta_{\mathrm{s}}$$

Exitance and radiance:

$$M = \frac{\partial\phi}{\partial\Omega_{\mathrm{s}}} \cong \frac{\phi}{\Omega_{\mathrm{s}}} \ \ \text{finite quantity} \ \ M = \pi L \ \text{Lambertian radiator}$$

Fundamental equation of radiation transfer:

$$\partial^2\phi = L\partial A_{\mathrm{s}}\cos\theta_{\mathrm{s}}\partial\Omega_{\mathrm{d}}$$

$$\phi \cong LA_{\mathrm{s}}\cos\theta_{\mathrm{s}}\Omega_{\mathrm{d}} \ \text{finite quantities}$$

AΩ product or optical invariant:

$$A_{\mathrm{s}}\Omega_{\mathrm{d}} = A_{\mathrm{d}}\Omega_{\mathrm{s}}$$

Equation Summary

Irradiance:

$$E_{\text{extended source}} = \frac{\partial \phi}{\partial \Omega_{\text{d}}} = \pi L \sin^2 \theta_{\max} = \frac{\pi L}{4(F/\#)^2 + 1}$$

$$E_{\text{point source}} = \frac{\phi}{A_{\text{d}}} \times 0.84 = \frac{0.84 I \Omega_{\text{optics}}}{\frac{\pi}{4} 2_{\text{diff}}^2} = \frac{0.84 I \Omega_{\text{optics}}}{\frac{\pi}{4} \left[2.44 \lambda (F/\#) \right]^2}$$

Planck's radiation law:

$$M_{\text{e},\lambda} = \frac{2\pi hc^2}{\lambda^5} \frac{1}{\exp(hc/\lambda kT) - 1} \quad [\text{W/cm}^2 \cdot \mu\text{m}]$$

$$M_{\text{p},\lambda} = \frac{2\pi c}{\lambda^4} \frac{1}{\exp(hc/\lambda kT) - 1} \quad [\text{photon/sec} \cdot \text{cm}^2 \cdot \mu\text{m}]$$

Rayleigh–Jeans radiation law:

$$hc/\lambda kT \ll 1 \quad M_{\text{e},\lambda} \cong \frac{2\pi ckT}{\lambda^4} \quad M_{\text{p},\lambda} \cong \frac{2\pi kT}{\lambda^3 h}$$

Wien's radiation law:

$$hc/\lambda kT \gg 1$$

$$M_{\text{e},\lambda} \cong \frac{2\pi hc^2}{\lambda^5} \exp\left(-\frac{hc}{\lambda kT}\right) \quad M_{\text{p},\lambda} \cong \frac{2\pi c}{\lambda^4} \exp\left(-\frac{hc}{\lambda kT}\right)$$

Stefan–Boltzmann law:

$$M_{\text{e}} = \sigma_{\text{e}} T^4 \quad \sigma_{\text{e}} = 5.7 \times 10^{-12} \quad [\text{W/cm}^2 \text{K}^4]$$

$$M_{\text{p}} = \sigma_{\text{p}} T^3 \quad \sigma_{\text{p}} = 1.52 \times 10^{-11} \quad [\text{photon/sec} \cdot \text{cm}^2 \text{K}^3]$$

Wien's displacement law:

$$\lambda_{\max,\text{e}} T = 2898 \ [\mu\text{m} \cdot \text{K}] \qquad \lambda_{\max,\text{p}} T = 3662 \ [\mu\text{m} \cdot \text{K}]$$

Peak exitance contrast:

$$\lambda_{\text{peak-contrast}} T = 2410 \ [\mu\text{m} \cdot \text{K}]$$

Emissivity:

$$\varepsilon(\lambda, T) = \frac{M_{\lambda,\text{source}}(\lambda, T)}{M_{\lambda,\text{BB}}(\lambda, T)}$$

Equation Summary

Kirchhoff's law:

$$\text{Absorptance} = a(\lambda, T) \equiv \varepsilon(\lambda, T) = \text{Emittance}$$

Atmospheric transmittance – Beer's law:

$$\tau_{\text{atm}} = e^{-\sigma \cdot r}$$

Sky-to-ground ratio (SRG):

$$\text{SGR} = \frac{L_{\text{pr}}}{L_{\text{b}_0}} \cdot \frac{1}{(1 - \tau_{\text{atm}})}$$

Contrast transmittance or transference:

$$\tau_{\text{c}} = \frac{C_{\text{r}}}{C_0} = \frac{1}{1 + \text{SGR}\left(\frac{1}{\tau_{\text{atm}}} - 1\right)}$$

Bibliography

Adams, J. H., "Specifications for optical grade germanium and silicon blanks," *Proc. SPIE* **0406** (1983) [doi: 10.1117/12.935669].

Bass, M., *Handbook of Optics*, Vols. I & II, McGraw-Hill, New York (1995).

Bentley, J. and C. Olson, *Field Guide to Lens Design*, SPIE Press, Bellingham, WA (2012) [doi: 10.1117/3.934997].

Born, M. and E. Wolf, *Principles of Optics*, Pergamon Press, New York (1986).

Boyd, R. W., *Radiometry and the Detection of Optical Radiation*, John Wiley & Sons, Inc., New York (1983).

Carslaw, H. S. and J. C. Jaeger, *Conduction of Heat in Solids*, Second Edition, Oxford Univ. Press, Oxford (1993).

Daniels, A., *Field Guide to Infrared Systems, Detectors, and FPAs*, Second Edition, SPIE Press, Bellingham, WA (2010) [doi: 10.1117/3.853623].

Dankin, J. P. and R. G. W. Brown, *Handbook of Optoelectronics*, Vol. **1**, CRC Press, Boca Raton, FL (2006).

Dereniak, E. L. and G. D. Boreman, *Infrared Detectors and Systems*, John Wiley & Sons, Inc. New York (1996).

Diamond, A. S. and D. S. Weiss, *Handbook of Infrared Materials*, Second Edition, Marcel Decker, Inc. New York, (2008).

Fischer, R. E., B. Tadic-Galeb, and P. Yoder, *Optical System Design*, Chapters 16 and 18, McGraw-Hill, New York (2008).

Gaskill, J. D., *Linear Systems, Fourier Transforms, and Optics*, John Wiley & Sons, Inc., New York (1978).

Ghosh, G., *Handbook of Optical Constants of Solids*, Academic Press, San Diego (1998).

Bibliography

Goldman, L. M., R. Twedt, S. Balasubramanian, and S. Sastri, "ALON optical ceramic transparencies for window, dome, and transparent armor applications," *Proc. SPIE* **8016**, 801608 (2011) [doi: 10.1117/12.886122].

Goodman, J. W., *Introduction to Fourier Optics*, McGraw-Hill, New York (1968).

Goodwin, E. P. and J. C. Wyant, *Field Guide to Interferometric Optical Testing*, SPIE Press, Bellingham, WA (2006) [doi: 10.1117/3.702897].

Greivenkamp, J. E., *Field Guide to Geometrical Optics*, SPIE Press, Bellingham, WA (2004) [doi: 10.1117/3.547461].

Guenter, R., *Modern Optics*, John Wiley & Sons, Inc. Cambridge (1990).

Harris, D. C., "Durable 3–5 μm transmitting infrared window materials," *Infrared Physics & Technology* **39**(4), 185–201 (1998).

Harris, D. C., *Materials for Infrared Windows and Domes: Properties and Performance*, SPIE Press, Bellingham, WA (1999) [doi: 10.1117/3.349896].

Hecht, E. and A. Zajac, *Optics*, Addison-Wesley, Boston (1974).

Hudson, R. D., *Infrared System Engineering*, John Wiley & Sons, Inc., New York (1969).

Jackson, J. D., *Classical Electrodynamics*, Second Edition, John Wiley & Sons, Inc., New York (1975).

Jenkins, F. A. and H. E. White, *Fundamentals of Optics*, McGraw-Hill, New York (1981).

Kingslake, R. and R. B. Johnson, *Lens Design Fundamentals*, Second Edition, Academic Press, Burlington, MA and SPIE Press, Bellingham, WA (2010).

Bibliography

Kingston, R. H., *Detection of Optical and Infrared Radiation*, Springer-Verlag, New York (1979).

Klein, C., "Diamond windows for high-power lasers: an initial assessment," *Proc. SPIE* **1624** (1991) [doi: 10.1117/12.60119].

Laikin, M., *Lens Design*, Third Edition, Marcel Dekker, Inc. New York (2001).

Lloyd, J. M., *Thermal Imaging Systems*, Plenum, New York (1975).

Malacara, D., *Optical Shop Testing*, John Wiley & Sons, Inc., New York (1978).

Meyer-Arendt, J. R., *Introduction to Classical and Modern Optics*, Fourth Edition, Prentice Hall, Upper Saddle River, NJ (1995).

Ramissety, M., S. Sastri, U. Kashalikar, L. M. Goldman, and N. Nag, "Transparent polycrystalline cubic spinels protect and defect," *American Ceramic Society Bulletin* **92**(2), 20–25 (2013).

Rogalski, A. and K. Chrzanowski, "Infrared devices and techniques," *Opto-Electronics Review* **10**(2), 111–136 (2002).

Rogers, J. R., "Homogeneity tolerances for optical elements," CODE V User Group Meeting 2011, Synopsis, Inc., pp. 1–35 (2011).

Roylance, D., *Mechanical Properties of Materials*, MIT (2008).

Saleh, B. E. A. and M. C. Teich, *Fundamentals of Photonics*, John Wiley & Sons, Inc., New York (1991).

Siegel, R. and J. R. Howell, *Thermal Radiation Heat Transfer*, Second Edition, Hemisphere Publishing, Philadelphia (1981).

Smith, W. J., *Modern Lens Design*, Second Edition, McGraw-Hill, New York (2005).

Bibliography

Smith, W. J., *Modern Optical Engineering*, Fourth Edition, McGraw-Hill, New York (2008).

Swab, J. J., R. Pavlacka, G. Gilde, S. Kilczewski, J. Wright, and D. Harris, "Determining the strength of coarse-grained AlON and spinel," *J. American Ceramic Society* **97**(2), 592–600 (2013).

Thomas, R. S., *Heat Transfer*, Prentice Hall, Upper Saddle River, NJ (1993).

Waynant, R. W. and M. N. Ediger, Eds., *Electro-Optics Handbook*, Second Edition, McGraw-Hill, New York (2000).

Welford, W. T., *Aberrations of Optical Systems*, Taylor & Francis, New York (1986).

Wolfe, W. L., *Introduction to Infrared Systems Design*, SPIE Press, Bellingham, WA (1996) [doi: 10.1117/3.226006].

Wolfe, W. L. and G. J. Zissis, *The Infrared Handbook*, Infrared Information Analysis (IRIA) Center, Ann Arbor, MI (1989).

Wu, R. L. C., A. W. McCormick, P. P. Pronko, and J. Keeley, "Surface hardening of ZnSe, ZnS, and ZnS/ZnSe optical materials by implantation of 1 MeV hydrogen ions," *Nuclear Instruments and Methods in Physics Research Section B* **59**, 1232–1235 (1991).

Index

Index

Index

Index

Index

Index

Arnold Daniels is a senior lead engineer with extensive experience in the conceptual definition of advanced infrared (IR), optical, and electro-optical (EO) systems. His background consists of technical contributions to applications for direct energy weapon systems, infrared search & track, thermal imaging, as well as ISR systems. His other areas of technical expertise include infrared radiometry, performance specification of thermal imaging systems, thermographic nondestructive testing, stray light analysis, optical design, precision optical alignment, adaptive optics, Fourier analysis, image processing, and data acquisition systems. He received a B.S. in Electro-Mechanical Engineering from the National Autonomous University of Mexico and a B.S. in Electrical Engineering from the Israel Institute of Technology (Technion). He earned an M.S. in Electrical Engineering from the University of Tel-Aviv and received a doctoral degree in Electro-Optics from the school of Optics (CREOL) at the University of Central Florida. In 1995, he received the Rudolf Kingslake medal and prize for the most noteworthy original paper to appear in SPIE's *Journal of Optical Engineering*. He currently develops electro-optical and infrared sensor systems for aerospace and defense applications.

Infrared Optics, Materials, and Radiometry

Arnold Daniels

The *Field Guide to Infrared Optics, Materials, and Radiometry* covers all aspects of infrared optics, including monochromatic and chromatic optical aberrations as well as important concepts such as depth of focus, depth of field, hyperfocal distance, warm shields, aspheric surfaces, and kinoforms. This Field Guide also provides a comprehensive introduction to the optical, mechanical, and thermal properties of infrared materials as well as the essentials of radiometry and sources necessary for the quantitative understanding of infrared signatures and flux transfer, spectral atmospheric transmittance, and path radiance. It serves as a companion to the *Field Guide to Infrared Systems, Detectors, and FPAs, Third Edition.*

SPIE Field Guides

The aim of each *SPIE Field Guide* is to distill a major field of optical science or technology into a handy desk or briefcase reference that provides basic, essential information about optical principles, techniques, or phenomena.

Written for you—the practicing engineer or scientist— each field guide includes the key definitions, equations, illustrations, application examples, design considerations, methods, and tips that you need in the lab and in the field.

John E. Greivenkamp
Series Editor

www.spie.org/press/fieldguides